Spring 1988

Experimental study of simulated micro-gravity vapor-liquid flow regimes

S B Reddy Karri
University of New Hampshire, Durham

Order Number 8816692

Experimental study of simulated micro-gravity vapor-liquid flow regimes

Karri, S. B. Reddy, Ph.D.

University of New Hampshire, 1988

U·M·I
300 N. Zeeb Rd.
Ann Arbor, MI 48106

PLEASE NOTE:

In all cases this material has been filmed in the best possible way from the available copy. Problems encountered with this document have been identified here with a check mark __✓__.

1. Glossy photographs or pages _____
2. Colored illustrations, paper or print _____
3. Photographs with dark background _____
4. Illustrations are poor copy _____
5. Pages with black marks, not original copy __✓__
6. Print shows through as there is text on both sides of page _____
7. Indistinct, broken or small print on several pages __✓__
8. Print exceeds margin requirements _____
9. Tightly bound copy with print lost in spine _____
10. Computer printout pages with indistinct print _____
11. Page(s) _____ lacking when material received, and not available from school or author.
12. Page(s) _____ seem to be missing in numbering only as text follows.
13. Two pages numbered _____. Text follows.
14. Curling and wrinkled pages _____
15. Dissertation contains pages with print at a slant, filmed as received __✓__
16. Other _____

_____

_____

EXPERIMENTAL STUDY OF SIMULATED MICRO-GRAVITY VAPOR-LIQUID FLOW REGIMES

by

S.B. Reddy Karri

B.Tech., Andhra University, 1981
M.S., University of New Hampshire, 1984

DISSERTATION

Submitted to the University of New Hampshire
in Partial Fulfillment of
the Requirements for the Degree of

Doctor of Philosophy

in

Engineering

May, 1988

This dissertation has been examined and approved.

Virendra K. Mathur

Dissertation director,
Virendra K. Mathur,
Professor of Chemical Engineering

Stephen S.T. Fan

Stephen S.T. Fan,
Chairman and Professor of Chemical Engineering

Russell T. Carr

Russell T. Carr,
Assistant Professor of Chemical Engineering

Horst Richter

Horst J. Richter,
Professor of Engineering, Dartmouth College

John A. Wilson

John A. Wilson,
Associate Professor of Mechanical Engineering

Feb. 10, 1988

Date

DEDICATION

To

My Parents, whose love and sacrifice make everything possible.

ACKNOWLEDGEMENTS

I am greatful to my dissertation director, Professor V.K. Mathur, for his valuable guidance, openness, and encouragement in directing the work that is presented in this thesis. I am fortunate to have had the benefit of his experience and confidence.

I thank my thesis committee members, Professors S.S.T. Fan, R.T. Carr of the Chemical Engineering Department, J.A. Wilson of Mechanical Engineering, and H.J. Richter of Dartmouth College who read the draft of the thesis, made constructive criticisms, and offered many invaluable suggestions for improvement.

I also thank Mr. Kenneth Palmer for his creativity relating to mechanical matters. In performing the experiments I received generous assistance from my friend, Mathew Miller. Stimulating conversations, which helped to determine the topical coverage, were held with Mr. Tom Lovell. Lastly, thanks are also due to all others who have contributed to the successful completion of this study.

I acknowledge the AETA Corporation, Portsmouth, New Hampshire; and US Air Force, Wright-Patterson Air Force Base, Dayton, Ohio, for providing funds for this project.

Finally, I acknowledge the ever present support and encouragement by my uncle and aunt.

S.B. Reddy Karri

TABLE OF CONTENTS

LIST OF TABLES

LIST OF FIGURES

NOMENCLATURE

a,b	Subscripts referring to liquids
A_G	Cross-sectional area occupied by gas, m^2
A_l	Cross-sectional area occupied by liquid, m^2
Bo	Bond number
$c_{p,l}$	Specific heat at constant pressure of liquid, J/kg-^oK
C_d	Drag coefficient given by equation 3.7
C_G	A constant in equation B.8
C_l	A constant in equation B.8
C_2	A Constant in equation 5.5
d	Diameter of vapor core in annular flow
D	Diameter of conduit, m
E	Defined by an equation 3.5, $m/\sqrt{s}$
E_G	Kinetic energy of gas, J
E_l	Kinetic energy of liquid, J
Eo	Eotvos number, $4g(\rho_l-\rho_v)R^2/\sigma$
f_l	Friction factor for liquid, dimensionless
F_b	Buoyancy force, N
F_d	Drag force, N
F_i	Inertial force, N
F_p	Excess pressure forces, N
F_s	Surface tension force, N
F_g	Gravity force, N
F_{int}	Interfacial force, N
Fr_t	Froude number defined by U_t^2/gD
Fr	Froude number
g	Gravitational field, m/s^2
g_n	Gravitational field on earth, m/s^2
G_{Gs}	Superficial mass velocity of gas, kg/m^2-s
G_{ls}	Superficial mass velocity of liquid, kg/m^2-s
G_t	Total phase mass velocty, kg/m^2-s
Gr	Grashof number
h	Height of liquid from a reference point, m
h_l	Liquid height in conduit, m
Ja	Jakob number, $\rho_l c_{p,l}\Delta T/\rho_v\Delta h_v$

k	Thermal conductivity of liquid, W/m-^{o}K
K_1	A constant given by equation 3.9
M_G	Mass flow rate of gas, kg/s
M_l	Mass flow rate of liquid, kg/s
p	Pressure, N/m^2
Pr	Prandtl number, $c_{p,l}\mu/k$
r	Capillary radius, m
R	Bubble radius, m
R_d	Bubble departure radius, m
R_s	Bubble base radius, m
Re	Reynolds number
Re_G	Reynolds number of gas
Re_l	Reynolds number of liquid
s	Sheltering coefficient in equation 5.3
S_i	Perimeter of gas-liquid interface, m
u_G	Gas velocity, m/s
u_l	Liquid velocity, m/s
U_{Gs}	Superficial velocity of gas, m/s
U_{ls}	Superficial velocity of liquid, m/s
U_t	Volume averaged velocity, m/s
We	Weber number
x	Axial length, m
x	Gas mass quality, dimensionless

Greek Symbols

α	Angle of inclination from horizontal, degrees
α_l	Thermal diffusivity of liquid, m^2/s
ϵ	Gas volume flux quality (void fraction), dimensionless
ρ_l	Liquid density, kg/m^3
ρ_v	Vapor density, kg/m^3
ρ_G	Gas density, kg/m^3
μ_G	Dynamic viscosity of gas, N-s/m^2
μ_l	Dynamic viscosity of liquid, N-s/m^2
ν_G	Kinematic viscosity of gas, m^2/s
ν_l	Kinematic viscosity of liquid, m^2/s
σ	Surface tension, N/m

γ_{ab}	Interfacial tension between two liquids, N/m
Δp_v	Excess vapor pressure, N/m^2
Δh_v	Latent heat of vaporization, J/kg
ΔT	Wall superheat, T_w-T_s, ^oK
τ	Bubble growth time, s
τ_l	Shear of liquid along the wall, N/m^2
τ_i	Interfacial shear between vapor and liquid, N/m^2
ϕ	Contact angle, degrees
λ	A dimensionless density parameter, defined by equation 5.1
ψ	Dimensionless parameter defined by equation 5.2

ABSTRACT

EXPERIMENTAL STUDY OF SIMULATED MICRO-GRAVITY VAPOR-LIQUID FLOW REGIMES

by

S.B. Reddy Karri
University of New Hampshire, May, 1988

Space missions in the near future will require power plants and cooling systems to operate in space. Such systems will often incorporate two-phase (vapor-liquid) heat transfer loops. Heat transfer processes such as boiling and condensation involve two-phase flow and are gravity dependent. Such unit operations would, therefore, be expected to behave differently in a micro-gravitational ("micro-g") environment. In this study, a unique approach to study the flow patterns of vapor-liquid flow in micro-g is presented. Simulation of a micro-g vapor-liquid flow on earth is accomplished by the use of two immiscible liquids of equal density. This equal density two-liquid system makes the buoyancy forces approach zero which is the case for real vapor-liquid flow in micro-g conditions. Water and properly selected oils are used in the experiments. In simulating micro-g vapor-liquid flow, the oil which is more viscous and more wettable liquid represents the "liquid" phase and water (less viscous and less wettable with respect to waxed tube surface) corresponds to the "vapor" phase.

The experiments are carried out in a horizontal pyrex glass tube (6.1 m long and 2.54 cm ID). Data are obtained for five different fluid systems to study the effect of viscosity ratio, interfacial

tension, and wettability of two fluids on flow regime boundary lines. Comparison of the simulated versus actual micro-g vapor-liquid flow regime data indicates the validity of this simulation approach. The experimental results are also compared against Taitel-Dukler and Weisman et al. model predictions under micro-g conditions. A flow regime map for vapor-liquid flow in a micro-g environment is developed for usage in designing two-phase systems in space applications.

The effect of gravity on nucleate boiling is also considered. The static and dynamic forces acting on a growing vapor bubble on heating surface are evaluated and how their interaction causes the bubble to detach from the surface is presented. By using a force balance, the bubble departure radius is calculated and compared with experimental measurements from literature under micro-g conditions.

I. INTRODUCTION

The exploration of space has brought with it a spectrum of effective gravitational environments, from zero-gravity to hyper-gravity through normal earth gravity. Zero-gravity is the state of apparent weightlessness within space vehicles when they move solely under the action of gravitation, either in free fall or in an orbit. Finite gravities may be as low as g/g_n of 10^{-6} or 10^{-5} when a vehicle experiences deceleration while coasting at the edge of a planetary atmosphere. Slightly higher gravities, i.e., in the range of $g/g_n = 10^{-4}$ to 10^{-2}, occur because of acceleration by electrical propulsion devices. Finally, there are fractional gravities in the vicinity and on the surface of celestial bodies which are early space flight destinations, such as g/g_n of : 1/6 on the Moon and Titan, 5/13 on Mercury and Mars, and 7/8 on Venus.

Both in the space vehicle and on the surfaces of a planet or satellite, fluid flow and heat transfer processes take place in propulsion, power-generation, and life-support systems. Frequently, these processes involve two-phase vapor-liquid or gas-liquid phenomena. Typical examples are processes in liquid-propellent storage tanks, vapor-liquid separators, evaporators, boilers, and condensers.

Space missions in the distant future envision the need for high power levels, which would be orders of magnitude greater than required by spacecraft launched at present. The power demands of future spacecrafts are expected to grow as high as one megawatt in the next

20 years (Mahefkey, 1982). According to Eastman et al. (1984), transport distances between the heat sources and the radiators could vary from 1 to 50 meters, and transport capabilities of up to 5 million watt-meters may be needed. The high operating power of the future spacecraft will require more effective thermal transport techniques.

Traditionally, excess heat from the power dissipating payload components is transferred by solid conductors to outer surfaces and then discarded to space by radiation. This is certainly not a viable means to handle high heat of dissipation since the unit gets heavier. Alternatively, "heat pipe" can be used for thermal transport in space applications. Liquid in the pipe is evaporated at the warmer part of the pipe. The vapor flows to cooler regions where condensation occurs. Surface tension in a wick or porous structure causes the liquid to flow from the condenser to the evaporator by capillary action and balances the pressure drop in the vapor. The advantages of using the heat pipes in space are: i) no pump is needed, ii) nearly isothermal operation and different fluids can be selected for the desired operating temperature, and importantly iii) the designs of heat pipes for space applications are expected to be the same as on the earth since the gravity has little effect on the flow of liquid and vapor in the wick (i.e., surface tension driven flows). However, the quantity of heat conducted through a heat pipe is limited by the low pressure differential generated in the wick. Some high capacity heat pipes are being developed to transport hundreds of watts for distances up to 15 m. or thousands of watts for 3 m. at ordinary temperatures. However, transport of high heat loads over long

distances by heat pipes is not yet an established capability. It is possible to put together many heat-pipes in series and/or parallel to overcome this problem, but, again the bundle gets heavier (Mahefkey, 1982).

The current space shuttle design uses a single-phase-fluid loop to transport heat to be dissipated to radiators. Theoretically, this cooling loop could be used to handle high heat loads. However, since only the sensible heat of the circulating fluid is used, these systems get large and heavy. In fact, in many cases, the equipment necessary to power the pump is much heavier than the cooling loop itself. Furthermore, the temperature drop between the source and the radiator is quite large.

Due to the shortcomings of the above mentioned methods, the use of two-phase-fluid-loops could offer a better alternative for the removal and transport of high waste-heat loads to space radiators. This system would allow the use of the latent heat of vaporization so that the flow rates would be sharply reduced. With a two-phase cooling loop, the operating flow rates and temperature drop can be considerably reduced and still one can obtain a higher heat transfer coefficient than a single-phase loop. According to Eastman et al. (1984), in a typical comparison with a single-phase-fluid loop, the pump power can be reduced by two orders of magnitude and the heat transfer coefficient increased by 10-100 times of magnitude. Furthermore, the entire loop is essentially isothermal making the radiators smaller and lighter.

Nuclear reactors are being considered for multi-mega-watt (MMW) power generation for future space applications such as space stations,

radar surveillance, communication platforms, etc. According to Krotiuk and Antoniak (1986), two-phase alkali-metal fluid loop is necessary for thermal transport in the space MMW nuclear reactors. The design and analysis of such loops require complete understanding of the flow regimes, pressure drops, and heat transfer in micro-gravitational environment.

Space missions in the near future would require power plants and cooling systems to operate in space. Such systems often need to incorporate two-phase (vapor-liquid) heat transfer loops. Heat transfer processes such as boiling and condensation involve two-phase flow and are gravity dependent. Such unit operations would therefore be expected to behave differently in a micro-gravitational ("micro-g") environment. Two-phase flow regime behavior in space may be significantly different from that on the earth, because vapor and liquid phases having different densities are affected to different extent by gravity. Therefore, there is a great need to study two-phase flow under micro-g environment. One reason for the lack of studies in this area is the complex nature of multiphase flow and the great difficulty in performing experiments in reduced gravity environment.

At present, two-phase experiments in micro-g require specialized facilities and equipment. The scope and extent of experiments in two-phase reduced-gravity flows have been determined largely by the methods and facilities employed for producing the reduced gravity. Generally, the reduced gravity experiments have been performed either in earth-based drop towers, airplane trajectories, and magnetic fields, or space-based long-term micro-g environment facilities such

as rockets, skylabs, or space shuttles. Some pertinent characteristics of these facilities are discussed below.

Drop Towers: The experimental package in perfectly free-fall with no resisting force provides a micro-gravity environment in the reference frame of the falling drop tower. This is because of the gravity (downward) and inertial (upward) forces acting on a free-falling experimental package are of the same magnitude and therefore would cancel each other resulting in a micro-g environment within the experimental module. There are several disadvantages in using this experiment: i) short duration of micro-g environment (~1 to 5 sec.) and therefore uncertainty of transient conditions, and ii) air from drop tower has to be evacuated prior to every experiment in order to achieve low g-levels (on the order of $g/g_n = 10^{-6}$). A drop tower facility at the NASA Lewis Research Center, consisting of a 2.2 sec. nonevacuated drop tower, and a 5.2 sec. evacuated drop tube, is available for experiments.

Airplane Trajectory: An aircraft flying a parabolic trajectory (see Figure 1.1) so that the experiment free floats within the cabin, can attain low g-levels. These micro-g levels can be sustained considerably longer than those in drop towers because the elevation change during free-fall is much larger. Two main advantages are that this technique offers more room for an experiment, and the experimenter can fly along with the experiment and is able to both observe and control the test while it is in progress. The magnitude and uniformity of the g-level produced is dependent on many factors, the chief one being the skill of the pilot. Note that prior to free fall maneuvers an acceleration of about $g/g_n = 2.5$ is experienced.

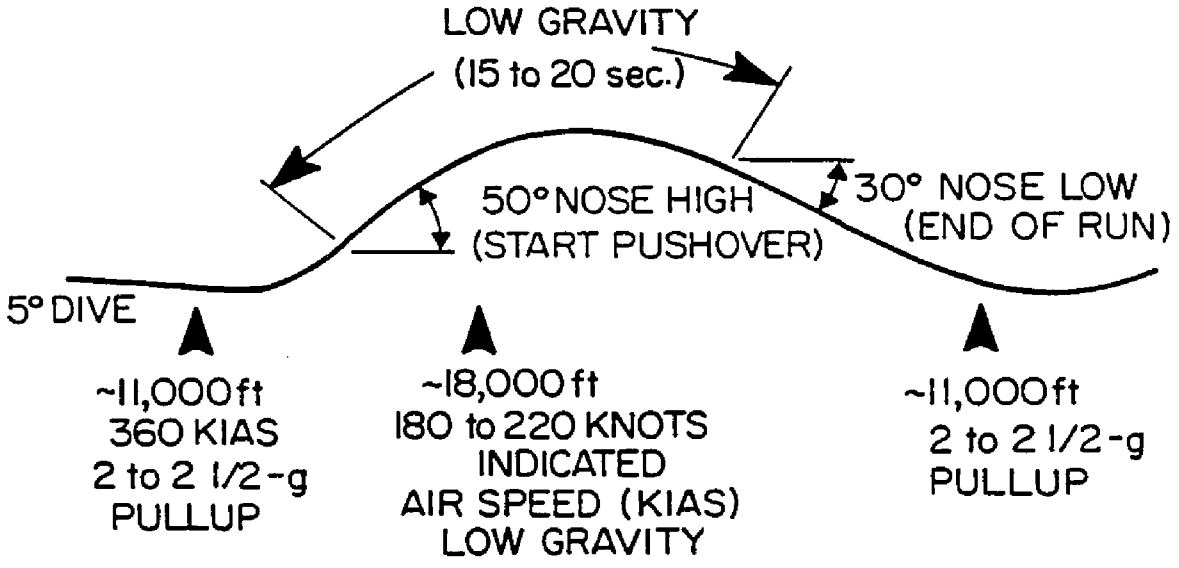

Figure 1.1: Typical "Low Gravity" Trajectory for Learjet.

This acceleration may perturb flow in the test loop, increasing the time required to establish a steady state once reduced gravity is achieved. If so, the period for taking valid data may be much shorter than the free-fall time. NASA owns two aircrafts for micro-g experiments: i) a Learjet at Lewis Research Center which can produce micro-g for 15 to 20 sec., and ii) a KC-135 aircraft at Johnson Space Center which can produce micro-g for about 25 sec.

Magnetic Field: Another technique (Petukov and Zhilin, 1973) that provides a range of gravity fields and can operate for long durations is the use of magnetic field with a fluid that has magnetic properties. The fluid is placed in a magnetic gradient such as in the core of a solenoidal magnet, and the magnetic force can be adjusted to counteract all or part of the gravitational body force. Some difficulties are encountered in obtaining magnetic fields that provide their force in a perfectly unidirectional manner because of end effects in a finite-sized magnet. Also, the liquid and vapor phases of the fluid, as would be present in a boiling or condensation experiment, are affected differently by the magnetic field due to their difference in magnetic permeability, and hence there is not an uniform reduced gravity simulation throughout the two-phase mixture.

Rocket: A rocket can perform essentially the same function as the aircrafts described earlier. Recently, a SPAR VIII rocket was used in a fluids experiment (Wilcox et al. 1981). This rocket provided over 4 minutes of an average acceleration near zero (actual g-level was not reported). Such tests, however, become quite costly. The experiments must be designed to withstand the high launch acceleration and hard

landing. It is not clear how low and steady a g-level is within rocket capabilities.

Space Shuttle: The advent of shuttle presents new opportunities for reduced-gravity experiments for a longer duration of time. Therefore, the shuttle-based experiments can be fully controlled and run until steady-state conditions prevail. However, the requirements for an experimental package are rather onerous in terms of development costs, safety considerations, size and weight of an experimental module, and the expense of the shuttle flight itself. Although it presents a significant improvement over the other facilities, the shuttle environment is by no means ideal. The reduced g-level during the orbit is $g/g_n = 10^{-3}$ to 10^{-4}; jitter can degrade it to 10^{-2}. A true micro-gravity condition ($g/g_n = 10^{-6}$) is achieved only at the shuttle's center of gravity (Salzman, 1985). In comparison, the space station of the 1990s has a g-level requirement of $g/g_n = 10^{-5}$ to 10^{-6}. This space station, which is still being designed, will represent the first true in-space laboratory to present a true micro-g environment.

In summary, the above discussed facilities and equipment can be used to study the flow patterns of vapor-liquid flow in micro-g. However, the earth-bound micro-g facilities are limited by the small size of the experimental module and short duration time of the experiment. So, there is always an element of uncertainty in judging whether the flow has reached steady state or not. On the other hand, the space-based facilities are very expensive to use, require the experimental package to meet many stringent safety regulations, and

present scheduling difficulties as there is always uncertainty of launching time.

Therefore, earth-based simulated two-phase experiments that replicate the conditions in space would offer enormous benefits such as long duration of tests, and a thorough understanding of vapor-liquid flow regimes that would occur in micro-g environment. In this investigation, a unique approach for simulating micro-gravity on earth to study the flow patterns of vapor-liquid flow in space is presented. A steady-state terrestrial method of simulating micro-gravity vapor-liquid flow is presented, discussed, and verified. The technique utilizes the use of two immiscible liquids of equal density which in turn offers the possibility of eliminating the buoyancy forces and thus simulating micro-gravity vapor-liquid flow on earth. The results of this simulated experiments are compared against model predictions and actual micro-g vapor-liquid flow regime data taken in either drop tower tests or airplane trajectory. Some of the chapters in this thesis stand by themselves and therefore will have their own results and discussion at the end of those chapters.

II. LITERATURE SURVEY

Future space missions envision the use of more effective thermal transport techniques utilizing either a single or a two-phase flow loops. The design and analysis of such loops require the detailed information regarding flow, pressure drop, and heat transfer characteristics in a micro-gravity environment. This chapter presents a brief review of the past reduced-gravity experiments reported in the literature including pool nucleate boiling, forced convective boiling, adiabatic vapor-liquid flow, and boiling and condensation experiments. These experiments are classified based on the methods and facilities employed for producing the micro-gravity environment.

a. Drop Tower Tests

Growth of single bubbles in a pool nucleate boiling under micro-gravity (g/g_n = 0.04 to 10^{-4}) has been studied by Cooper et al. (1978) for three fluid systems, namely water, toluene, and hexane. They have concluded that there was no sudden departure of the bubbles from the wall. The lack of large temperature difference (between wall and saturation temperatures, ΔT) was considered responsible for this. The shapes of the bubbles were found to be a function of surface tension, growth rate, departure time, and the 'g' value. A relationship was also found between bubble departure diameter and the gravitational field, 'g'.

A review article by Siegel (1967) discusses the effects of reduced gravity on heat transfer for all experimental and theoretical

studies published until 1966. Most experiments used the drop tower facilities, although some also utilized aircraft. For pool boiling, the critical heat flux was found to correlate well with $g^{1/4}$ for g/g_n of 1 to 10^{-2}. The basic physical principles governing bubble dynamics were used in obtaining simple expressions for the forces acting on a growing vapor bubble. These forces were calculated and plotted versus time. Short duration saturated pool nucleate boiling seems independent of gravity, but requires experimental substantiation.

Oker and Merte (1973) conducted a series of pool boiling experiments using liquid nitrogen and Freon-113 and heat flux from 10^3 to 10^5 W/m^2. A rather short drop tower was used, which gave < 1.4 sec. of free fall; it is uncertain if steady state conditions ever prevailed during the test. The gravitational fields as low as g/g_n of 4×10^{-3} were achieved. The data indicate that surface superheat at boiling inception is a function of gravity and is claimed to be less at micro-g than in normal gravity. However, an examination of the data shows that generally the ΔT increases significantly in the transition from normal to micro-g, which is what one would expect in the absence of natural convective heat transfer at micro-g. Oker and Merte's paper also presents a summary table, listing earlier nucleate pool boiling reduced-gravity experiments. In some cases the data appear to be somewhat contradictory.

An earlier experimental program (Cochran 1970) studied forced-convection boiling at low heat flux and low velocities in micro-gravity. The liquid used was slightly subcooled (0.4 to 1.5°C below saturation temperature) distilled water, heated from bottom with a flat Chromel strip. The experiments were conducted during the 2.2

sec. free fall in a drop tower. Bubble growth exhibited a cyclical trend; it is not clear whether steady state conditions prevailed or not. Eighty five percent of the bubbles remained attached to the heater surface, essentially forming a bubble boundary layer. The bubble diameter was found to correlate well with saturation layer thickness. The relevance of work is probably restricted to storage tanks containing cryogenic fluids. Insufficient data are available for drawing any conclusions regarding forced convection heat transfer.

Labus et al. (1972) examined the proportion of vapor generated at the surface of saturated freon-11, and in the bulk liquid (i.e., bubbles), upon venting to vacuum. The 5 sec drop test facility was used. No bulk vapor was generated at zero-g (i.e., all of the vapor was generated at the surface); however, small amounts of bulk vapor (boiling) were generated at measurable micro-gravity levels.

b. Aircraft Tests

Heppner et al. (1975) have conducted experiments to study the effect of gravity on flow regime transition boundaries and pressure drop. Two-phase flow of air and water in a pipe of 2.54 cm ID and 25.4 cm long (horizontal) was examined first on earth, then in a KC-135 aircraft simulating micro-g for about 20 sec. per trajectory. The flow regimes that are observed are annular, slug, plug (elongated bubble), and bubble flow. An analytical model indicated a downward shift of regime boundaries at reduced gravity. Experimental data reduction confirmed this trend, but not its magnitude. Pressure drop measurements showed significant increase for the micro-gravity environment when compared with normal gravity conditions.

Feldmanis (1966) conducted an experimental study (aircraft trajectory) on pressure and temperature changes in forced convective boiling at micro-gravity. It is reported that the system pressure increased and boiling oscillations damped out in micro-gravity. A similar experimental effort was devoted to condensation of Freon-12 in small diameter (2.62 mm ID and 3.66 m long) quartz tubes (Williams et al. 1973; Keshock et al. 1974; Williams, 1974). Although the test section was well instrumented, only qualitative results were reported. It appears that the flow regimes observed conform reasonably well to Baker-chart predictions (Collier, 1972). A qualitative difference in flow regimes at micro-g and normal-g flow conditions was notably less irregular, which is somewhat at variance with the trend noted earlier. The flow regimes observed are annular, slug, and bubble flow. The micro-gravity annular flow is stable, smoother, more regular, and less wavy than at earth gravity condition. Based on little discernible difference in condensation lengths, it was also hypothesized that condensation heat transfer was not appreciably affected by g-level.

Two preliminary studies investigating the flow condensation of a non-wetting mercury in pipes, were conducted by Albers and Macosko (1965), and Namkoong (1967). Both studies employed a Navy AJ-2 bomber flying a Keplerian (parabolic) trajectory to attain the micro-g environment. Steel pipes used ranged from 0.686 to 1.245 cm ID. Albers and Macosko reported practically the same pressure losses at normal- and micro-g. Both losses were greater than predicted by the Lockhart-Martinelli correlation (Collier, 1972) at low vapor qualities. But in the high-quality region of the condensing pipe, the

pressure drop from the Lockhart-Martinelli correlation agreed within 70% with the measured pressure loss. It was felt that the fog-flow correlation best explained the data. Namkoong reported that the distribution of liquid drops in the pipe was at the bottom of the pipe under normal-g, while uniformly distributed along the cross-section under micro-g.

Recently Hill et al. (1987) have conducted experiments in a NASA-JSC KC-135 using a very controlled instrumentation to study the effect of gravity on flow regime boundaries and pressure drop. Observations were made of an adiabatic two-phase flow of freon-114 in a tube of 1.58 cm ID and 1.83 m long. The flow regimes that are observed are typically classified into slug and/or annular flows. The bubble flow regime was not observed in this study.

c. Rocket Tests

A 4 min. rocket flight provided the micro-gravity environment for an experiment on bubble migration in molten glass ("fining") as reported by Wilcox et al. (1981). During the micro-g portion of the flight, distinct migration of the vapor bubbles toward the hotter portion of the sample was noted. This is due to the Marangoni effect (surface tension driven flows).

d. Shuttle Tests

The shuttle program has planned a series of fluid mechanics experiments (NASA, 1984) in the near future. Recently, a shuttle has been used for the production of super-glass, and crystal growth in micro-gravity environment.

e. Magnetic Field Tests

Several experiments have been performed with magnetic fields and a liquid metal (mercury). The objective was not to counteract gravity, but rather to note any perturbations engendered by the field on the boiling process. Petukhov and Zhilin (1973) discuss a number of experiments performed with single-phase liquid metals in magnetic fields. Hsu and Graham (1976) reported that the heat transfer was little perturbed by magnetic fields oriented horizontally.

In conclusion, a literature survey showed that very little work has been done on understanding and modeling two-phase (vapor-liquid) flow under micro-g environment. The few studies conducted on two-phase flow have a number of shortcoming such as the small size and length of the test section, short duration of experiment, thereby creating uncertainty as to whether a steady state has been achieved or not during this short time. These limited studies, however, do provide some qualitative information about the flow regimes that will occur for a vapor-liquid flow in micro-gravity. The literature survey indicated that annular, slug, and bubble flow are common micro-g vapor-liquid flow regimes.

III. DYNAMICS OF BUBBLE DEPARTURE IN MICRO-GRAVITY

In the literature survey a brief review of the past micro-g experiments including pool nucleate boiling and forced convective boiling has been presented. The effect of gravity on physical phenomena such as nucleate boiling is receiving greater attention with the advent of space travel and the associated micro-g environment. Nucleate boiling is one of the few modes of heat transfer which is affected by gravitational forces. The objective of this investigation is to understand the two-phase flow under micro-g which would finally be helpful in predicting heat effects. Therefore, it is important to understand the fundamentals of nucleate pool boiling in reduced gravity environment before attempting to study the complex micro-g two-phase flow. In this chapter, the static and dynamic forces acting on a growing vapor bubble on a heated surface are evaluated as to how their interaction causes the bubble to detach from the surface. This will give very good understanding of interaction of various static and dynamic forces acting on a vapor-liquid flow. It is important to be able to estimate the nucleate boiling parameters such as departure time and bubble radius at the moment of bubble detachment under micro-g conditions.

The effect of gravity on the bubble dynamics for saturated pool boiling of water has been experimentally studied by Siegel and Keshock (1964). They found that the bubble departure radius increases approximately as $g^{-1/3}$ for fields between g/g_n of 0.1 and 1, and for lower gravities increases as $g^{-1/2}$. It is a coupled problem of fluid

mechanics and thermodynamics where the fluid mechanics alone may involve inertia, drag, surface tension, pressure force, and gravity. The thermodynamics can be regarded as determining the rate of growth, which thus depends on many thermal properties and initial temperature fields in the fluid and wall. By using a force balance, an estimate of the departure radius is calculated and compared with experimental data of Siegel and Keshock (1964) for various g/g_n values. Five well known bubble departure diameter correlations which have 'g' as a parameter are extrapolated to several g/g_n values and the predicted departure diameters are compared.

Theory

Forces Acting on a Growing Bubble

When the bubble is small during nucleate pool boiling, the forces that hold the bubble to the wall (negative) are larger than the forces that pull the bubble from the wall (positive). As the bubble grows, the positive forces grow faster than the negative forces until they cross at a point which signifies the condition for bubble detachment. The forces that act on a growing bubble on a heated wall of constant temperature are shown in Figure 3.1. Hatton and Hall (1966), and Beer et al. (1977) have shown that bubble departure can be determined by a force balance:

drag force + surface tension force = liquid inertia force + pressure force + buoyancy force (3.1)

or

$$F_d + F_s = F_i + F_p + F_b \quad (3.2)$$

or

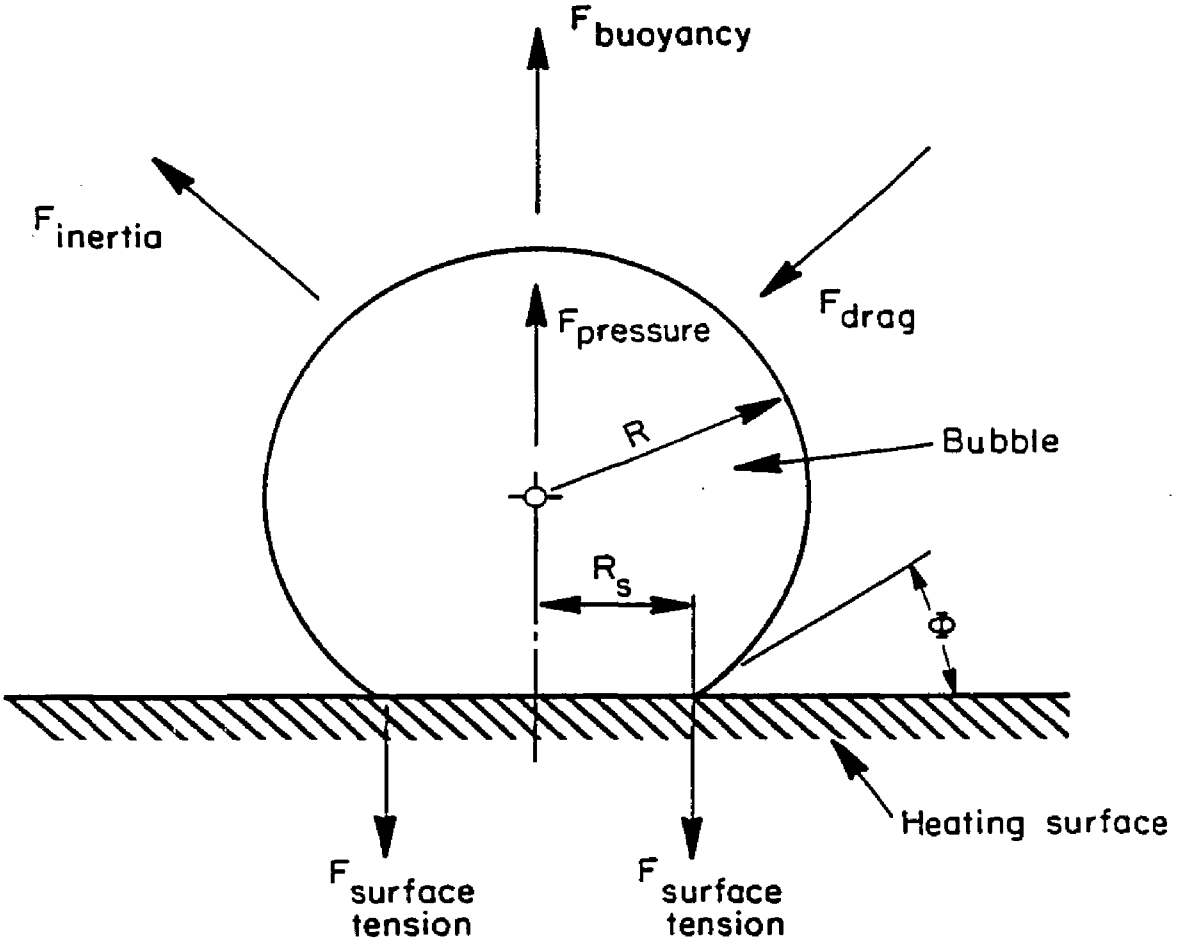

Figure 3.1: Forces Acting on a Vapor Bubble Growing on a Heating Surface.

$$C_d \frac{\rho_l}{2}\left[\frac{dR}{d\tau}\right]^2 \pi R_s^2 + 2\pi R_s \sigma \sin\phi = -\frac{4}{3}\pi R_d^3 \rho_l \frac{d^2R}{d\tau^2} + \left[\frac{2\sigma}{R_d} + \Delta p_v\right]\pi R_s^2$$

$$+ \frac{4}{3}\pi R_d^3 (\rho_l - \rho_v) g \qquad 3.3$$

Among these, the forces of surface tension, inertia, and buoyancy at any moment of bubble growth can be determined from the known values of R, ϕ, R_s, $dR/d\tau$, and $d^2R/d\tau^2$. Once the R-τ and ϕ-τ relationships are known, the last three variables, namely R_s, $dR/d\tau$, and $d^2R/d\tau^2$, can be easily computed. For micro-g applications, Siegel and Keshock (1964) have concluded from their experimental data that the growth curves can be approximated fairly well by $\tau^{1/2}$ behavior and ϕ is essentially independent of gravity. Therefore, radius-time relationship is evaluated from a general form,

$$R = E\tau^{1/2} \qquad 3.4$$

where E can be obtained from the Cole-Shulman (1966) correlation

$$E = 1/2 \sqrt{\pi}\ (Ja \sqrt{\alpha_l}) \qquad 3.5$$

This radius-time relationship has been used by a number of other investigators (Cooper et al., 1978; Pike, 1977). Therefore, the bubble growth rate can be calculated from $dR/d\tau = E / 2\sqrt{\tau}$. Pike has observed that the rate of growth of the bubble predicted by this equation is consistent with the experimental results.

And the base radius R_s is given by

$$R_s = (7/11)\ R \qquad 3.6$$

This relationship is only valid for large dimension heating surfaces and not applicable for thin wires.

To compute the drag forces, the drag coefficient C_d of growing

bubbles needs to be calculated. Beer et al. (1977) suggest that the drag coefficient can be calculated from

$$C_d = \frac{5360}{[R(dR/d\tau)\ \rho_l\ /\ \mu_l]^{0.79}} \qquad 3.7$$

The dynamic excess vapor pressure inside a bubble as shown by Beer et al. (1977) can be estimated by a force balance on an unattached growing bubble. This is given as

$$\Delta p_v 4\pi R^2 = -\frac{4}{3}\pi R^3 \rho_l \frac{d^2R}{d\tau^2} + C_d \frac{\rho_l}{2}\pi R^2 \left[\frac{dR}{d\tau}\right]^2 \qquad 3.8$$

After determining the C_d and Δp_v, all the positive and negative forces acting on a growing bubble can be computed by means of equation 3.3. The condition for bubble departure is assumed to be the point at which the net force goes from negative to positive. The corresponding radius refers to departure radius.

Bubble Departure Diameter Correlations

Several theoretical correlations have been proposed for predicting the size of the bubble at departure. Recently Jensen and Memmel (1986) have reviewed twelve bubble departure diameter correlations and compared their predictions against over five hundred data points culled from the literature covering a very wide range of experimental conditions. They have concluded that the correlation developed by Kutateladze and Gogonin (1979) was the most successful in predicting the data and Cole's (1967) correlation was the next best. The bubble departure radius can be computed from Eotvos number, Eo. Some of the correlations are briefly presented below.

Kutateladze and Gogonin (1979) developed a differential equation for the forces acting on a bubble at the moment of detachment from the wall. From this they obtained two dimensionless groups, Eo & K_1 with which they correlated data (≈180 points, 7 fluids) from the literature as given below:

$$Eo^{0.5} = 0.25(1 + 10^5 K_1)^{0.5} \quad \text{for } K_1 < 0.06 \qquad 3.9$$

$$\text{where } K_1 = \frac{Ja}{Pr}\left[\left\{\frac{g\rho_l(\rho_l-\rho_v)}{\mu_l^2}\right\}\left\{\frac{\sigma}{g(\rho_l-\rho_v)}\right\}^{1.5}\right]^{-1}$$

Jensen and Memmel (1986) modified this correlation to

$$Eo^{0.5} = 0.19(1.8 + 10^5 K_1)^{0.67} \qquad 3.10$$

Cole (1967) developed a correlation taking into consideration the effect of pressure as

$$Eo^{0.5} = 0.04\ Ja \qquad 3.11$$

Ruckenstein (1963) made a balance between the buoyancy and the drag forces to develop:

$$Eo^{0.5} = \left[\frac{3\pi^2\rho_l\alpha_l^2 g^{0.5}(\rho_l-\rho_v)^{0.5}}{\sigma^{1.5}}\right]^{1/3} Ja^{4/3} \qquad 3.12$$

Growth of single bubbles in a pool nucleate boiling under micro-g (g/g_n = 0.04 to 10^{-4}) has been studied by Cooper et al. (1978) for three fluid systems, namely, water, toluene, and hexane. They have concluded that there was no sudden departure of the bubbles from the wall. The lack of large temperature difference was considered responsible for this. The shapes of the bubbles were found to be functions of surface tension, growth rate, departure time, and the 'g' value. A relationship between bubble departure diameter and the gravitational field, 'g' based on empirical fit was found to be:

$$R_d\,(g/b^4)^{1/3} = 6 \qquad 3.13$$

where $b = Ja\sqrt{\alpha_l}$.

All these correlations have 'g' as a parameter and can be extrapolated to various g/g_n values. The predicted values of these extrapolations to low gravity fields are compared with the experimental data of Siegel and Keshock (1964).

Results and Discussion

The bubble departure radius is calculated from static and dynamic force balance (equation 3.3) along with equations 3.4 through 3.8 for saturated water boiling on a wall heated to 379.17°K at 1 atm under various values of 'g' accelerations. A contact angle of 45° is used for all g/g_n values. The departure radius is also computed from the well known theoretical correlations 3.9 through 3.13 at various g/g_n values. The variation of departure radius as a function of the fraction of normal gravity, g/gn, is given in Table 3.1. The second column lists the average departure radius at reduced gravity. The experimental data was taken by Siegel and Keshock (1964) in a drop tower which can produce micro-gravity environment for a duration of about 1.2 sec.

From a comparison of percentage absolute error, it is evident that the static and dynamic force balance approach (equation 3.3) is the most accurate in predicting the departure radius at micro-g environment. The correlation developed by Ruckenstein (1963) shows the next best results. It predicts within 10% error for g/g_n greater than 0.126 and about 25% error for lower g/g_n values. This equation is derived by making a force balance between buoyancy and drag

Table 3.1: Bubble Departure Radius : Comparison of Experimental and Predicted Data

g/g_n	Bubble Departure Radius, mm					
	Experimental	Force balance	Equations			
		Equation 3.3	3.9	3.10	3.11	3.12	3.13
1	1.18	1.13	0.85	0.96	0.93	1.08	4.19
		(4.2)	(28.0)	(18.6)	(21.2)	(8.5)	(255)
0.429	1.53	1.56	1.08	1.19	1.42	1.44	5.56
		(2.0)	(29.4)	(22.2)	(7.2)	(5.9)	(263)
0.229	1.83	1.99	1.31	1.42	1.94	1.77	6.85
		(8.7)	(28.4)	(22.4)	(6.0)	(3.3)	(274)
0.126	2.36	2.53	1.59	1.7	2.62	2.16	8.37
		(7.2)	(32.6)	(28.0)	(11.0)	(8.5)	(255)
0.061	3.42	3.41	2.03	2.16	3.76	2.76	10.65
		(0.3)	(40.6)	(36.8)	(9.9)	(19.3)	(211)
0.03	4.61	4.62	2.62	2.79	5.36	3.49	13.5
		(0.2)	(43.2)	(39.5)	(16.3)	(24.3)	(193)
0.014	6.0	6.4	3.5	3.75	7.85	4.5	17.4
		(6.7)	(41.7)	(37.5)	(30.8)	(25.0)	(190)

Note: the numbers in the parenthesis represent the % absolute error from the experimental values.

forces. It is clear from these two approaches that the drag force is important and cannot be neglected in predicting the departure radius. The equations 3.9 and 3.10 consistently predicts considerably low values. The Cooper et al. correlation (equation 3.13) which was developed based on micro-g data for three fluid systems appears to be predicting considerably high values for bubble departure radius. Comparison of bubble departure radius predicted by force balance approach (equation 3.3) and experimental data of Siegel and Keshock (1964) as a function of the fraction of normal gravity, g/g_n, is given is Figure 3.2. These two are in good agreement.

The forces acting on a growing vapor bubble are computed using equation 3.3 along with equations 3.4 through 3.8 for saturated water boiling under g/g_n = 1, 0.126, and 0.014. These forces acting on a bubble versus the radius of the bubble for various g/g_n values are shown in Figures 3.3 through 3.5. The inertial force (F_i) is generally found to be the smallest among all the forces. The drag (F_d), inertial (F_i), and excess vapor pressure forces (F_{p2}) are essentially constant for all bubble radii. The increase in excess capillary pressure (F_{p1}) (a function of surface tension) alone is insufficient to overcome the growing surface tension force (F_s). As the bubble continue to grow, the buoyancy force (F_b) begins to increase from initial low values of the magnitude of 10^{-6} N. The latter eventually surpasses the remaining resultant forces so that the bubble must detach. The total net force (F_{net}) which is the sum of positive (upward) and negative (downward) forces is shown as a broken line in these figures. When this total net force going from negative to positive gives the condition at which the bubble begins to detach.

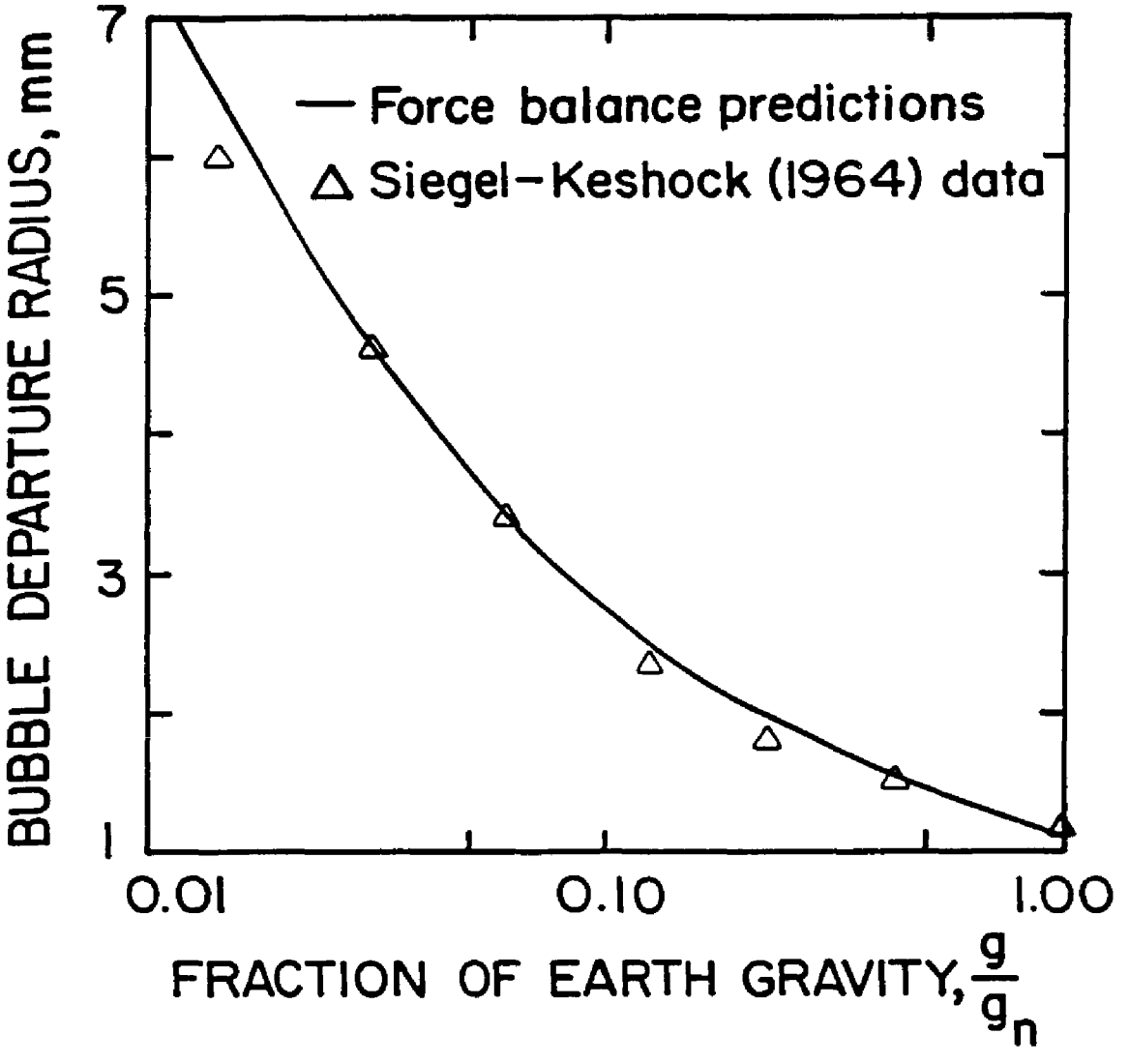

Figure 3.2: Comparison of Theoretical Predictions and Experimental Data.

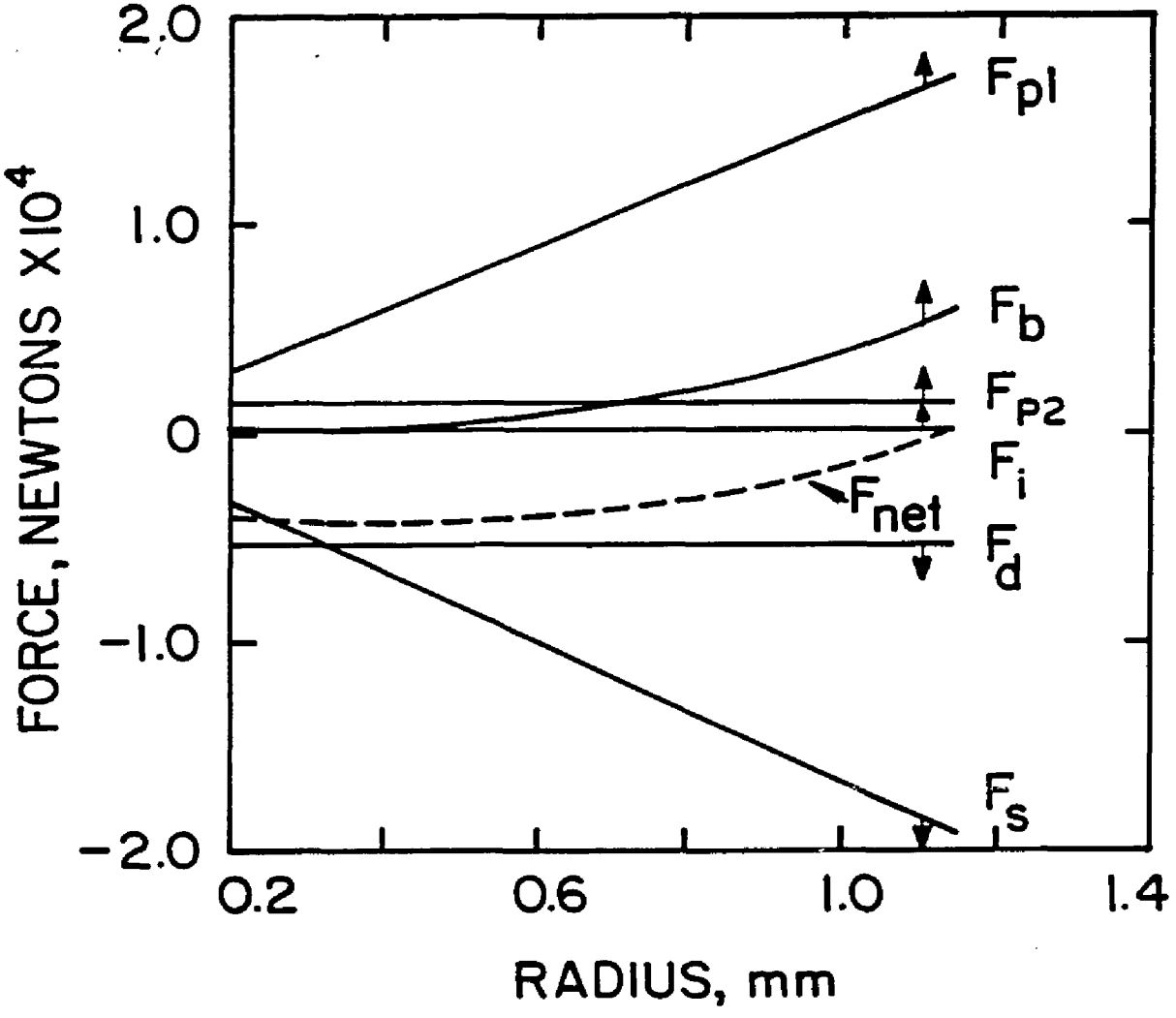

Figure 3.3: Forces Acting on a Bubble Growing in a Saturated Water on a 379.17°K Heating Surface under $g/g_n = 1$. (F_b - buoyancy, F_d - drag, F_i - inertial, F_{pl} - excess capillary pressure, F_{p2} - excess vapor pressure, F_s - surface tension, and F_{net} - total net forces)

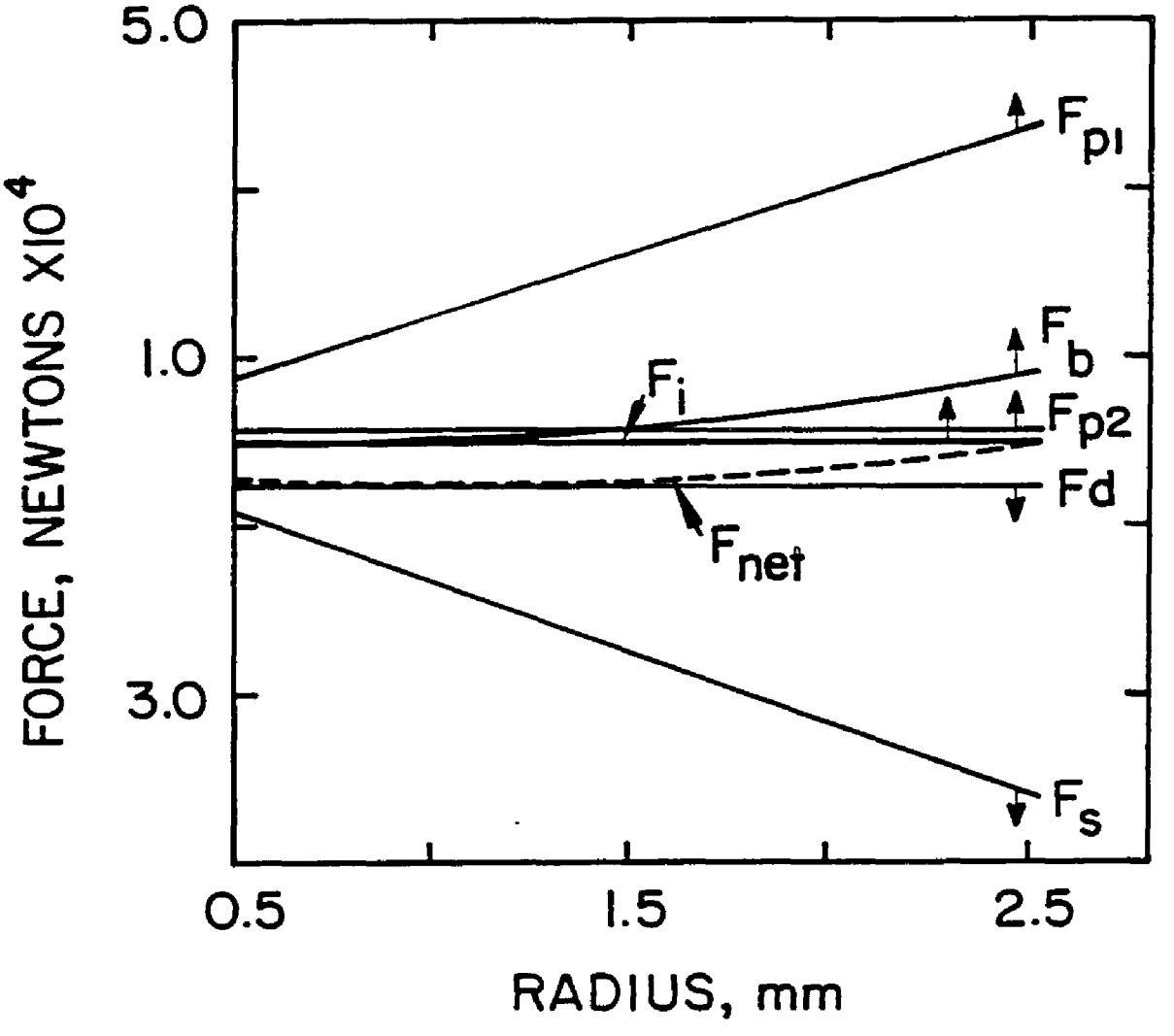

Figure 3.4: Forces Acting on a Bubble Growing in a Saturated Water on a 379.17°K Heating Surface under $g/g_n = 0.126$.

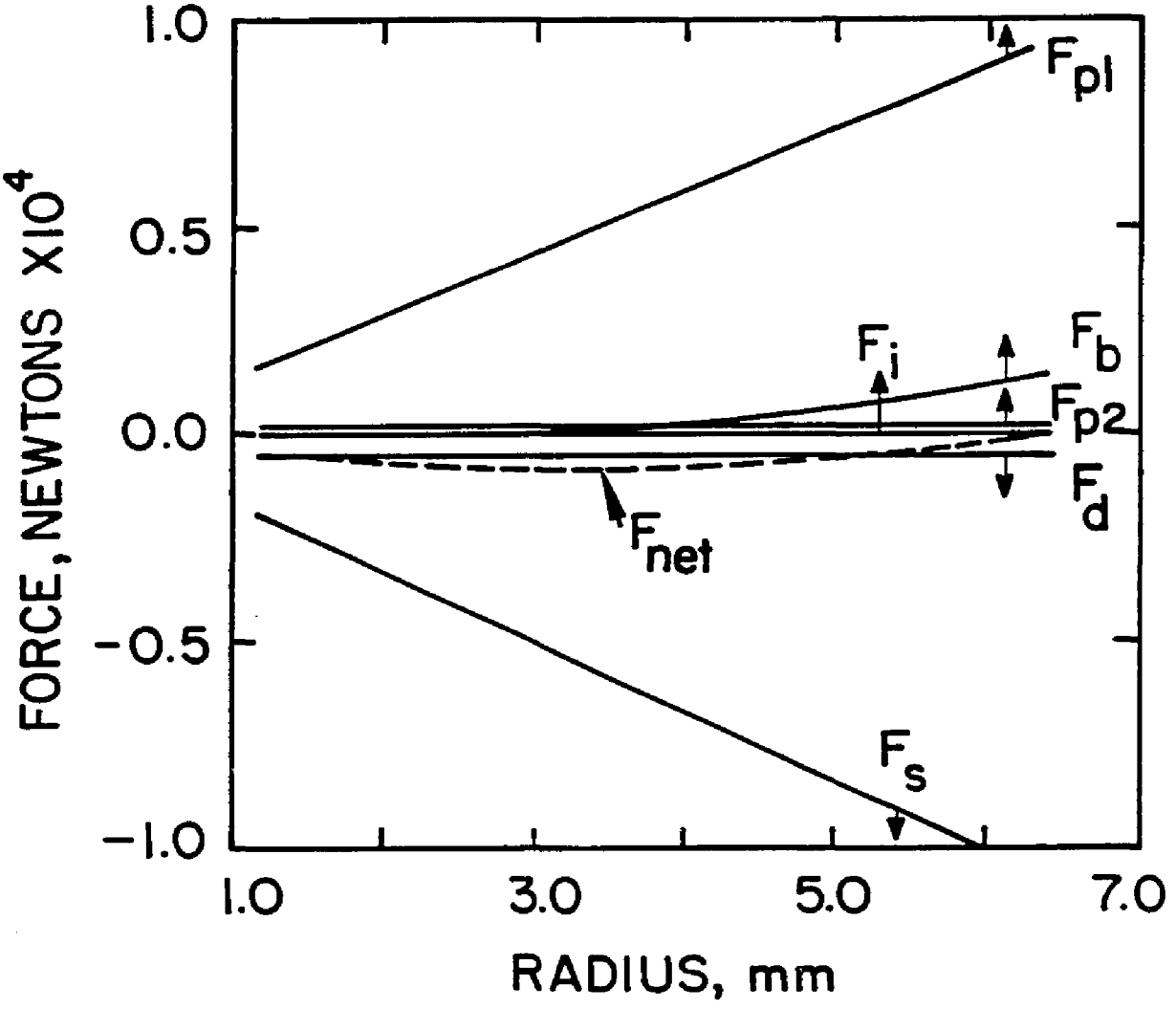

Figure 3.5: Forces Acting on a Bubble Growing in a Saturated Water on a 379.17°K Heating Surface under $g/g_n = 0.014$.

It is also important to note that the overall effect of surface tension (F_s - F_{pl}) is to delay, not to assist, the departure of bubbles in many circumstances. The only effect of reducing gravity is an increase in the bubble departure radius or total growth time. It should also be noted that a steam bubble growing on a 379.17^{o}K wall under exact zero-g conditions and with no interference from other bubbles will not detach from the surface. This phenomenon is due to the total absence of the buoyancy force which is essential for bubble departure. However, for other fluids or for water under different conditions (like increase in wall temperature), nucleate boiling may exist under zero-g conditions.

Conclusions

Bubble departure radii from micro-g data of Siegel and Keshock (1964) are compared against predictions from the proposed static and dynamic force balance approach and five well known correlations. The static and dynamic force balance approach predictions are in good agreement with the experimental data. It is evident that the drag forces can not be neglected in departure radius calculations. In particular, the overall effect of surface tension is to delay, not to assist, the bubble departure. The only data needed for predicting the departure radius are the wall superheat, contact angle, and the physical properties of the fluid system. In micro-gravity, the bubbles become quite large and the growth times are longer compared with those in earth gravity.

IV. TWO-PHASE (VAPOR-LIQUID) FLOW PATTERNS

In order to design an advanced two-phase cooling loop for spacecraft applications, it is necessary to analyze the flow within the system and predict heat transfer coefficients and pressure drops for normal gravity and "micro-g" operation. Unfortunately, there are no comprehensive mathematical models to relate pressure drop with other parameters (Heppner, et al, 1975) for analysis and design involving two-phase flows. Many investigators have developed empirical correlations for heat transfer coefficients and pressure drop, but these correlations are good only for specific flow regimes. The key, then, for estimating heat transfer and pressure drop is to first be able to predict the flow regime that would occur for given operating conditions. Baker (1954) and others emphasize that predicting the flow regime is an important step in predicting pressure drop.

Flow Regime Map Analysis - Selection of Coordinate Systems

Flow regime information is one of the most essential key when designing devices in which a two-phase flow occurs. The flow ranges of occurrence of particular two-phase flow regimes are generally presented in diagrams, called flow regime maps, in the form of areas divided by transition lines. For a quantitative description of the conditions which lead to the transition lines from one pattern to another it is necessary to define a set of parameters or parameter groups which have a direct bearing on such transitions.

One simplistic two-dimensional coordinate system is defined by using the superficial phase velocities of vapor and liquid (mass flow rate of the particular phase divided by its density and total flow area). Such a simple coordinate system is perhaps adequate for identifying the operating conditions that specify various regimes for a given fluid in a fixed geometry (pipe diameter and nature of wall surface). But it would not be useful in making any generalization to other fluid systems or other geometries regarding the conditions at which flow regime transitions would occur. This is because many parameters such as viscosity, surface tension, density, etc. affect the occurrence of various flow regimes and it is not possible to represent flow regime transition criteria in terms of only two simple variables.

Flow regime maps are plotted using various parameters as ordinate and abscissa (as shown in Table 4.1) and can be divided into three groups:

(1) Phase velocities or fluxes (U_{Gs}, U_{ls}, or G_{Gs}, G_{ls}, or M_G, M_l). This group of parameters, though the most convenient when used, does not assure universal flow regime maps for different two-phase systems,

(2) Parameters such as U_t, G_t, Fr_t, ϵ, x used in homogeneous models for two-phase flow, are the transformations of the parameters from group (1) and they are useful only for some flow regimes,

(3) Parameters such as dimensionless groups of phases, Re_l, Re_G, λ, ψ, E_G, E_l may provide a possibility for working out universal flow regime maps.

Table 4.1: Coordinate systems used for flow regime maps of two-phase flow in both horizontal and vertical flows

Authors	Coordinate System x	y
Abou-Sabe and Johnson (1952)	M_G	M_l
Baker (1954)	$(G_{ls}/G_{Gs})\lambda\psi$	G_{Gs}/λ
Goldman et al. (1961)	x	G_t
Govier et al. (1958)	U_{Gs}/U_{ls}	U_l
Griffith and Wallis (1961)	Fr_t	ϵ
Hewitt and Roberts (1969)	$U_{Gs}^2\rho_g$	$U_{ls}^2\rho_l$
Hoogendoorn (1959)	U_t	ϵ
Mandhane et al. (1974)	U_{Gs}	U_{ls}
Schroter (1962)	Re_G	Re_l
White and Huntington (1955)	G_{Gs}	G_{ls}

The coordinate systems of base maps should be general, convenient, accurate, and easy to use for practical applications. It is apparent from the studies of Mandhane et al. (1974) that the superficial phase velocities represent discrimination criteria of all flow regimes. In this study the flow regime data is presented on log-log plots using the following three coordinate systems:

(i) U_{Gs} vs. U_{ls}

(ii) $U_{Gs}^2\rho_G$ vs. $U_{ls}^2\rho_l$

(iii) Re_G vs. Re_l

Forces Acting on a Vapor-Liquid Flow

Co-current flow of vapor and liquid in a horizontal pipe may show different flow patterns. Most of the flow regimes in a

horizontal pipe show a non-symmetric pattern which is due to the effect of gravity on fluids with different densities. In general, the forces that act on the flow to cause the various flow regimes are: gravity, surface tension, inertia, viscosity, dynamically generated body forces, and the Bernoulli effect.

Gravity tends to stabilize the flow and generates a tendency for stratification in the vertical direction, i.e. liquid flow shows a tendency to occupy the lower part of the pipe, forcing the vapor to the upper parts. Surface tension tends to wick the liquid around the circumference of the pipe creating annular flow and also it tends to create strong interfacial forces which lead to slug flow. The inertial force manifests itself in turbulent fluctuations which create disperse flows, while the viscous force causes pressure differentials that tend to create stratified and annular flows. Viscosity and dynamically generated body forces act mainly in horizontal direction, the former against and the latter with the flow, respectively. At high vapor velocities the frictional and dynamic forces become dominant. Hence various flow regimes are the result of interaction of the various forces on the flow components. Flow regimes are classified into those which are gravity-surface tension dominated and those which are dominated by inertial, viscous and dynamically generated body forces. The low velocity flow regimes such as stratified smooth and wavy, elongated bubble, and low velocity slug flow are dominated by gravity-surface tension forces. The high velocity flow regimes such as annular-mist, the dispersed bubble flow, and the high velocity slug flow are all dominated by inertial, viscous and dynamically generated body forces.

A flow regime is a characteristic spatial distribution of the liquid and vapor flow. When various forces dominate the flow, different flow regimes will be encountered. The various flow regimes or flow patterns will have different effects on the hydrodynamic conditions near the wall and cause different frictional pressure drops and different modes of heat transfer.

Micro-g Vapor-Liquid Flow

In the case of horizontal co-current flow of liquid and vapor in the micro-gravity environment, fluid derived forces, such as momentum, inertial, viscosity, surface tension and dynamically generated body forces, can and will predominate and will dictate the location of the liquid and vapor phases in the pipe. Thus, in micro-gravity, one would expect major flow pattern changes during the conditions at which low velocity flow regimes would normally occur under normal gravity conditions, i.e., gravity dominated flow regimes. On the other hand, the high velocity flow regimes are largely uninfluenced by micro-g environment since gravity force is only a secondary effect (inertial, viscous, etc. being primary effects). Figure 4.1 shows the flow regime map for any vapor-liquid flow under earth gravity environment, in which two regions are indicated by shaded lines. The low velocity region in which gravity is a dominant force, gravity determines the type of flow regimes. On the other hand, the high velocity region in which gravity is insignificant force, the type of flow regimes will not be affected by micro-g environment. In fact, there is some support for this behavior to occur from the results of the Sky Lab experiments (Keshock et al, 1974).

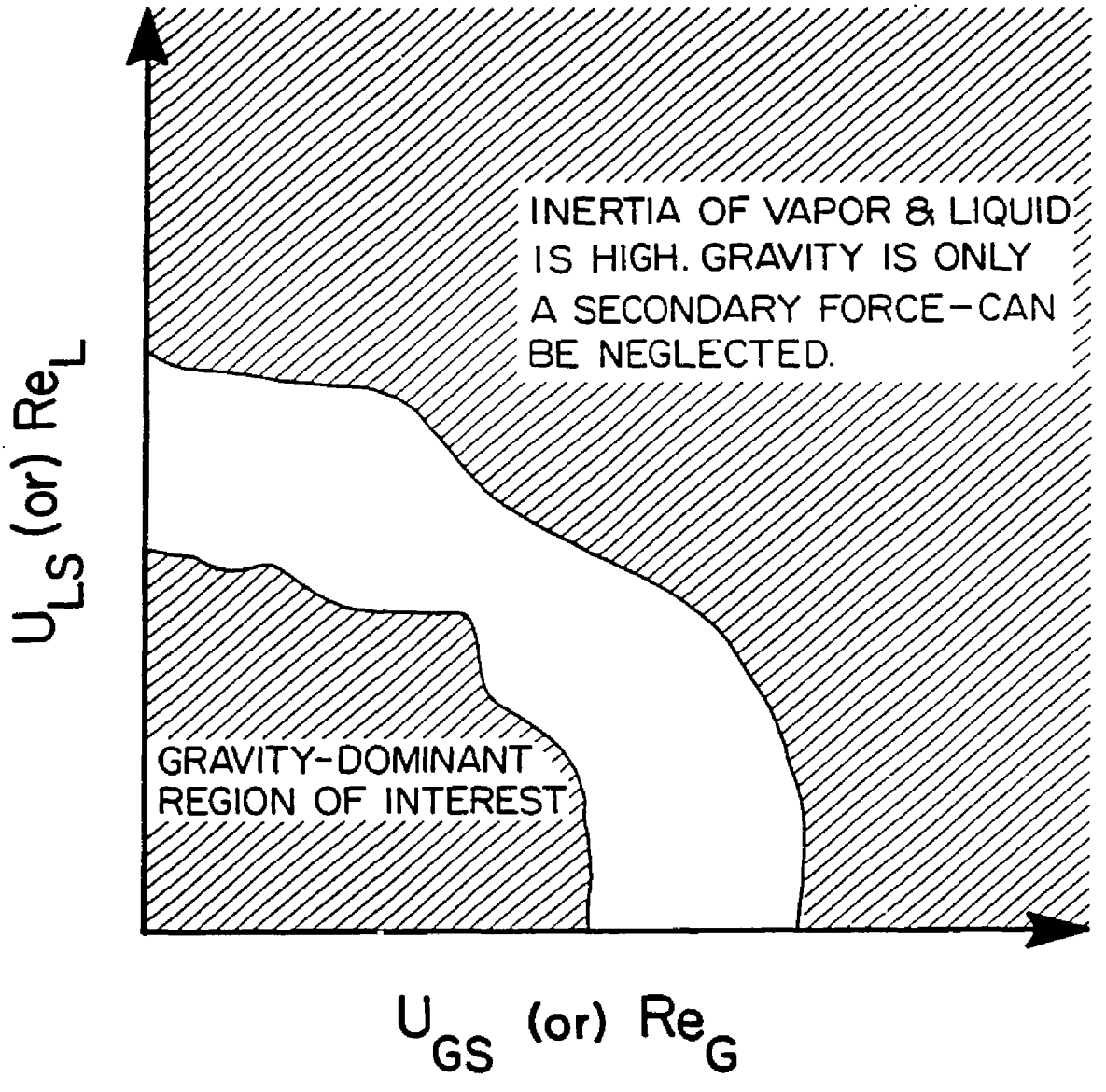

Figure 4.1: Flow Pattern Map.

Figure 4.2 shows the flow regime map predicted by Taitel-Dukler (1976) model for freon-11 vapor-liquid system (25°C, saturation pressure of 1 atm, 2.54 cm ID horizontal tube) under normal earth gravity conditions. The transition lines are represented by dashed lines. The window drawn by solid lines represents the low velocity region in which flow regimes such as stratified smooth and wavy, elongated bubble, and low velocity slug flow are dominated by gravity-surface tension forces. At higher velocities, i.e., outside the window, gravity force has a secondary effect and therefore the flow regimes are largely uninfluenced by micro-g environment. The major thrust of this study is to investigate what flow regimes would exist in the gravity dominated region. The simulated micro-g experiments are carried out to cover this region of interest. Additional work is required to quantitatively define this region of interest as stated under recommendations chapter.

Thus, in order to design heat transfer equipment for micro-g environment, it is essential that we have an understanding of the vapor-liquid flow regimes that are likely to actually occur. Such two-phase flow regimes are complex and often difficult to characterize and predict. Types of liquid-vapor flow regimes that are likely to occur under simulated micro-g environment are presented in Table 4.2.

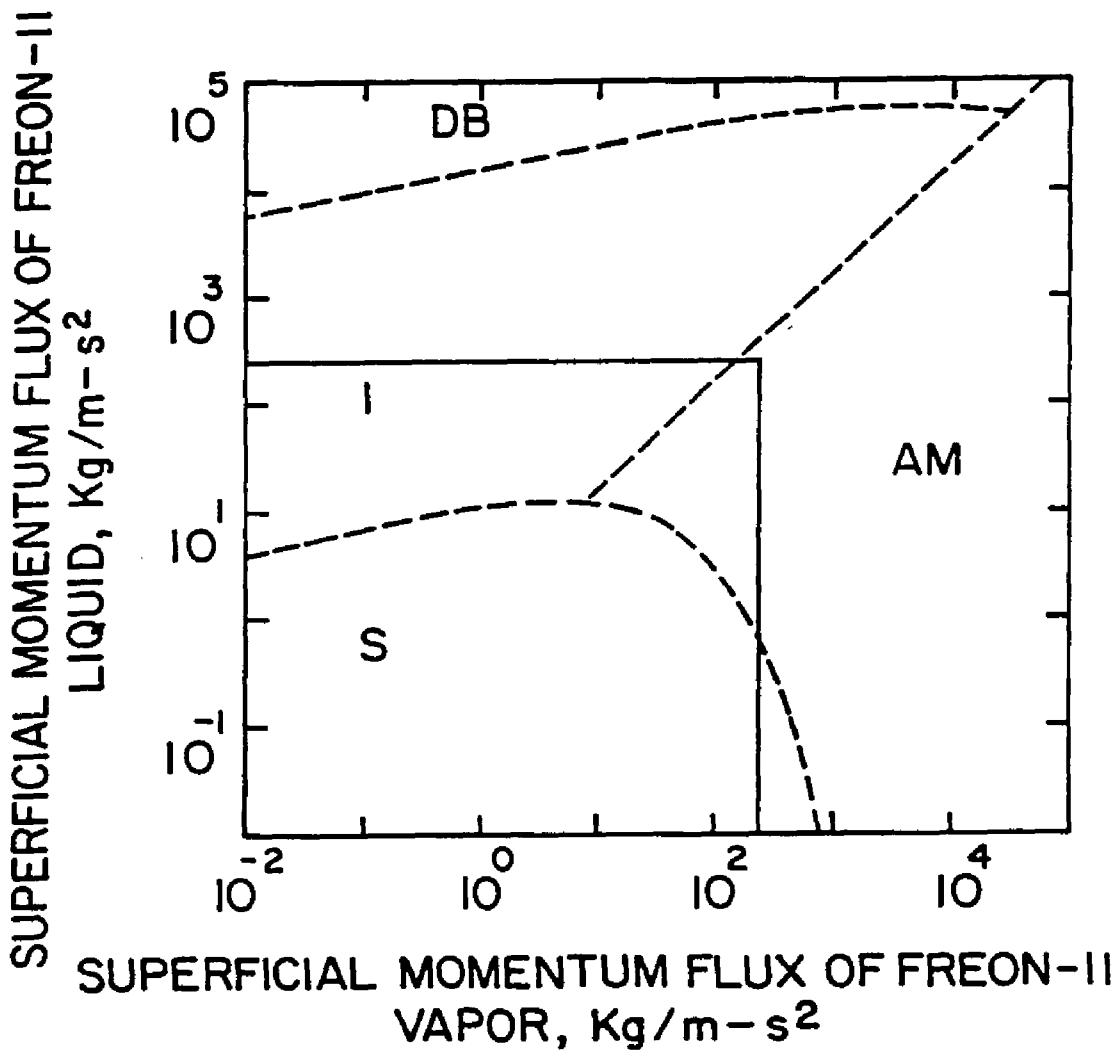

Figure 4.2: Freon-11 Flow Regime Map; Horizontal, 2.54 cm ID, 25°C, Sat. Press., g/g_n = 1.0, - - -Taitel-Dukler Model (1976).

Table 4.2. Flow Regime Definitions of Two-Phase Flow in Simulated Micro-G

–Stratified Smooth Flow (SS). In this regime, both liquid and vapor phases are continuous. The liquid flows as one or more smooth surface, narrow streams or rivulets that wet portion of the pipe. The vapor is in contact with, and flows above the liquid rivulets as well as the bare portions of the pipe.

–Stratified Wavy Flow (SW). Similar to the stratified flow regimes described above; however, with increased vapor velocities, the smooth interface with liquid becomes rippled and wavy. These include stratified plus roll wave and stratified plus inertial wave.

–Annular Flow (A). It is a form of stratified flow. In this regime the liquid phase completely wets the circumference of the pipe and the vapor flow is confined to central core of the pipe area. An alternate form of annular flow, the **Inverse Annular Flow (IA)**, can also occur where the liquid phase occupies central core and the vapor phase flows mostly through an annular zone, like a thick layer on the pipe wall. The liquid flow in the central core of an inverse annular flow may entrain some bubbles and, in some cases, the vapor layer may also entrain small portion of the liquid phase in the form of droplets. This regime sometimes called "burn out" or "departure from nucleate boiling" (DNB) and is characterized by heat transfer coefficients typical of vapor phase.

–Drop or Entrained Flow (D). At higher vapor velocities, the waves on the liquid surface grow, causing droplets to break off and to flow in the vapor core. At sufficiently high vapor qualities and vapor velocities the whole liquid phase flows almost entirely as a dispersion of droplets or mist within the continuous vapor phase.

–Bubble or Dispersed Bubble Flow (B). At relatively large liquid flow velocities, with little vapor flow, the liquid phase is continuous and fills the flow pipe while the vapor is in the dispersed form of the scattered bubbles.

–Slug Flow (S). Under appropriate conditions, the liquid waves created in the stratified wavy flow regime can bridge the pipe. This creates a flow regime characterized by alternating "bullet" shaped slugs of vapor followed by liquid phase flow that completely fills the pipe cross-section. **Inverse Slug** Flow (IS) would, of course, correspond to liquid slugs flowing in a continuous vapor stream.

–Churn Flow (C). Similar to both the annular and slug flow regimes, however, churn flow is more chaotic, lacking the well-defined "bullets" slugs. Moreover, the liquid-vapor interface moving in the direction of flow is rough and some bridging occurs to interrupt the continuity of the vapor phase in the core. **Inverse Churn Flow (IC),** as implied, corresponds to a similar flow regime in which the liquid and vapor phases are reversed.

V. VAPOR-LIQUID (TWO-PHASE) FLOW REGIME MAP PREDICTIONS UNDER MICRO-GRAVITY

Introduction

Research in two-phase flow has been in progress for over four decades owing to its application in nuclear and chemical industries. Consequently, knowledge about two-phase flow and heat transfer has advanced greatly during recent times. Almost all the work in the two-phase flow has been conducted for earth gravity applications, and very little has been done in the area of micro-gravity. Lack of knowledge of two-phase flow behavior in reduced gravities has prevented its use in space applications.

In this section, a brief review of the literature on earth gravity two-phase models to predict the flow regime transitions is presented.

Analytical Approach to Transitions

In this section, some of the analytic criteria that have been proposed for predicting the conditions, at which two-phase flow regime would change from one pattern to another have been examined. There have been a number of theoretical or semitheoretical attempts to describe flow-regime transitions. For such attempts to be successful, it would be necessary to include pipe diameter, liquid viscosity, liquid surface tension, liquid density, vapor density, and gravity in the mathematical models. Our primary objective is to analyze how the models available in the literature predict flow-regime transitions in micro-gravity.

Horizontal Flow

One of the most widely used flow pattern maps for horizontal two-phase flow has been presented by Baker (1954). The work is based on observations on cocurrent flow of gaseous and condensate petroleum products in horizontal pipes. The equations derived are entirely empirical. Baker took account of the fluid properties by introducing the following parameters:

$$\lambda = \left[\frac{\rho_G \rho_l}{\rho_a \rho_w}\right]^{1/2} \qquad 5.1$$

$$\psi = \left[\frac{\sigma_w}{\sigma}\frac{\mu_l}{\mu_w}\left[\frac{\rho_w}{\rho_l}\right]^2\right]^{1/3} \qquad 5.2$$

where ρ, σ, and μ represent the density, surface tension, and viscosity, respectively, the subscripts G and l represent the gas and liquid phases, and the subscripts a and w represent the values for air and water at atmospheric conditions (typically 20°C and atmospheric pressure). In SI units, appropriate values for the air-water at standard conditions are

$\rho_a = 1.205$ kg/m^3 $\quad \mu_w = 0.001002$ kg/m-s

$\rho_w = 1000$ kg/m^3 $\quad \sigma_w = 0.0728$ N/m

It is convenient to plot the Baker map in terms of the modified coordinates G_G/λ and $G_l\psi$ (Bell et al., 1970). A plot in this form is shown in Figure 5.1. The transitional empirical equations do not include an acceleration due to gravity, "g" term and therefore cannot be extrapolated to low "g" values.

For horizontal flow, Mandhane et al. (1974) examined 5935 flow pattern observations and proposed a new flow pattern map using superficial velocities of gas and liquid phases as coordinates. But

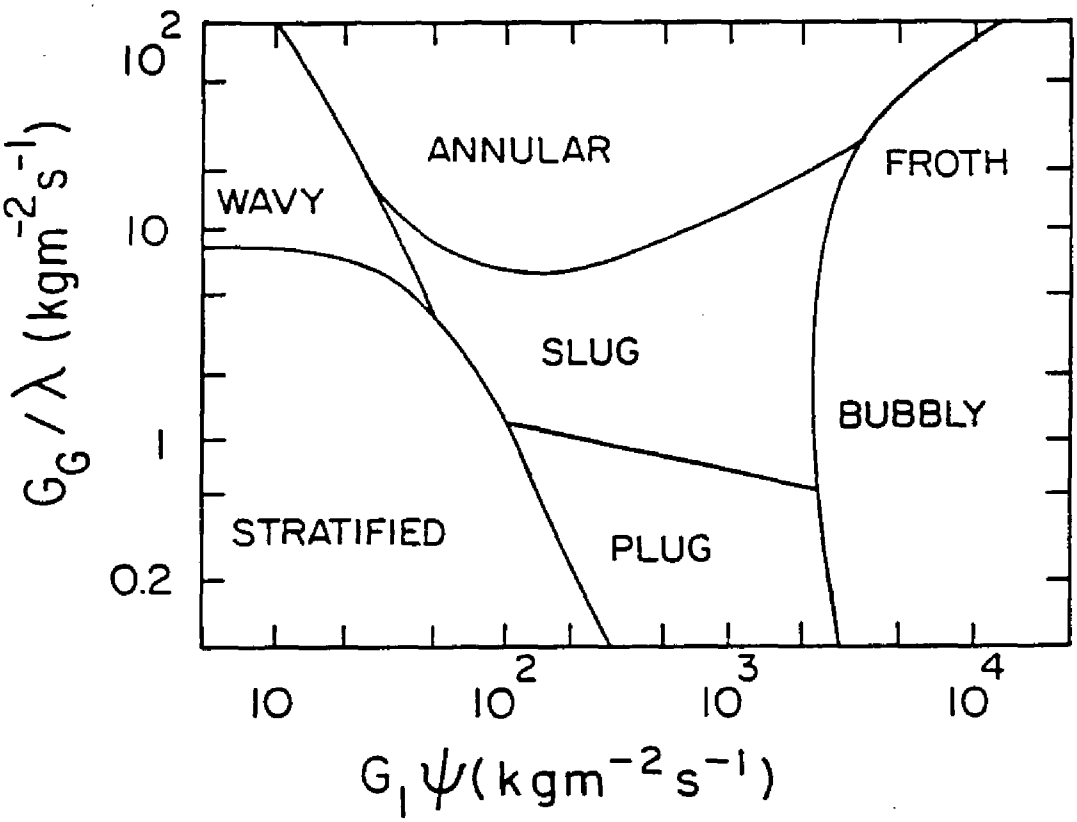

Figure 5.1: Flow Pattern Map of Baker (1954).

they did not report any correlations, based upon theoretical consideration or experimental data, for transitions between different flow patterns. Perhaps the most comprehensive treatment of flow-regime transitions in horizontal flow on a semitheoretical basis is that of Taitel and Dukler (1976). They are the first ones to provide expressions for various transitions, based upon theoretical and empirical logic. Weisman and his co-workers (1979) at the University of Cincinnati have conducted numerous experiments to determine the effects of different parameters on flow pattern transitions. Using an air/aqueous loop, they systematically varied pipe diameter, liquid viscosity, liquid surface tension, liquid density, and vapor density. Based on their experimental results, they proposed a set of mean transition curves. Although empirical in nature, their work seems to be the most complete and accurate to date.

The two models by Taitel-Dukler and Weisman et al. have been found to be more suitable for extrapolation to wide range of system parameters than the other horizontal two-phase flow regime maps available in the literature. Both use the same set of flow regimes and definitions and therefore it is easy to compare the transition predictions by these two models at any system parameter. The flow regimes used in both the models are: stratified (smooth and wavy), intermittent (slug and plug), annular-mist, and dispersed bubble. These two models have been reviewed in depth by several authors (Rouhani and Sohal, 1983 and Hewitt, 1981). The following are the criteria governing the transition regions for both the models:

Transition between stratified smooth and stratified wavy flow regimes. Taitel and Dukler (1976) have given a theoretical criterion for this transition. They used a modified form of Jeffreys (1925, 1926) model for interfacial instabilities and gave the criterion for this transition:

$$u_G \geq \left[\frac{4\nu_l(\rho_l - \rho_G)g\cos(\alpha)}{s\,\rho_G u_l}\right]^{1/2} \qquad 5.3$$

where s, the 'sheltering' coefficient is assumed to be 0.01 and α is the angle of inclination from horizontal.

Weisman et al. (1979) gave the condition for transition from stratified to wavy flow regime as:

$$\left[\frac{\sigma}{gD^2(\rho_l-\rho_G)}\right]^{0.2}\left[\frac{DU_{Gs}}{\nu_G}\right]^{0.45} \geq 8\left[\frac{U_{Gs}}{U_{ls}}\right]^{0.16} \qquad 5.4$$

This relationship is general in defining this transition, since it includes the effects of surface tension as well as other physical properties. Both these models have "g" as a parameter and can be extrapolated to low "g" values. In this study, the transition line between stratified smooth and stratified wavy is not plotted for the clarity of the figures, and both flow regimes are referred as stratified flow as commonly done in the literature.

Transition between stratified and intermittent or annular-mist flow regimes. Taitel and Dukler described this transition in terms of the classical Kelvin-Helmholtz instability and presented the criteria for this transition as:

$$u_G \geq C_2 \left[\frac{(\rho_l - \rho_G) g \cos(\alpha) A_G}{\rho_G \, dA_l/dh_l} \right]^{0.5} \qquad 5.5$$

where $C_2 = 1 - h_l/D$, and $dA_l/dh_l = 2 (h_l D - h_l^2)^{0.5}$ and h_l is the liquid height in the pipe.

Weisman et al. gave their transition criteria by defining a mean curve fit through a large number of data points. Their stratified intermittent transition criteria is given by:

$$\frac{U_{Gs}}{\sqrt{gD}} \geq 0.25 \left[\frac{U_{Gs}}{U_{ls}} \right]^{1.1} \qquad 5.6$$

These two transition criteria (equations 5.5 and 5.6) do not take into consideration the effect of surface tension on this transition boundary. However, both these equations do have "g" as a parameter, thus, can be used to predict this transition at low "g" values.

Transition between intermittent and annular-mist regimes. Taitel and Dukler hypothesized that development of intermittent or annular flow from stratified flow, depended uniquely on the liquid level in the equilibrium stratified flow. If the value of $h_l/D > 0.5$, then a sinusoidal wave growing on the interface would touch the top of the tube before its trough reaches the bottom of the tube. Thus, if $h_l/D > 0.5$, intermittent flow would develop, and if $h_l/D < 0.5$, annular or annular-mist flow is likely to occur. The constant value of $h_l/D = 0.5$ represents the criteria for intermittent to annular flow transition. Some confirmation of this view of the transition is given by Kubie (1979).

Weisman et al. proposed the following curve-fit correlation for a transition from annular to intermittent/stratified flow:

$$1.9\left[\frac{U_{Gs}}{U_{ls}}\right]^{0.125} \leq \left[\frac{U_{Gs}\rho_G^{0.5}}{\{g\sigma(\rho_l-\rho_G)\}^{0.25}}\right]^{0.2}\left[\frac{U_{Gs}^2}{gD}\right]^{0.18} \qquad 5.7$$

This transition is a function of "g" in both the models and can be extrapolated to low "g" values.

Transition between intermittent and dispersed bubble regimes. Taitel and Dukler see this transition as a case where turbulent fluctuations within the liquid are sufficient enough to overcome the buoyant forces tending to keep the gas at the top of the pipe. An approximate analysis gives the condition for the flow regime to change from intermittent to dispersed bubble as:

$$u_l \geq \left[\frac{4A_G}{S_i}\frac{g\cos(\alpha)}{f_l}\{1-\rho_G/\rho_l\}\right]^{0.5} \qquad 5.8$$

where S_i is the perimeter of gas-liquid interface, and f_l is the friction factor for liquid.

Weisman et al. fitted all the available experimental data on intermittent to dispersed bubble regime transition with the following slightly modified relation which included the effect of surface tension:

$$\left[\frac{(dp/dx)_l}{(\rho_l-\rho_G)g}\right]^{0.5}\left[\frac{\sigma}{(\rho_l-\rho_G)gD^2}\right]^{-0.25} \geq 1.94 \qquad 5.9$$

The predictions of this transition by these criteria can be obtained at extrapolated low "g".

Vertical Flow

Two recent studies have been reported on flow pattern transitions in vertical two-phase flow. These are by Taitel et al.

(1980) and Weisman and Kang (1981). They both have used the same set of flow regimes and their definitions. The flow regimes used in both the models are: bubble, intermittent (slug and churn), annular, and dispersed bubble. The following are the criteria governing the transition for these models:

Transition between bubble and intermittent regimes. Taitel et al. gave the following condition for the flow to change from bubbly to intermittent flow:

$$U_{ls} \geq 3.0U_{Gs} - 1.15 \left[\frac{g(\rho_l - \rho_G)\sigma}{\rho_l^2}\right]^{0.25} \qquad 5.10$$

Weisman and Kang correlated the data for transition from bubbly to intermittent flow and gave the following criterion for this transition:

$$\frac{U_{Gs}}{\sqrt{gD}} \geq 0.45 \left[\frac{U_{Gs} + U_{ls}}{\sqrt{gD}}\right]^{0.78} (1 - 0.65\cos\alpha) \qquad 5.11$$

where α is the angle of inclination with the horizontal.

Transition between dispersed bubble and bubble/intermittent regimes. Taitel et al. arrived at the following condition for transition from bubbly to dispersed bubbly flow:

$$U_{ls} + U_{Gs} \geq 4.0 \left[\frac{D^{0.429}(\sigma/\rho_l)^{0.089}}{\nu_l^{0.072}} \left[\frac{g(\rho_l - \rho_G)}{\rho_l}\right]^{0.446}\right] \qquad 5.12$$

And also the curve computed by this equation, delimiting dispersed bubble flow must terminate at another curve relating U_{ls} and U_{Gs} for a void fraction of 0.52.

The criteria of Weisman and Kang for this transition is the same as given for horizontal flow, i.e. equation 5.9.

Transition between intermittent and annular regimes. Taitel et al. proposed the criterion for this transition as:

$$\frac{U_{Gs}\rho_g^{0.5}}{[\sigma g(\rho_l - \rho_g)]^{0.25}} \geq 3.1 \qquad 5.13$$

Weisman and Kang used their own earlier correlation (equation 5.7) for horizontal flow to predict this transition.

All the above equations have "g" as a parameter, thus, can be used to predict these transitions under micro-gravity.

RESULTS AND DISCUSSION

The flow regime maps for the above mentioned models have been presented at earth gravity conditions. As mentioned earlier space program requires models for obtaining flow transition criteria under micro-gravity conditions which are not available in the literature. In this study, efforts have been made to examine these models by successively reducing the value of g/g_n from 1 to 10^{-5}

Micro-Gravity Flow Regime Transitions: Horizontal Flow

The flow transition equations of Taitel-Dukler and Weisman et al. for horizontal flow, have been used to generate flow pattern boundaries at micro-gravity levels, as presented in Figures 5.2 through 5.4.

These figures show computed flow regimes for an air-water system (25^oC, 1 atm, 2.54 cm ID horizontal pipe) for various values of g/g_n, namely, 1, 10^{-2}, and 10^{-5}. Figure 5.2 shows the flow regime map predicted by Taitel-Dukler and Weisman et al. models at $g/g_n = 1$. Transition predictions of the Weisman et al. model are represented by

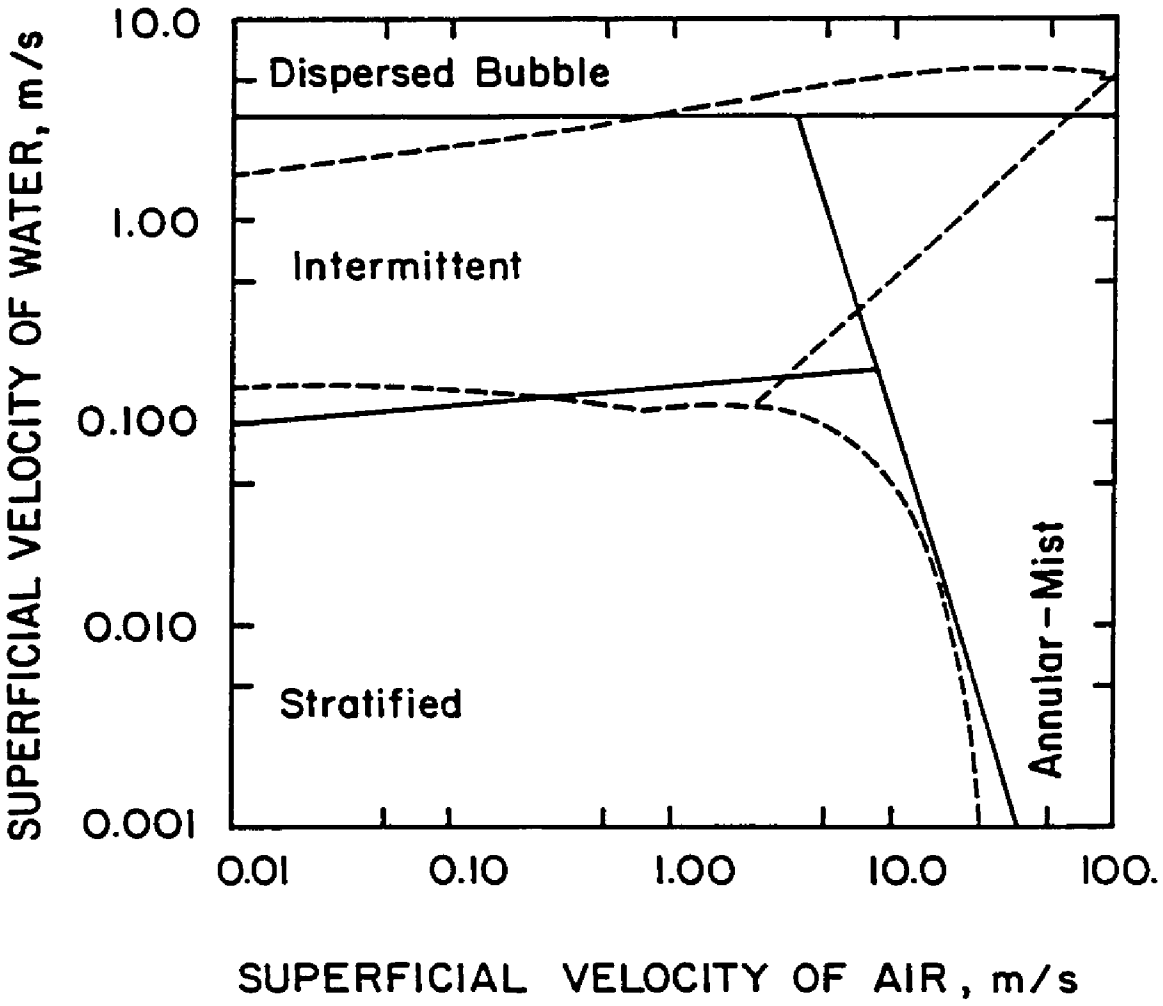

Figure 5.2: Horizontal Air-Water Flow, 2.54 cm ID, 1 atm, 25°C, $g/g_n = 1$,- - -Taitel-Dukler Model,——Weisman et al. Model.

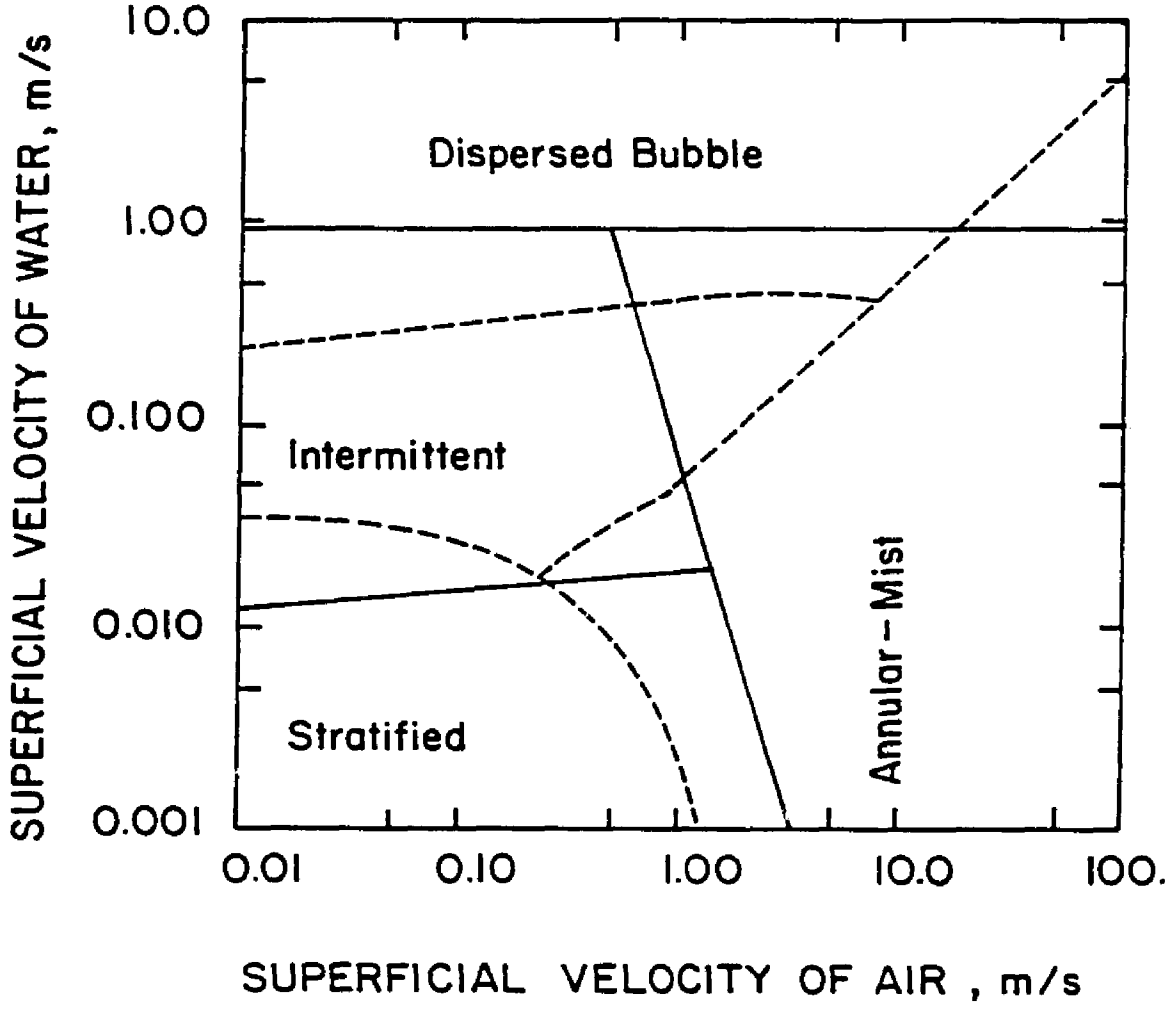

Figure 5.3: Horizontal Air-Water Flow, 2.54 cm ID, 1 atm, 25°C, $g/g_n = 10^{-2}$, - - -Taitel-Dukler Model, ——Weisman et al. Model.

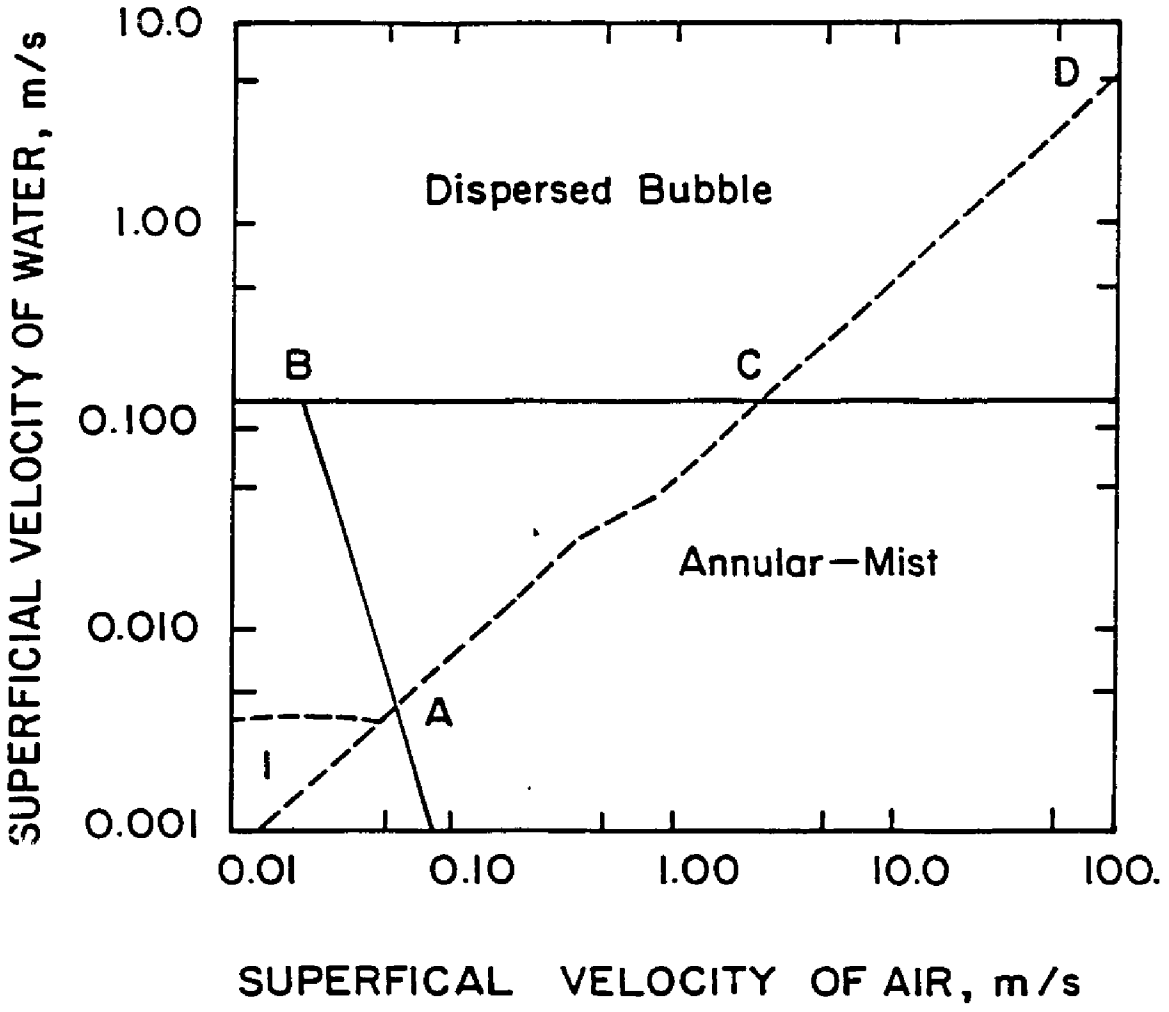

Figure 5.4: Horizontal Air-Water Flow, 2.54 cm ID, 1 atm, 25°C, $g/g_n = 10^{-5}$,- - -Taitel-Dukler Model,——Weisman et al. Model.

solid lines, those of the Taitel-Dukler model by broken lines. A comparison of these two models reveals that the same flow regimes are identified in roughly the same regions of the plot. However, the slope of the transition line between intermittent and annular-mist is positive for the Taitel-Dukler model and is negative for the Weisman et al. model. Figure 5.3 shows the flow regime map at $g/g_n = 10^{-2}$. The boundaries between stratified and intermittent, intermittent and dispersed bubble, and stratified and annular-mist regimes all move toward lower superficial velocities of both phases as g/g_n is reduced. This trend is similar for both models. However, the region of intermittent flow regime for the Taitel-Dukler model is much smaller than that predicted by the Weisman et al. model.

At very low gravitational accelerations, i.e., $g/g_n = 10^{-5}$, Figure 5.4 shows that stratified flow will not exist, as predicted by both models. The Taitel-Dukler model predicts that essentially dispersed bubble and annular-mist flows will occur, whereas the Weisman et al. model predicts three flow regimes: intermittent, dispersed bubble, and annular-mist. For the Weisman et al. model: (i) AB is the transition line between intermittent and annular-mist flow, and (ii) BC is the transition line between dispersed bubble and annular-mist. ACD is the transition line between dispersed bubble and annular-mist for the Taitel-Dukler model. From this map it is clear that predictions by these two models differ considerably in the type, size, shape, and extent of the flow regimes at low g/g_n values.

Micro-Gravity Flow Regime Transitions: Vertical Flow

For vertical flow, Taitel et al. (1980) and Weisman and Kang (1981) have proposed theoretical and/or empirical correlations for various flow regime transitions. Both these models have used the same set of flow regime definitions, namely, bubble, intermittent (slug and churn), annular, and dispersed bubble. These flow transition equations have been used to generate flow pattern boundaries at micro-gravity levels, as presented in Figures 5.5 through 5.7.

These figures show typical flow regimes for an air-water system (25°C, 1 atm, 2.54 cm ID vertical pipe) for various values of g/g_n, namely, 1, 10^{-2}, 10^{-5}. Figure 5.5 shows the typical flow regime map predicted by the Taitel et al. and Weisman-Kang models at $g/g_n = 1$. The Weisman-Kang model transition predictions are represented by solid lines, those of the Taitel et al. model by broken lines. A comparison of these models reveals that these two models agree reasonably well at $g/g_n = 1$. Figure 5.6 shows the flow regime map at $g/g_n = 10^{-2}$. The boundaries between bubble and intermittent, bubble-intermittent and dispersed bubble, and intermittent and annular-mist flows all move toward lower superficial velocities of both phases as g/g_n is reduced. This trend is similar for both these models. However, the region of intermittent flow regime for the Taitel et al. model is much larger than that predicted by the Weisman-Kang model.

At low gravitational values, i.e., $g/g_n = 10^{-5}$, Figure 5.7 shows that bubble flow will not exist, as predicted by both models. The three flow regimes predicted by both models are intermittent, annular-mist, and dispersed bubble. The Taitel et al. model predicts that annular-mist flow would predominate for all values of large air

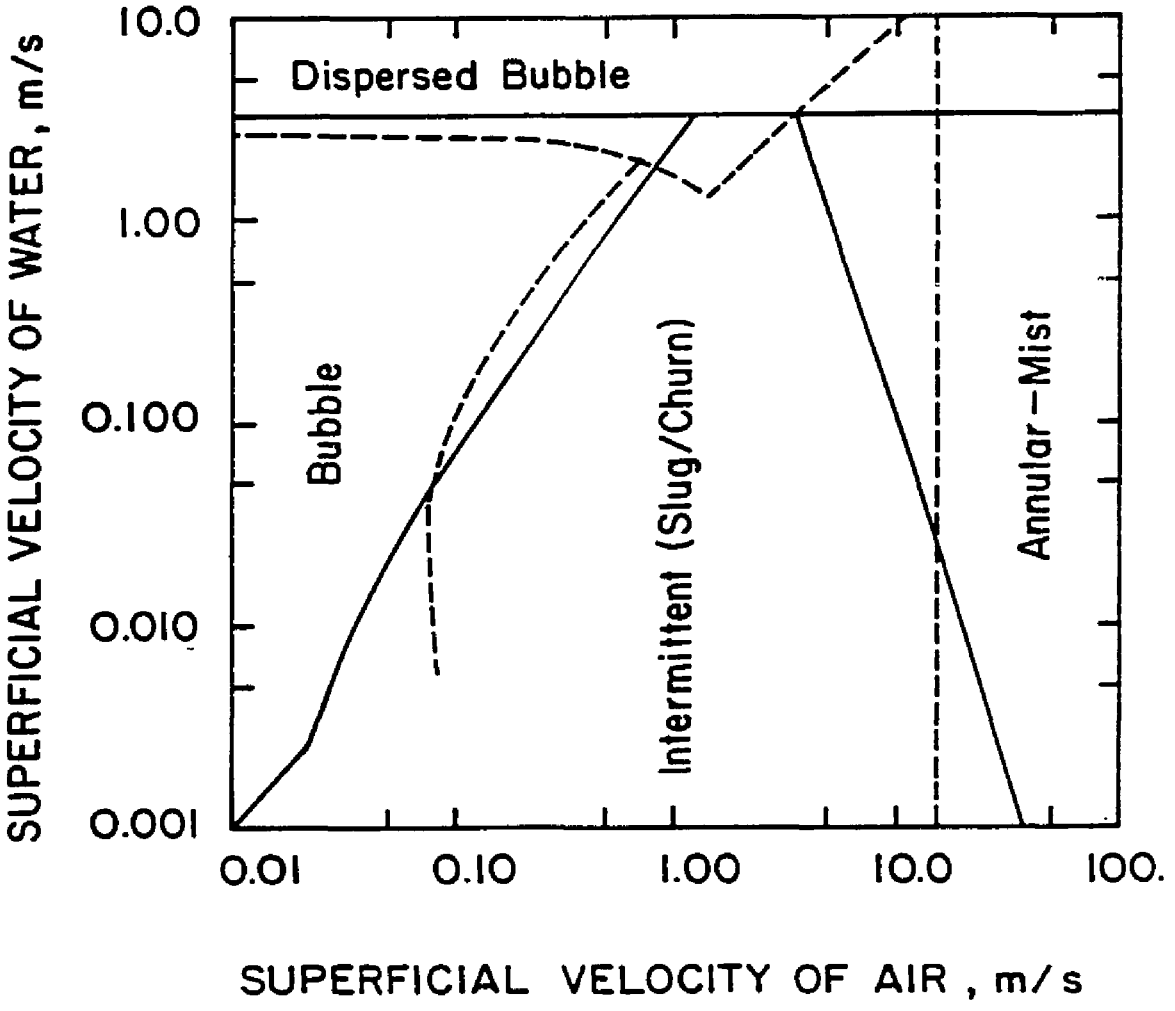

Figure 5.5: Vertical Air-Water Flow, 2.54 cm ID, 1 atm, 25°C, g/g_n = 1,- - -Taitel et al. Model,——Weisman-Kang Model.

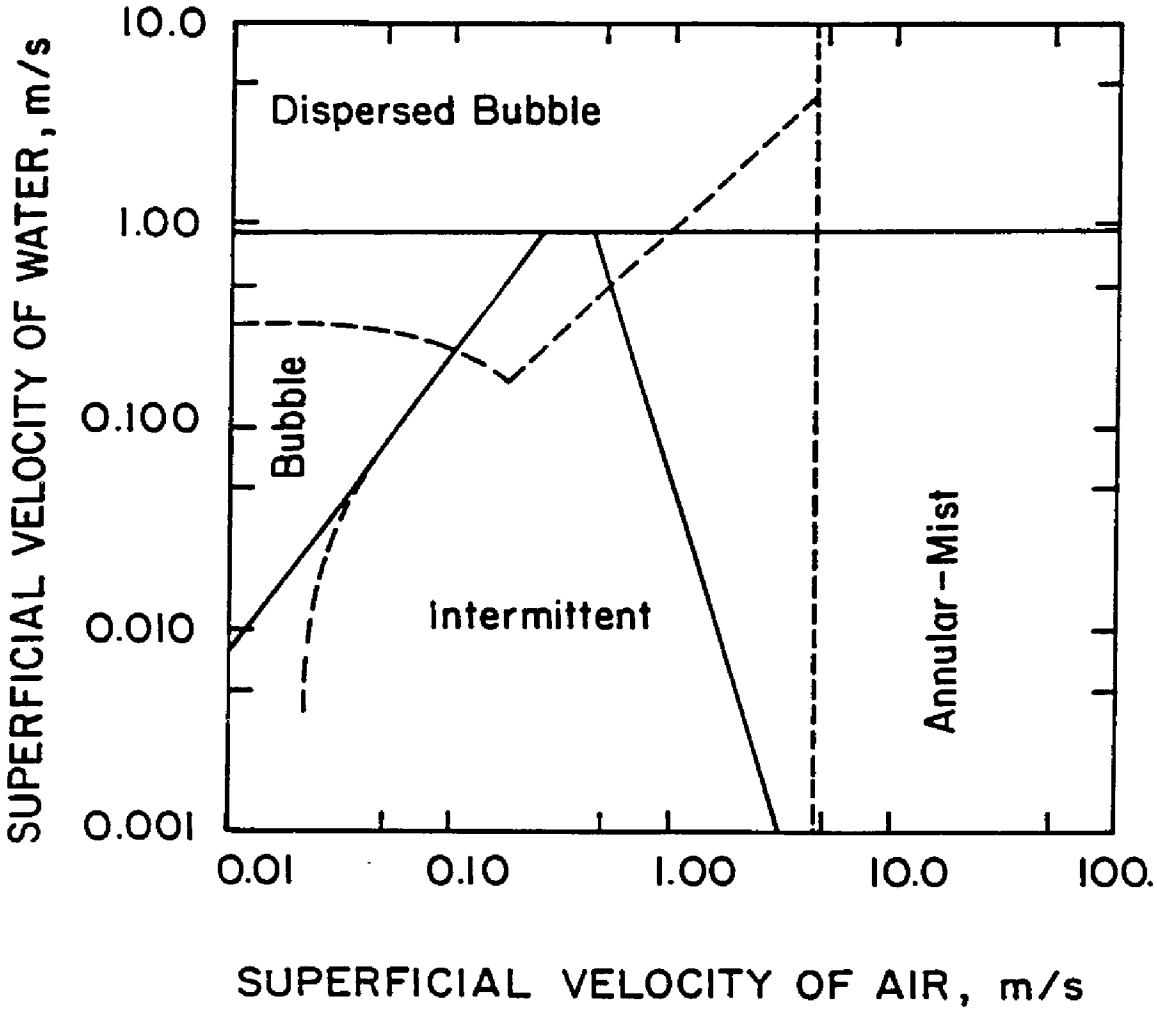

Figure 5.6: Vertical Air-Water Flow, 2.54 cm ID, 1 atm, 25°C, $g/g_n = 10^{-2}$,- - -Taitel et al. Model,——Weisman-Kang Model.

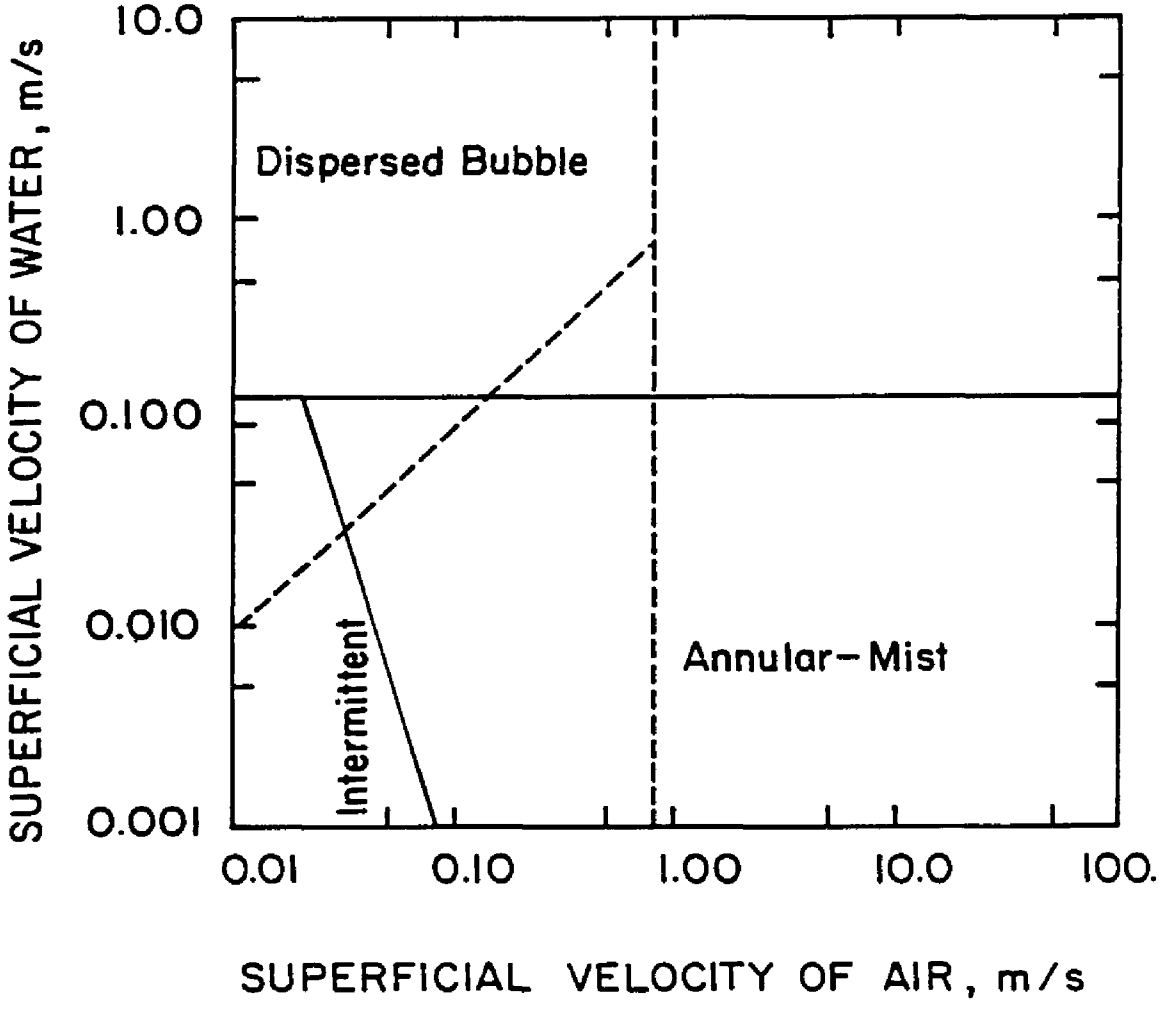

Figure 5.7: Vertical Air-Water Flow, 2.54 cm ID, 1 atm, 25°C, $g/g_n = 10^{-5}$,- - -Taitel et al. Model,——Weisman-Kang Model.

flow. The Weisman-Kang model predicts that dispersed bubble would occur for all values of large water flow. In the case of vertical flow, these two models differ considerably at low g/g_n values.

Comparison of Horizontal and Vertical Models

In the absence of gravity force, the orientation of the tube should not have an effect on a flow regime map, i.e., one would see the same flow regimes and their transition lines for both horizontal and vertical gas-liquid flow. Therefore, ideal horizontal and vertical models should reflect this phenomena.

A comparison of the Taitel-Dukler models for horizontal and vertical flow at $g/g_n = 10^{-5}$, Figures 5.4 and 5.7, respectively, reveals that two flow regimes (dispersed bubble and annular-mist) are predicted for horizontal and three regimes (intermittent, dispersed bubble, and annular-mist) for the vertical flow. It is also observed that the orientation of the transition line between dispersed bubble and annular-mist flow is different; this line has a positive slope in the case of horizontal and infinite slope in the case of vertical flow. The flow regime maps do not coincide for horizontal and vertical flow models.

Weisman et al. and Weisman-Kang have not proposed different flow regime transition correlations for horizontal and vertical flow, except for stratified to intermittent in the case of horizontal and bubble to intermittent for vertical flow. A comparison of flow regime maps at $g/g_n = 1$, Figures 5.2 and 5.5, shows that the horizontal stratified and intermittent flow regimes are replaced by the bubble and intermittent regimes in the case of vertical flow. The other

transitions are the same. At the reduced gravity of $g/g_n = 10^{-5}$ the flow regime maps, Figures 5.4 and 5.7, are almost identical. The stratified and bubble flow regimes for horizontal and vertical flow, respectively, move towards the region of very low phase velocities whereas positions of other flow regime transitions remain unchanged.

CONCLUSIONS AND SIGNIFICANCE

The four two-phase flow models namely, horizontal Taitel-Dukler (1976), horizontal Weisman et al. (1979), vertical Taitel et al. (1980), and vertical Weisman-Kang (1981), are analyzed. These models are extrapolated to micro-gravity levels for an air-water system. It is observed that both models predict similar flow regime maps at $g/g_n = 1$. However, as the g/g_n values are reduced from 1 to 10^{-5}, the predictions begin to differ in both horizontal and vertical flow, showing the greatest deviation at the low values of g/g_n. The results show that the dispersed bubble and annular-mist flow regimes dominate at reduced gravity fields for both horizontal and vertical flow. Stratified and intermittent flow regimes are restricted to lower air and water superficial velocities. While these four models, in general, predict similar flow regimes under micro-gravity, they differ considerably in calculating flow regime boundaries.

The results of this study provide an evaluation of models proposed by Taitel-Dukler and Weisman et al. under micro-gravity fields. The results strongly suggest the necessity of reliable vapor-liquid flow regime experimental data in low gravity environment to modify the existing models or develop new ones.

VI. Scientific Rationale for the Technique of Simulating Micro-Gravity Vapor-Liquid Flow

The term zero-gravity has been used to denote a situation more accurately defined as apparent weightlessness. This condition occurs during the purely gravitational motion of a body when the inertial forces of the body are exactly balanced by the forces due to its weight. To understand the physical conditions existing within such a body, the significance of the gravitational field and its relationship to accelerated motion must be reviewed (Congelliere et al., 1963).

Material bodies at rest or moving with uniform velocity, with respect to a fixed-reference system (i.e., stationary with respect to the Earth), experience body forces in proportion to their mass. These forces are uniformly distributed and influence every particle in the reference system; they are called a gravitational field. The acceleration produced by the field is termed the strength of the gravitational field, expressed in g's, where $g_n = 1$ g is the strength of the Earth's gravitational field at mean sea level, 45^o north latitude.

The gravitational field acts uniformly on all mass points of a body, tending to produce a uniform acceleration of each point in the body, but does not tend to cause relative movement between mass points. When a body is supported, it is done by applying forces along the boundaries of the body or system of mass points. The force acting on the internal mass points of a body are, thus, the result of the gravitational and mechanical/body forces transmitted through the body from the supporting structure. In liquids, forces are transmitted

through hydrostatic pressure; in solids, they are transmitted through stresses.

Thus, it is not the gravitational field which causes vapor/gas bubbles to rise in a liquid, but the gradient of pressure field within the fluid. This gradient is, in turn, a result of the support given to the liquid container to prevent its acceleration by the field. If the support of the container is removed (i.e., it is dropped), the hydrostatic pressure gradient within the fluid disappears and, because the vapor/gas within the bubble is accelerated at the same rate as the liquid surrounding the bubble and the walls of the container, there will be no forces tending to create relative movement between the bubble and the liquid or the container.

The foregoing discussion is an illustration of the fundamental postulate of Einstein's General Theory of Relativity, which states that it is impossible to distinguish between a uniform gravitational field and a uniformly accelerated coordinate system. The apparent gravitational field, $\bar{G}$, experienced by a body will be given by

$$\bar{G} = \bar{g} - \bar{a} \qquad 6.1$$

where $\bar{g}$ is the local gravitational field experienced by an unaccelerated coordinate system, and $\bar{a}$ is the acceleration of the body coordinates. (In this expression, $\bar{a}$ is positive in the direction of the field.)

When a liquid container and its contents are stationary, the system is said to be in a gravitational field of $g/g_n = 1$. Supporting the container so that it remains at rest in Earth coordinates, results in a hydrostatic pressure gradient which, in turn, causes the bubbles in the liquid to rise. If the container is

accelerated downward at 9.8 m/sec^2 by removing all support from it, the acceleration of the container will be

$$\bar{a} = \bar{g} \qquad 6.2$$

and the apparent gravitational field for the container and its contents will be

$$\bar{G} = 0 \qquad 6.3$$

Under these circumstances, the bubble will not move relative to the fluid or to the sides of the container. Satellites, ballistic missiles, and other objects which are not supported in relation to the Earth's coordinate system experience $\bar{G} = 0$, because they are in free fall and $\bar{a} = \bar{g}$.

Steady-Flow, Micro-g Vapor-Liquid Simulation

The advantages of a steady-state, terrestrial-laboratory, micro-g vapor-liquid simulation method are many. These are : (i) conventional instrumentation can be used, (ii) direct visual observation can be achieved, (iii) starting transients as well as steady state conditions can be studied due to virtually unlimited test duration time, (iv) unlimited equipment size (i.e., L/D ratio, etc.), and (v) reproducibility and close control for test conditions are easier to achieve which, in turn, results in reliable data with economy in time and equipment.

The steady-state, micro-g simulation method presented here has an unique approach for studying the flow patterns of vapor-liquid flow in space. The use of two immiscible liquids of equal density offers the possibility to eliminate the buoyancy forces (which is directly

proportional to density difference of the two fluids). This results in an equal vertical static pressure gradient in both fluids, so that no relative vertical movement of liquids in the stream can occur, for example, the liquid drop in the pool of second liquid experiences no forces tending to displace it. Considering a real vapor-liquid system in a micro-g field, the vapor bubble will not move relative to the fluid or to the sides of the container due to the absence of a hydrostatic pressure gradient, as discussed in the previous section. Therefore, this steady state, micro-g vapor-liquid simulation technique has, theoretically speaking, the equivalence of a gravitational field and an accelerated coordinate system, as discussed in the previous section.

Thus, the simulation of a micro-g environment for vapor-liquid flow is accomplished by the use of liquid/liquid systems. The two liquids used are immiscible and possess essentially equal densities. In simulating micro-g vapor-liquid flow, the fluid which is more viscous and more wettable represents the "liquid" phase and the second liquid (less viscous and less wettable with respect to tube surface), corresponds to the "vapor" phase. In order to maintain the similitude between the real micro-g vapor-liquid system and simulating liquid/liquid system, it is essential to match the following physical characteristics:

a. viscosity ratio

b. interfacial tension

c. relative wettability of liquids with respect to tube surface

VII. EXPERIMENTAL SET-UP AND PROCEDURE

The experimental set-up to study the simulated micro-g liquid-vapor flow regime transitions is shown in Figure 7.1. It consists of 6.4 m (21 feet) of 0.0254 m (1 inch) ID pyrex glass tube with two entrance ports for the introduction of two immiscible liquids. Hot and cold water lines are run to a storage tank (Feed 1) to allow for maintenance of a constant temperature water supply. Water is pumped from the constant temperature storage tank while the flow is controlled by hand valves and measured with Dwyer rotameters of appropriate range (2.1×10^{-6} to 2.2×10^{-4} m^3/s or 2 to 210 gph).

Various oils are used as the second liquid. The second liquid which is simulating the "liquid" phase in micro-g, is pumped from a 55 gallon drum (Feed 2) placed on its side on a weighing scale. Flow is controlled by hand valves and measured with rotameters of appropriate range. The temperature of the second liquid is kept constant at 25 $\pm$ 1°C by a combination of two methods. The 55 gallon drum is wrapped with a resistance tape heater which is turned on prior to conducting experiments if the temperature is below 25°C. It is observed that the viscous liquid heats up over a period of time, particularly at the low flow rates, due to continuous recirculation through the pump (heat due to viscous dissipation). For such cases, a countercurrent heat exchanger is installed in the bypass line to cool the viscous liquid and return it to the 55 gallon drum at the desired temperature of 25°C. The temperature of the viscous liquid passing through the bypass line can be monitored at all times and the flow rate of the heat exchanger's cold side fluid (water) is adjusted continually to

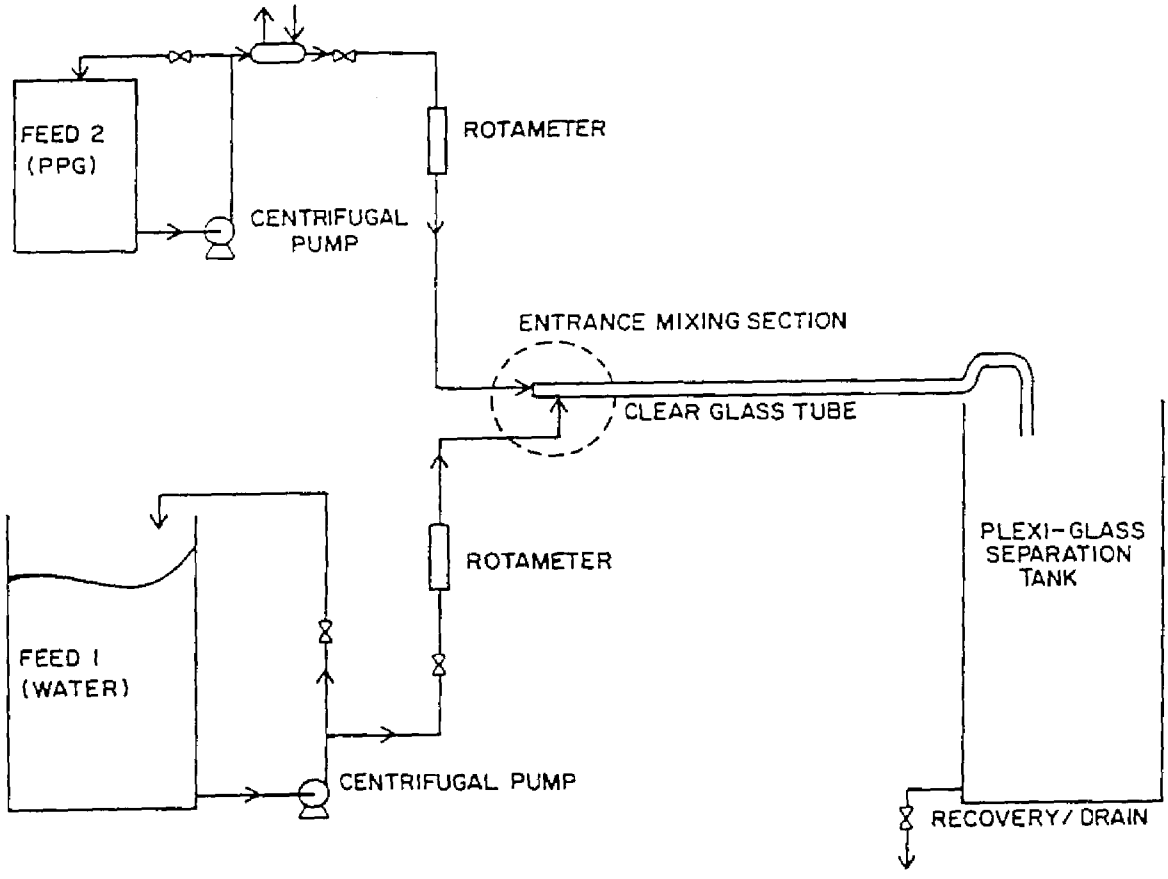

Figure 7.1 : Two-Phase Flow Experimental Set-Up.

maintain "liquid" phase temperature at 25 $\pm$ 1^{o}C throughout each experimental run. Two rotameters are installed in parallel for each liquid in order to cover the full range of flow rates. In addition, two manometers, one filled with carbon tetrachloride and the other filled with mercury, are placed in parallel to measure pressure drop across the two pressure taps located at each end of the glass tube. The connecting tubes are filled with water.

Visualization Section

The flow behavior/pattern is observed in a visualization section located approximately 75 diameters downstream of the entrance region to ensure a fully developed flow. Weisman et al. (1979) have found 60 diameters to be sufficient to attain fully developed flow over the full velocity range for a 0.0254 m I.D. horizontal system. In this study, it is found that the flow is fully developed at about 75 diameters downstream. This visualization section is fitted with a rectangular duct of plexi-glass filled with water. This arrangement reduces the optical distortions which are observed through the pyrex glass tube during the flow of the two immiscible liquids. The flow regimes/patterns are recorded on videotapes to allow for more in-depth off-line analysis (e.g., using slow motion and stop action) and to facilitate discussion with other researchers.

Separation Tank

The two immiscible liquids, after passing through the tube, discharge into a separation tank. Since the two liquids are of equal density, they form dispersions and therefore do not stratify. A small

amount of sodium chloride (regular salt) is added to this tank and mixed thoroughly to increase the density of water slightly above its normal value. The solubility of sodium chloride in the more viscous oily liquids is found to be negligible. After allowing approximately 12 hours for maximum recovery, water separates into a distinct layer visible through the side of the collection tank. The water is then discharged into the drainage and the top layer of viscous liquid is pumped off for recovery. The viscous liquid is heated to 120°C to evaporate off any water which may be present and to break the emulsion which sometimes forms at the higher flow rates. After cooling the liquid, the viscosity, specific gravity, and interfacial tension are measured prior to returning the recovered liquid to the 55 gallon drum for reuse. By this arrangement, approximately 90% of the viscous liquid is recovered. This is a time consuming operation, requiring approximately twelve hours to recover 30 gallons of the liquid, enough to complete one experimental run.

Measurement of Physical Properties

In simulating micro-g vapor-liquid flow, the physical properties of the two liquids of equal density need to be considered carefully to have similitude between real and simulating systems. The physical properties important to the analysis are : density, viscosity, and interfacial tension. The measurement techniques for these properties are discussed as follows:

Density - Since this property is so important to this project, the density of the liquids is measured carefully using a specific gravity bottle in a temperature controlled environment.

Viscosity - A spindle-type viscometer supplied by Brookfield Laboratories, MA is used in conjunction with a eight grams sample adaptor. The adaptor is provided with a water jacket, connected to a hot bath to maintain the sample at a desired temperature.

Interfacial Tension - In the absence of a gravity force, interfacial forces play an important role, especially in the low velocity region, in determining the flow regimes/patterns of vapor-liquid flow. A new method has been developed to measure the interfacial tension. The basic principle and the details of the apparatus and procedure are presented in the following chapter.

VIII. MEASUREMENT OF INTERFACIAL TENSION OF IMMISCIBLE LIQUIDS OF EQUAL DENSITY

The use of two immiscible liquids of equal density offers the possibility of eliminating the buoyancy forces and thus simulating micro-gravity environment on earth. This technique can be used to study micro-gravity fluid physics such as: 1) interfacial tension driven flows (Marangoni effect) on earth, e.g., drop migration in a liquid matrix with temperature gradient, and 2) two-phase (vapor-liquid) flow regimes (Karri and Mathur, 1987 & 1988) likely to occur in micro-gravity.

For the study of micro-gravity fluid physics, one of the most important liquid properties is the interfacial tension. In the absence of gravity force, interfacial forces play an important role in determining the thermocapillary flows driven by a temperature gradient and type of flow regimes in the case of two-phase flow. In order to use this technique, it is essential to know the interfacial tension between two immiscible liquids of equal density. The measurement of interfacial tension in such liquid systems is quite complex because of the absence of a liquid density difference. The equations used in the traditional interfacial tension measurement techniques such as capillary height method (Reynolds, 1921), ring method (Zuidema and Waters, 1941), and drop weight method (Harkins and Humphrey, 1916), contain a density difference term and, therefore, become invalid as the density difference approaches zero. In short, since two equally dense liquids forming an interface represent a relatively buoyancy free situation, these classical measurement techniques cannot be used,

as they use the resultant gravity force at the interface giving rise to a density difference term in the final expression.

A new approach which was originally developed by Bartell and Miller (1928) to measure the interfacial tension between two liquids of equal density is used in our experiments. They used this method to measure the interfacial tension of dark liquids with water since they were unable to observe a falling drop in the dark liquid as required with the drop weight method, or to delineate the meniscus once the capillary was wetted with the dark liquid as in the capillary rise method.

THEORY

A number of textbooks have discussed various methods which have been used for interfacial tension measurement. The most commonly used techniques are capillary rise, drop weight, and ring method. However, these traditional interfacial tension measurement techniques can not be used for systems of equal density liquids. Some of the interfacial tension measurement techniques and their analysis are briefly discussed below.

Capillary Rise Method: The capillary rise method has been used with several modifications by Reynolds (1921) and others. When the two liquids are in equilibrium inside a capillary, the interfacial and buoyancy forces can be equated to give an expression for interfacial tension, γ_{ab}:

$$\gamma_{ab} = 1/2\ rhg(\rho_a - \rho_b) \qquad 8.1$$

where r = capillary radius, h = total height of liquid rise in the capillary, ρ = density of liquid, and subscripts a and b refer to

liquid 'a' and liquid 'b', respectively.

Drop Weight Method: The drop weight method described by Harkins and Humphrey (1916), uses the size of a drop of liquid 'a' suspended in a liquid 'b' before falling (as opposed to height of liquid rise in the capillary rise method) as a measure of interfacial tension. A force balance on the drop leads to the correlation:

$$\gamma_{ab} = [V(\rho_a - \rho_b)g/r]F \qquad 8.2$$

where V = volume of the suspended drop at the point of breakaway, and F = correction factor, used since actual drop that falls is only a fraction of the drop that forms; this is a function of density for which standard tables are available.

Both the capillary rise and the drop weight methods require a $(\rho_a - \rho_b)$ term for calculation of γ_{ab} and, therefore, are not valid for determining interfacial tension between two liquids of equal density. The same reasoning applies to ring-method (Zuidema and Waters, 1941) and it can not be used for measuring interfacial tension of equal density liquids. In short, since two equally dense liquids forming an interface represent a relatively gravity free situation, these classical measurement techniques cannot be used, as they use the resultant gravity force at the interface giving rise to a density difference term in the final expression.

Principle of the new method: The simple device shown in Figure 8.1 is based on the capillary rise principle (Karri and Mathur, 1988). The apparatus consists of two cups, A and B, connected by a U-shaped tube, one leg of which is a capillary tube. Liquid 'b' is added to the cup B until it reaches the end of the U-tube at the

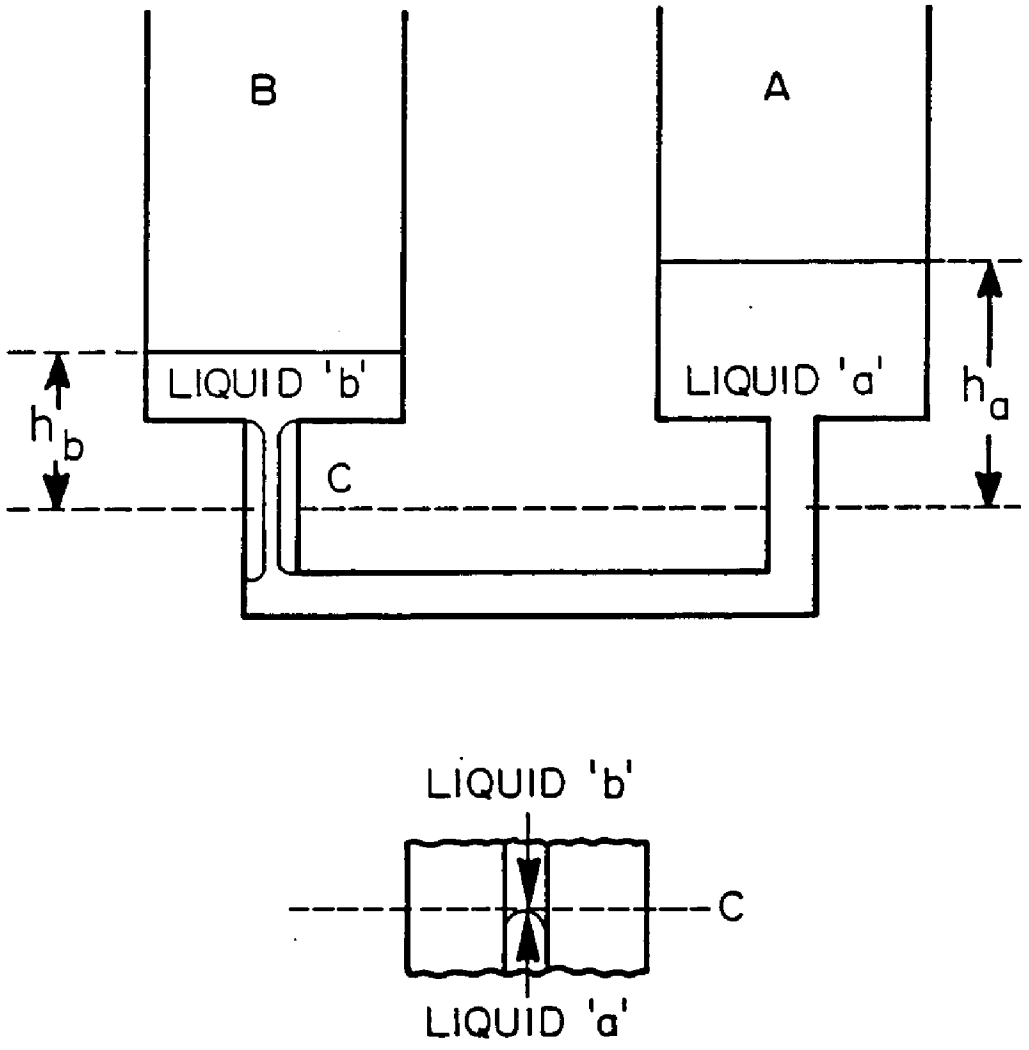

Figure 8.1: Apparatus for Interfacial Tension Measurement of Equal Density Fluids.

bottom of cup A. Liquid 'a' is, then, added slowly from a buret to cup A, so that liquid 'b' is forced back until the liquid meniscus enters the lower end of the capillary and finally stabilizes at some reference point 'C'. The heights h_a and h_b of liquid 'a' and liquid 'b', respectively, above this reference point or meniscus, are measured using a cathetometer. The forces acting on the meniscus are:

gravity force :

$$F_g = \pi r^2[\rho_a h_a - \rho_b h_b]g \qquad 8.3$$

where r = capillary radius, and ρ the corresponding densities (F_g is acting in the downward direction)

vertical force due to the interfacial tension :

$$F_{int} = 2\pi r\gamma_{ab} \qquad 8.4$$

Equating equations 8.3 and 8.4 for mechanical equilibrium-condition at the meniscus, one obtains:

$$\gamma_{ab} = 1/2\ gr\ [\rho_a h_a - \rho_b h_b] \qquad 8.5$$

It is noteworthy that the term $(\rho_a h_a - \rho_b h_b)$, which contains the difference between the products of corresponding density and height, does not approach zero even for equal density liquids. This method is general and therefore can be used to measure the interfacial tension of any combination of two immiscible liquids irrespective of their densities.

APPARATUS AND MEASUREMENT

The apparatus as shown in Figure 8.1, is constructed with pyrex-glass. The two cups, A and B, are about 0.022 m ID and 0.12 m in height. These are connected by a U-type glass tubing, one arm of which is a capillary tube of approximately 0.75 mm, radius. The diameter of the capillary is determined from the weight difference between capillary tube when filled with mercury and when empty.

For constant temperature conditions, the apparatus is immersed in a constant temperature water bath with plane glass sides for visibility and recording. For the determination of interfacial tension, liquid 'b' (organic liquid or oil) is slowly added to cup B until it fills just below the top of the U-tube in the bottom of cup A. It is important to ascertain that there are no air-bubbles caught along the wall of the U-tube including capillary. Liquid 'a' (water) is then slowly added from a buret to cup A until the meniscus or interface is forced downward along the U-tube and stabilizes in the capillary at some reference point 'C'. The height of each liquid above this reference point is then readily measured by means of a cathetometer.

The density of the liquid 'b' is measured using a specific gravity bottle. Knowing the densities and heights, the interfacial tension can readily be calculated using equation 8.5.

EXPERIMENTAL RESULTS

Several liquid systems of unequal densities with known interfacial tension are used for calibration of this apparatus. The results are presented in Table 8.1. The results are within acceptable

accuracy. The chemicals used are of analytical grade purity. The use of high purity chemicals may have reduced the percent error. For ordinary accuracy requirements, no capillary corrections for meniscus height readings are necessary, as indicated by Bartell and Miller (1928).

TABLE 8.1: Interfacial Tension of Various Systems of Unequal Densities at 25°C

System	Density of Organic Liquid (kg/m^3)	Interfacial Tension (N/m)		%Error
		Measured	Literature	
Aniline : Water	1022	0.00541	0.00577	-6.3
Benzaldehyde : Water	1050	0.01478	0.01551	-4.7
Carbon Tetra-chloride : Water	1583	0.0443	0.045	-1.6

This apparatus has been used to measure the interfacial tension of eleven different systems of approximately equal densities. Water is used as liquid 'a' throughout these experiments. Liquids 'b' used in these experiments are either pure organic liquids or oils. In case of heavy mineral oil and silicone oil, a small amount of carbon tetrachloride is added to adjust the density. All 'b' liquids have densities almost equal to that of water. The temperature of the apparatus is maintained at 25°C. The apparatus is cleaned with acetone followed by washing with NOCHROMIX solution. The washed apparatus is rinsed with distilled water and dried overnight at about 110°C. Table 8.2 presents the experimental results for eleven

TABLE 8.2: Interfacial Tension of Various Systems of Equal Densities at 25°C

System	Density of Organic Liquid/Oil (kg/m^3)	Interfacial Tension (N/m)
Amyl Benzoate : Water	988	0.033
Anisole : Water	993	0.035
Benzonitrile : Water	1002	0.028
Butyl Benzoate : Water	1002	0.034
Diethyl Adipate : Water	1004	0.018
Diethyl Dimethyl-malonate : Water	1018	0.019
n,n-Diethyl-1-Naphthyl Amine : Water	1075	0.016
3-Phenyl-1-Propanol : Water	998	$\sim$0
Poly Propylene Glycol-2000 : Water	1003	0.005
Heavy Mineral Oil(+CCl_4) : Water	998	0.031
Silicone Oil (+CCl_4) : Water	998	0.047

different liquid systems. Densities and interfacial tensions are also listed.

The liquid systems are so selected that the measured interfacial tension would cover a wide range of values. In the case of 3-phenyl-1-propanol and water system, the densities are almost equal and the measured heights are about the same, giving an interfacial tension of about 0 N/m. The highest interfacial tension of about 0.047 N/m (47 dynes/cm), is obtained for the liquid system of Dow Corning 200 silicone fluid (50 cSt at 25°C) (+CCl_4) and water. The apparatus is sensitive enough to measure interfacial tension ranging from 0 to 0.05 N/m. From Table 1, the accuracy of this method is within ±6% for liquids of unequal densities. Since the interfacial tension of liquid systems of equal density is unknown, it is anticipated that the accuracy of this instrument would be within ±10%.

This device can be used to measure the interfacial tension as a function of temperature for two liquids exhibiting equal or unequal density. This can be achieved by immersing the apparatus in a constant temperature water bath, maintaining the temperature at any desired value.

This apparatus was used for measuring the interfacial tension of the various fluid systems used in this study. The development of this tensiometer is considered as one of the major contributions of this project.

IX. SELECTION OF ENTRANCE CONFIGURATION AND CRITERIA FOR EXPERIMENTAL PARAMETERS

Simulation of micro-g vapor-liquid (two-phase) flow is accomplished by the selection and use of unique test fluids. The two fluids (fluid system #1) chosen for this study are water and polypropylene glycol-2000 (PPG), which are immiscible and possess essentially equal densities. In simulating micro-g two-phase flow, the PPG, more viscous liquid represents the "liquid" phase and the water (less viscous) although a liquid as well at test conditions, corresponds to the "vapor" phase.

In this section, the effects of entrance configuration on flow regimes and the fluid system #1 flow regime map are presented. The limitations of this system in simulating micro-g vapor-liquid flow are discussed. Finally, the criteria for selection of parameters such as viscosity ratio, interfacial tension, and relative wettability of the equi-density fluid systems are also discussed. These parameters are critical in matching simulated flow characteristics with the actual micro-g vapor-liquid flow patterns.

Entrance Effects

There is, at present, a considerable understanding of two-phase (vapor-liquid) flow on earth. It is known that entrance configurations have little effect on two-phase flow behavior under normal gravity. Gravity tends to stabilize the flow and creates a stratified flow pattern and thus minimizes the entrance effects. However, entrance configurations could have pronounced effect on flow

pattern in the absence of gravity. In order to study these effects, experiments with different entrance mixing configurations are conducted. The designs of these configurations are shown in Figures 9.1 through 9.3. In all these configurations, one fluid is dispersed into the other in order to achieve mixing at the entrance. The subsequent flow regime patterns are observed 120 diameters down the tube to study the flow behavior.

The observed flow regimes are defined as given in Table 4.2. The flow regimes observed for two-phase flow namely polypropylene glycol (PPG)-water for all entrance configurations are presented in Table 9.1. All the experiments are conducted using a constant water ("vapor") flow rate of 3.785 liters/min. (1 gpm). The flow regime pattern and pressure drop data are recorded for an increase in PPG ("liquid") flow rates from 0.01 to 0.36 m/s (based on total cross-sectional area of the tube). At first glance, data in Table 9.1 for various configurations do not indicate any definite order. However, despite the changes caused by entrance conditions, a pattern of flow regimes emerges. Moving vertically top to bottom in each column (increasing "liquid" flow rates) the results show a general trend beginning with drop flow, then inverse slug, and finally inverse annular flow. Pressure drops were measured using an inclined manometer filled with carbon tetrachloride. The data are presented in Table 9.1 in inches of water. Pressure drop increases with PPG flow rate as expected.

One-Nozzle Configuration (see Figure 9.1): Configuration 1(a) in which "vapor" is introduced through a nozzle and "liquid" flows through annulus is shown in Figure 9.1(a). The nozzle is designed

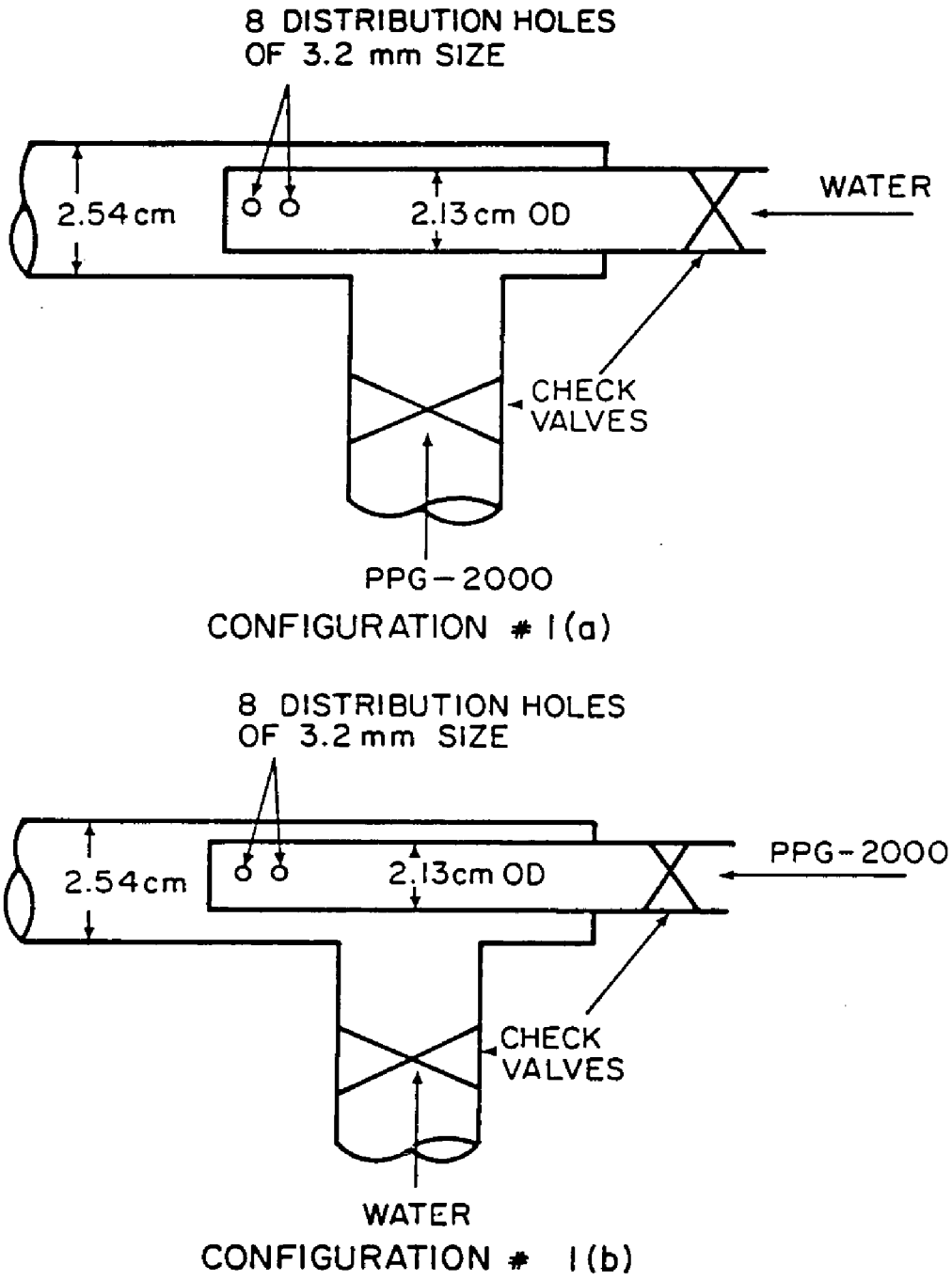

Figure 9.1: One-Nozzle Configuration.

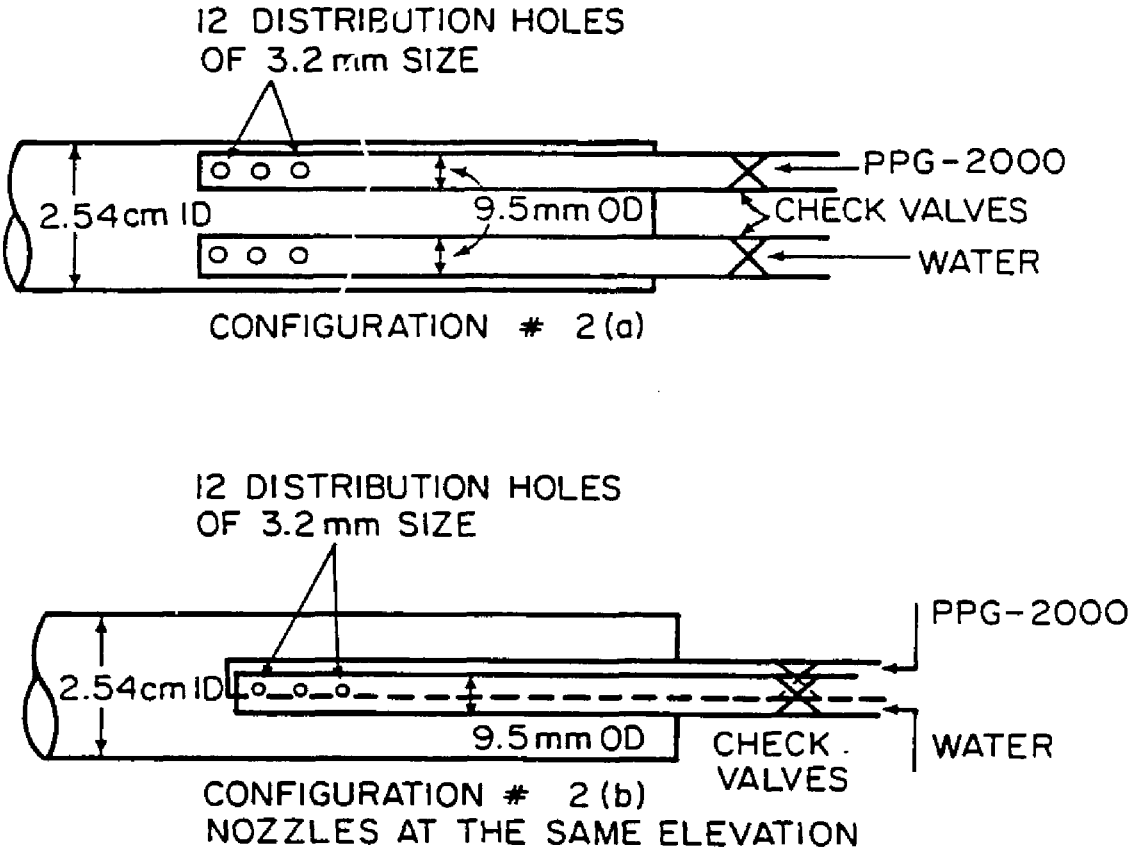

Figure 9.2: Two-Nozzle Configuration.

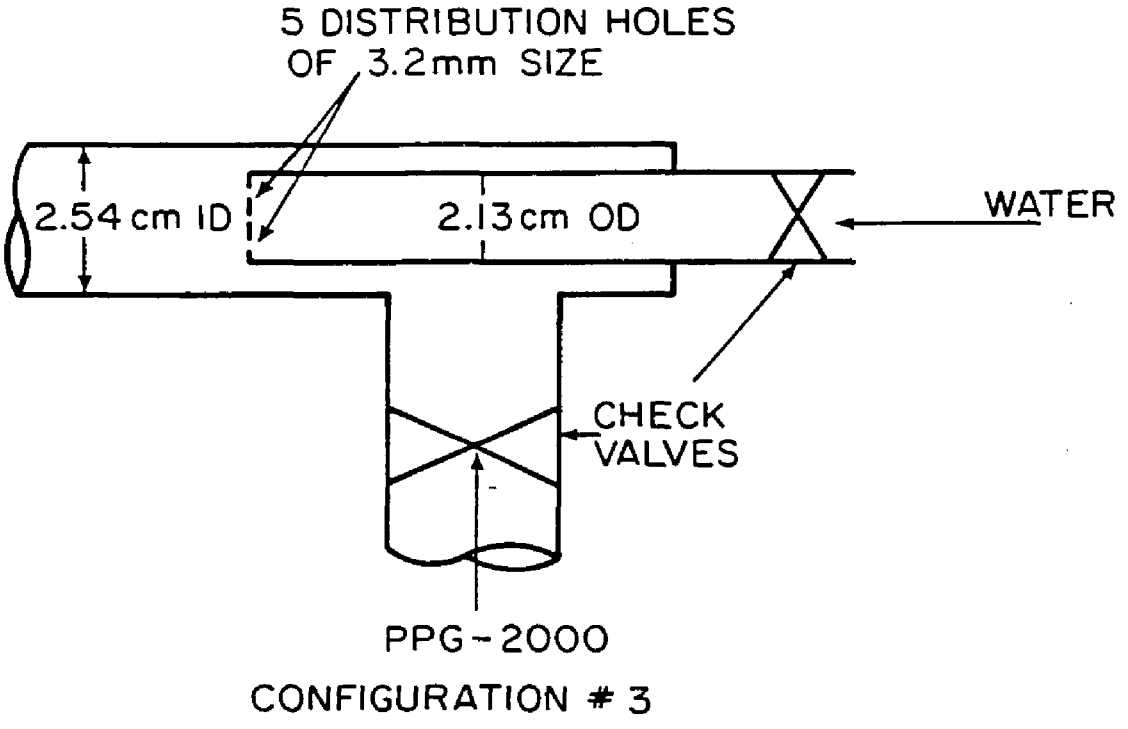

Figure 9.3: One-Orifice Type Nozzle Configuration.

Table 9.1: Entrance Effects : Flow Regime Data

Constant Water Flow Rate = 3.785 m^3/min. (0.12 m/s)

Flow Rate of PPG (m/s)	Configurations				
	# 1(a)	# 1(b)	# 2(a)	# 2(b)	# 3
0.01	D (0.3)	D (0.3)	D (0.46)	D (0.43)	D (0.36)
0.0396	D (0.44)	D (0.59)	D (0.54)	D (0.619)	D (0.49)
0.0821	IS (0.53)	IS (0.65)	IS (0.75)	IS (0.75)	D (0.69)
0.1342	IA (0.74)	IS (1.13)	IS (0.97)	IS (1.2)	D (0.93)
0.2087	IA (1.01)	IS (1.37)	IA (1.78)	IA (1.79)	IS (1.18)
0.2834	IA (1.25)	--	--	--	IA (1.31)
0.3579	IA (1.72)	--	--	--	IA (2.08)

Note: Numbers in parenthesis give pressure drop across 5.56 m long tube in inches of water. D - drop/mist, IS - inverse slug, IA - inverse annular.

such that the fluid is dispersed through eight holes of 3.2 mm size on the side of a 2.13 cm OD PVC tube. The front end of the nozzle is closed. The configuration 1(b) is the same as 1(a) in all respects except that the flow of "vapor" and "liquid" are interchanged.

A comparison of data for configurations 1(a) and 1(b) (Table 9.1) shows that the transition from drop flow to inverse slug is not effected by entrance conditions and occurs at a "liquid" flow rate of 0.08 m/s. However, an earlier transition to inverse annular is quite pronounced in the case of configuration 1(a) compared to 1(b). The region for which inverse slug occurs broadens for configuration 1(b). This region is observed for a range of flow rates of "liquid" between 0.08 to 0.21 m/s. Pressure drop for configuration 1(a) is less than that of 1(b) for all flow rates of "liquid".

Two-Nozzle Configuration (see Figure 9.2): Each of these two nozzles is designed the same way as described under one-nozzle configuration. In configuration 2(a) the two nozzles are positioned such that one is below the other, whereas in configuration 2(b) two nozzles are placed horizontally at the same level. As one would expect, the flow regime patterns and pressure drops are about the same for both configurations 2(a) & 2(b).

Comparing data for configurations 1(a) and 2(a), the transition from drop flow to inverse slug remains at the same flow rate of "liquid" at 0.082 m/s. Transition from inverse slug to inverse annular shifts to higher flow rate of "liquid" (0.21 m/s) for configuration 2(a). Pressure drop for configuration 2(a) is higher than that of 1(a) for all flow rates.

One-Orifice Type Nozzle Configuration (see Figure 9.3): An orifice type nozzle has been fabricated by soldering an aluminum orifice plate having five holes of 3.2 mm size at the end of the 2.13 cm OD aluminum tube. Water enters through the nozzle and "liquid" flows through the annulus. It has been observed that in this configuration the transition from drop flow to inverse slug shifts to higher flow rate of "liquid" at 0.21 m/s (Table 9.1). Inverse annular flow occurs only at high flow rates of "liquid" (0.28 m/s) as compared with that "liquid" flow rate of 0.13 m/s for configuration 1(a). Pressure drops are comparable in both cases.

It is concluded that entrance configurations under micro-gravity conditions do have an effect on flow rates of "liquid" at which transitions from one flow regime to other occurs. However, it doesn't effect the sequence of flow regime patterns. Without the gravity effect to act as an stabilizing force, flow regime transitions are sensitive to entrance configurations in the immediate area of the nozzles. Thus, the design of entrance configuration in heat transfer loops may be one of the factors to control a specific flow regime. For example, inverse annular flow might enhance the vapor condensation. Therefore one would design entrance configuration like 1(a) so that inverse annular flow would occur for a wide range of flow rates of "liquid" (0.13 to 0.36 m/s).

The range of velocities of "liquid" for which inverse slug flow regime occur appear to be strongly influenced by the entrance configurations. Because little is known about these flow regimes on earth, their presence in a spacecraft heat transfer system could be considered undesirable. Heat exchanger performance can be

characterized by significant pressure fluctuations in the fluid and by variations of the stress levels within the tube walls, the latter as a result of local temperature changes. Proper selection of the entrance configuration may be a satisfactory approach to control the flow regimes, thus improving the heat exchanger performance.

Flow Regime Map - Fluid System #1

The object is to observe the flow behavior of PPG with water over a wide range of flow rates in a tube and to obtain pressure drop data for various flow patterns observed. Flow patterns are observed over a range of PPG superficial velocity from 0.01 to 0.5 m/s and a range of water superficial velocity from 0.01 to 0.5 m/s. One-nozzle configuration #1(a) is used to introduce the liquids into the pipe. The physical properties of PPG are measured and the values at 25°C are given as:

$$\text{Viscosity} = 310 \text{ cP}$$

$$\text{Density} = 1005 \text{ kg/m}^3$$

Interfacial tension between PPG and water = 0.005 N/m. Wettability of water on pyrex glass is more than that of PPG.

A series of flow patterns are observed for an increase in the "liquid" flow rate at a constant "vapor" flow rate. The observed flow patterns are classified into corresponding regimes based on the definitions presented in Table 4.2.

Experimentally observed vapor-liquid flow pattern maps for horizontal flow are shown in Figure 9.4. Data is presented on log-log plot with superficial "vapor" velocity, U_{Gs} versus superficial "liquid" velocity, U_{ls} as a coordinate system. A key

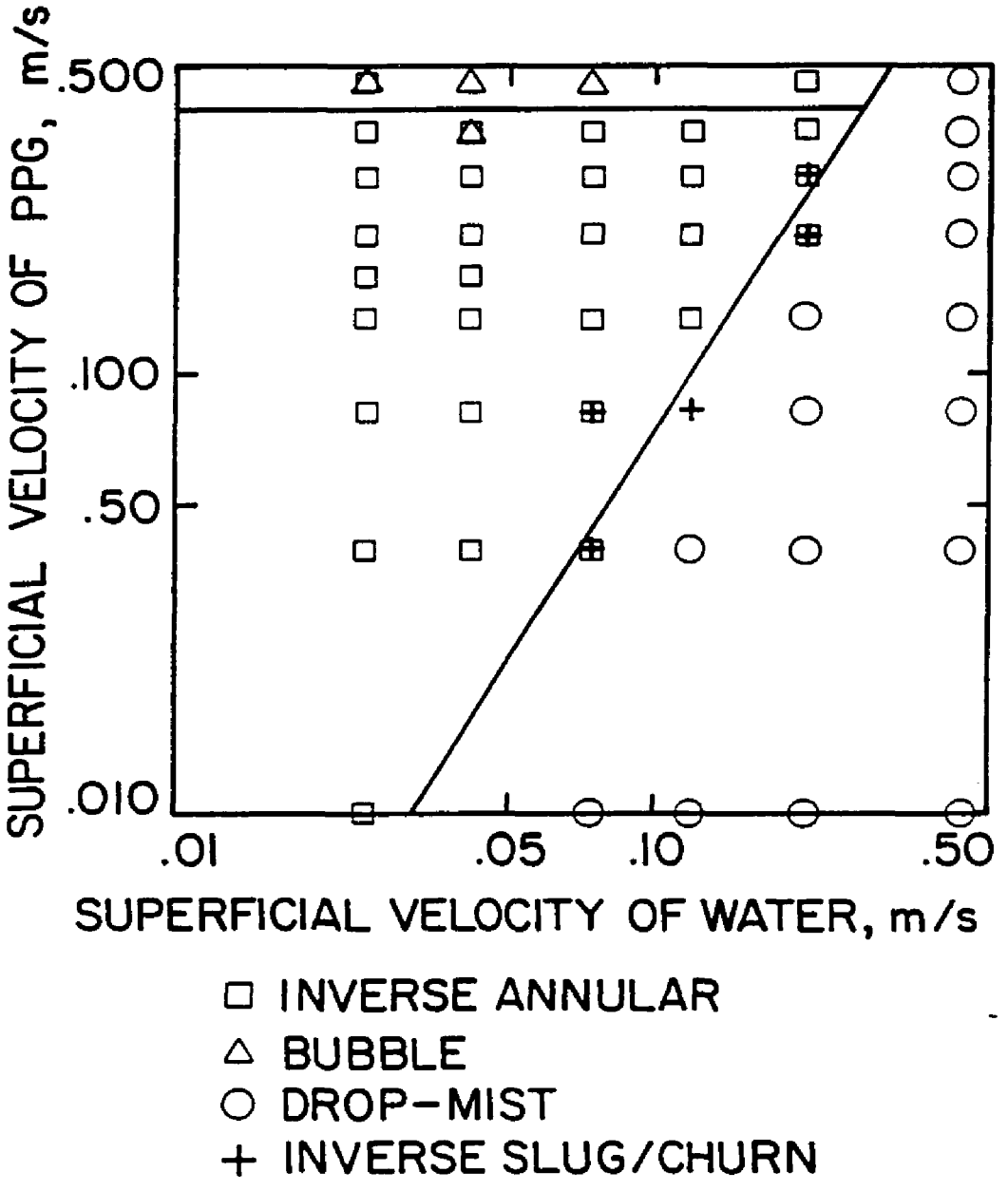

Figure 9.4: Simulated Micro-g Vapor-Liquid Flow Regime Map - Fluid System #1 (Equi-Density PPG and water).

shows the flow regimes indicated by the various symbols. The lines (fitted by visual observation) are drawn between the various flow regime data as obtained in this study. The change from one regime to another is not always well defined, however, the lines represent the gradual transitions.

The effect on the flow pattern of increasing the "liquid" velocity at a relatively low "vapor" velocity of 0.025 m/s can be seen in Figure 9.4. At low "liquid" velocities both phases are continuous and stratified wavy. However, a thin layer of "vapor" along the tube circumference is observed even at these low velocities and therefore the flow regime is classified as an inverse annular flow. An increase in "liquid" velocity to about 0.2 m/s causes the "liquid" phase to occupy central core and the "vapor" phase flows as an annular layer near the pipe wall. Both phases are still continuous. This is characteristic of inverse annular. A further increase in "liquid" velocity at a "vapor" velocity of 0.025 m/s results in the "vapor" phase becoming discontinuous and forms bubbles. This is a typical of bubble or dispersed bubble flow.

The effect on the flow pattern of increasing "liquid" velocity at the relatively moderate "vapor" velocity of 0.12 m/s shows similar flow behavior. However, at low "liquid" velocities the "liquid" drops in continuous "vapor" phase are observed. As the "liquid" velocity increases from 0.04 to 0.13 m/s, the flow pattern changes from drop to inverse annular flow through an intermediate regime, inverse slug at 0.08 m/s of "liquid" velocity.

The effect on the flow pattern of increasing "liquid" velocity at

a higher "vapor" velocity of 0.44 m/s is quite different. For all "liquid" velocities, a drop or mist flow is observed.

For a wide range of "liquid" and up to a moderate range of "vapor" velocities, the flow pattern leads to the formation of inverse annular flow. In general, as the "vapor" flow rate is increased for a definite low "liquid" velocity, the "liquid" surface is observed to pass successively from ripple waves to roll waves. At high "vapor" velocities "liquid" droplets are detached from the interface giving drop flow. A further increase in vapor velocities, causes the flow to become completely drop or mist in nature. At high "vapor" velocities the central "liquid" core breaks up to give a drop or mist flow condition. At high initial "liquid" flows, bubble flow is observed; and as the "vapor" velocity is increased the drop or mist flow condition is developed. Inverse slug flow is observed only during the transition from inverse annular to a drop flow regime.

Charles et. al. (1961) are the first ones to study the flow regimes of equal density oil-water systems. For an oil-water flow system in a 2.54 cm horizontal tube (3.05 m long), and using oils with viscosities of 6.3 and 16.8 cP and a density of 998 kg/m^3, they prepared flow regime maps with superficial water and oil velocities as parameters. In all these systems, water is more wettable with the tube surface than the oils. They considered a range of superficial oil velocities of 0.015 - 0.9 m/s and a range of superficial water velocities of 0.03 - 1.07 m/s. The flow patterns observed in their study are reinterpreted to fall into our classification Table 4.2 for simulation of micro-g vapor-liquid flow. These are:

water drops in oil - bubble flow

oil in water concentric - inverse annular flow

oil slugs in water - inverse slug flow

oil bubble/drops in water - drop or mist flow

Their data are converted to SI units and the transition lines between reinterpreted flow patterns are shown in Figure 9.5 with superficial velocities as coordinate system. The positions of the transition lines between inverse annular to inverse slug and inverse slug to drop flow observed for two different oils of different viscosities were identical. Figure 9.5 also show that the transition line to bubble flow (shown by broken lines) for the 16.8 cP oil is at a somewhat higher oil velocity than for the 6.3 cP oil.

Comparison of Figures 9.4 and 9.5 shows that the similar flow regimes are observed in both the studies except there is no definite region of inverse slug in the case of fluid system #1. As shown in the entrance effects section, the entrance configuration has considerable effect on the occurrence of inverse slug. Charles et al. (1961) have used a concentric nozzle in which oil was introduced inside a water annulus and have found definite region of inverse slug. When configuration # 1(a) was used in which water was introduced through a tube with holes on its side and PPG through annulus, the inverse slug region was not observed. Figure 9.5 shows that the transition line between inverse annular and bubble flow has a positive slope and this slope decreases as viscosity of oil goes up. Figure 9.4 shows that this transition line has a slope of about zero and is located at a oil velocity of 0.4 m/s. This is consistent with the trend shown in Figure 9.5. The transition line from inverse annular

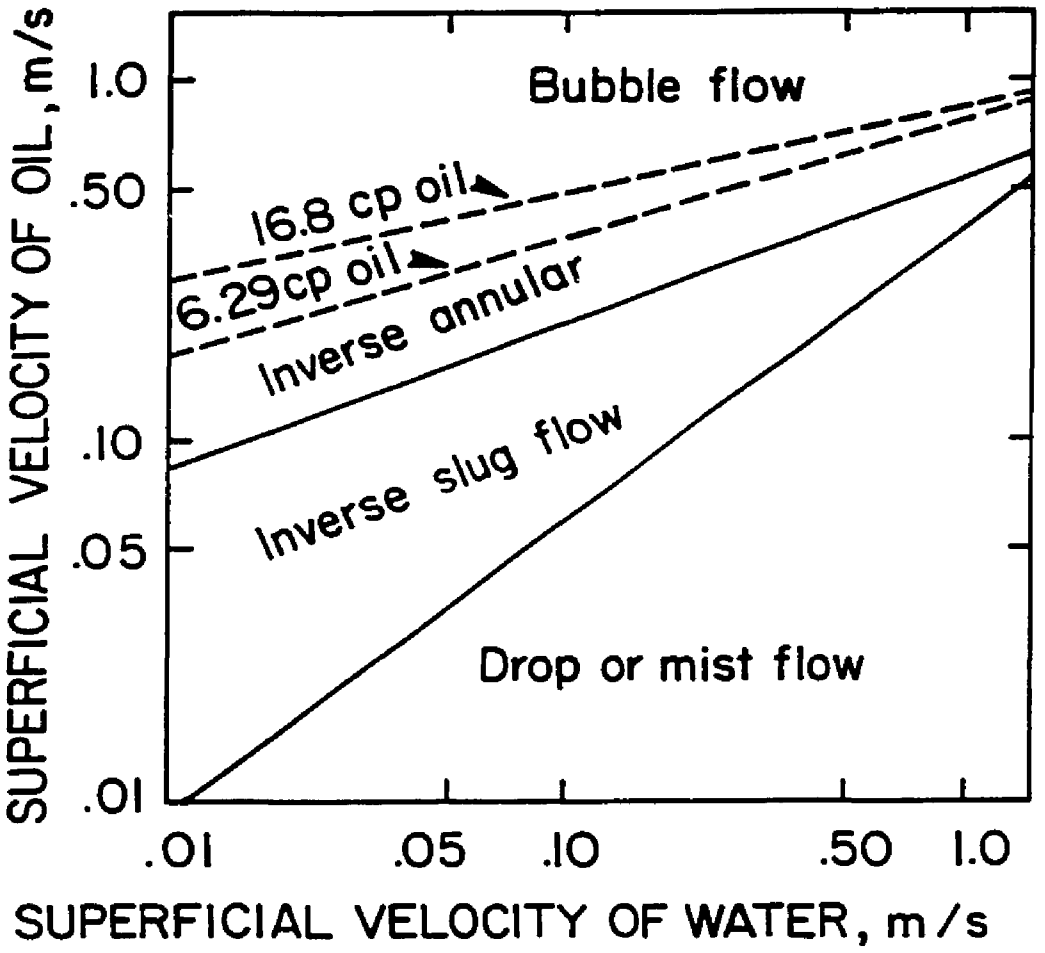

Figure 9.5: Charles et al. (1961) Flow Regime Map for Equi-Density Oil-Water Flow (Oils of Viscosities 6.29 and 16.8 cP).

flow to drop flow have positive slopes in both the Figures 9.4 and 9.5. In conclusion, the flow regimes observed for a two immiscible liquids of equal density fluid system in which less viscous fluid (water) is more wettable with the tube surface than the high viscous fluid (oils), are bubble, inverse annular, inverse slug, and drop or mist flows.

These equi-density fluid experiments are an attempt to simulate micro-g vapor-liquid flow to determine what flow regimes and their transitions will exist in micro-g environment. The objective of this study is to control experimental parameters in the equi-density fluid system so that the results best simulate micro-g vapor-liquid flow regimes. The literature survey (Chapter II.) has shown that some limited number of vapor-liquid flow experiments were conducted in actual micro-g conditions. These studies show that annular, slug, and bubble flows are commonly observed micro-g vapor-liquid flow regimes. The most radical difference between the simulated experiments and the actual micro-g experiments are the absence of annular and slug flows and the presence of inverse annular and inverse slug flow in the equi-density fluid experiments. This shows that there is a need to control other experimental parameter(s) in the equi-density fluid system to match closely with the actual micro-g vapor-liquid flow.

Selection of Fluid Systems

The difficulty with the fluid system #1 (water-PPG) in simulating micro-g vapor-liquid flow regimes, is the improper wettability, viscosity, and interfacial tension characteristics of PPG. In simulating micro-g vapor-liquid flow, the viscosity ratio and

interfacial tension of two fluids comprising the system are to be comparable to that of typical vapor-liquid systems, e.g. viscosity ratio of water-air system, μ_l/μ_G = 45 and that of freon-11, μ_l/μ_G = 41 at 25°C. The viscosity ratio of PPG to water is about 310 and the interfacial tension between these two liquids is about 0.005 N/m. Therefore, the criteria for the selection of the fluid systems is to have a higher interfacial tension and lower viscosity ratio than obtained using the fluid system #1. Water would remain as the primary liquid due to its low cost and high availability. The search for suitable fluids has resulted in a number fluid mixtures as the second liquid. The physical properties of these equi-density fluid systems measured at 25°C are shown in Table 9.2. These fluids are mixture of various oils and appropriate amounts of carbon tetrachloride such that the density of the mixture is the same as that of water. The fluids are selected to cover the full range of viscosity ratios and interfacial tension of typical vapor-liquid systems.

Method of Mixing the Fluids - A literature review (Chapter II.) has revealed that annular, slug, and bubble flow are commonly observed in micro-gravity vapor-liquid flow. Annular flow seems to be more predominant under the micro-gravity conditions (Williams et al., 1973; Hill et al., 1987). After testing a number of nozzles, the annular type (concentric) nozzle configuration #4 as shown in Figure 9.6 is chosen to be used throughout this study as it provides annual flow at the entrance section. A procedure has been adopted to introduce the high viscous fluid first through the annular space followed by water

Table 9.2: Physical Properties of Equi-Density Fluid Systems

	System	Density kg/m3	Viscosity cP (25 C)	Interfacial Tension (N/m)x10^3
Fluid #1	**PPG-2000**	**1003**	**300**	~ 5
Fluid #2	**Heavy Mineral Oil and Carbon Tetrachloride**	**998**	~31	~32
Fluid #3	**Dow Corning Fluid and Carbon Tetrachloride**	**998**	~35	~47
Fluid #4	**Same as Fluid #3 with Surfactant**	**998**	~35	~ 5
Fluid #5	**Kerosene and Carbon Tetrachloride**	**998**	1.3	~38

Properties of Air-Water system : @ 25°C

$\mu_l/\mu_G = 45$

$\gamma = 0.072$ N/m

Properties of Freon-11 : @ 25°C

$\mu_l/\mu_G = 41$

$\gamma = 0.018$ N/m

Properties of Freon-12 : @25°C

$\mu_l/\mu_G = 17$

$\gamma = 0.0085$ N/m

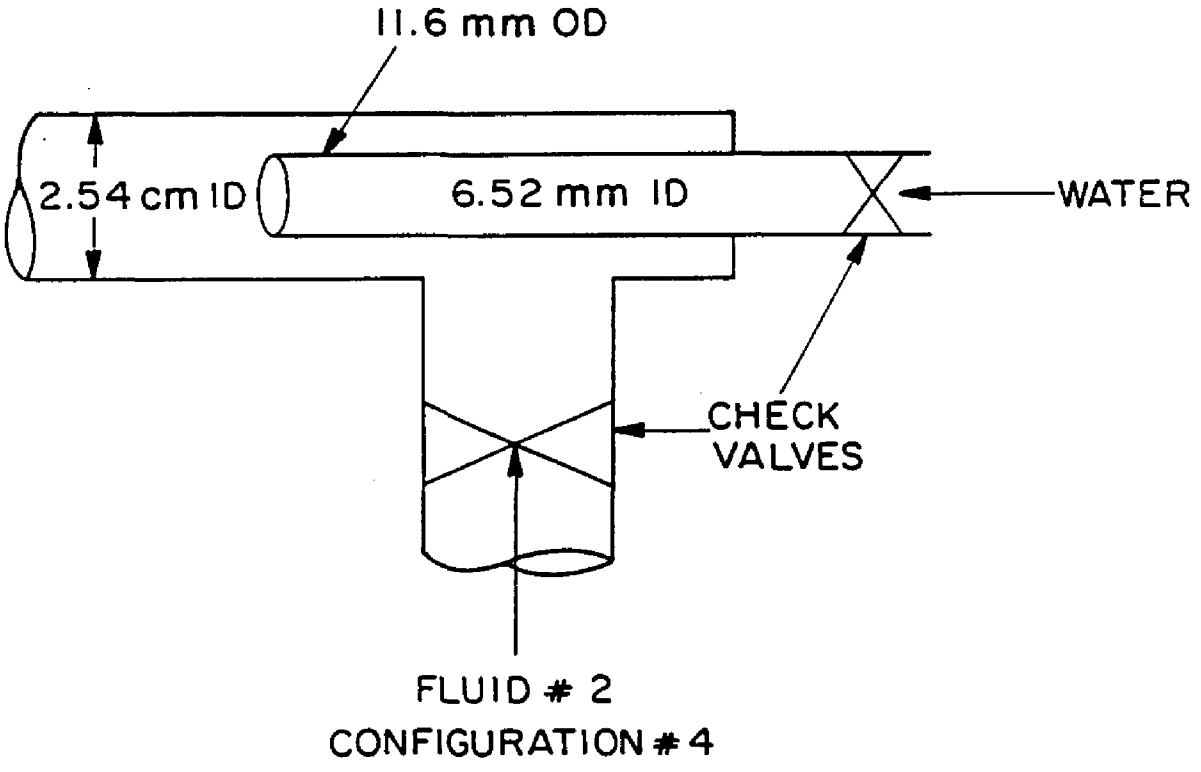

Figure 9.6: Annular-Type Nozzle Configuration.

through the inner tube. This procedure allows the flow to start as an annular. The resulting flow regime is noted only after three to five minutes from the start of the experiment allowing sufficient time to reach steady state conditions.

Effect of Wettability - Under an actual vapor-liquid system, the liquid is usually more wettable with the pipe surface than vapor. In simulating micro-g vapor-liquid flow, the water, simulating the "vapor" phase, is more wettable with the tube surface. The relative wettability of simulated "vapor" phase with the tube surface must be decreased which is achieved by using the following procedure.

Surface Waxing - The surface property of the pyrex glass is altered by coating the surface with hard carnauba wax which is commonly used as a mold release agent. The qualitative experiments to study wetting ability of water and fluid #2 for an unwaxed and waxed flat glass surface yielded the following results:

(i) fluid #2 exhibited no discernible difference in wetting between the waxed and unwaxed glass surfaces showing only a "moderate" tendency to wet the glass in either case.

(ii) water showed a dramatic difference in wetting characteristics between the waxed and unwaxed glass surfaces. Water drops wet the unwaxed surface quite well. It took an extreme tilt of the glass surface to force the water to roll down. When a drop of water rolls down, it moves slowly and leave a trail of water film behind; thus, the water drop became smaller as it rolled. On the other hand, water drops wet a waxed glass surface hardly at all. The water droplets bead up nearly to spheres. It took little tilt to

cause the droplets to roll down. When a water drop rolls, it rolls freely and leave no track at all.

(iii) waxed glass even when subjected to flowing water for several hours shows no change in its wetting characteristics.

These results suggest that waxing reduces water's affinity for glass but leaves fluid #2's affinity for glass unchanged.

In our experiments, the wetting ability of water is reduced by coating the inside of the 2.54 cm ID pyrex glass tube with carnauba wax. The two liquids are introduced into the tube as described in the method of mixing the fluids section. The flow regime patterns are observed through the viewing section to study the flow behavior. The observed flow regime data for both non-waxed and waxed tube surface are presented in Table 9.3. The experiments are conducted for two water flow rates of 0.02074 and 0.1244 m/s. The flow regime patterns and pressure drop data are recorded for an increase in fluid #2 flow rates from 0.0067 to 0.4605 m/s. A comparison of data for non-waxed and waxed surfaces at a water flow rate of 0.02074 m/s shows that an inverse annular flow regime for non-waxed surface is replaced by a slug flow when the pipe surface is waxed. Similarly, comparing the data at a water flow rate of 0.1244 m/s shows that drop flow in the case of non-waxed surface is replaced by an annular-drop flow for waxed surface. This clearly indicates that the change in wettability characteristics of water (simulating "vapor") with respect to tube surface would replace the flow regimes such as inverse annular, inverse slug, etc., by flow regimes like slug, annular, etc. The pressure drops for flow regimes with waxed surface are greater than

Table 9.3. Effect of Wettability: Flow Regime Data

Flow Rate of Fluid #2, U_{ls} (m/s)	Flow Rate of Water, U_{Gs} = 0.02074 m/s		U_{Gs} = 0.124 m/s	
	Non-Waxed Tube Surface	Waxed Tube Surface	Non-Waxed Tube Surface	Waxed Tube Surface
0.0067	D (0.16)	S (1.56)	D (0.96)	AD (1.56)
0.0218	IA (0.32)	S (3.83)	D (1.28)	AD (4.63)
0.0439	IA (0.96)	S (6.54)	D (1.6)	D (3.83)
0.0748	IA (1.12)	S (9.09)	D (2.39)	AD (7.82)
0.1144	IA (2.55)	S (12.6)	D (3.19)	AD (---)
0.1316	IA (3.19)	B (12.76)	D (3.83)	AD (17.8)
0.3382	IA (9.57)	B (16.7)	B (---)	AD (16.3)
0.4605	B (>30)	B (19.0)	-	B (20.4)

Numbers in parenthesis indicate pressure drop across 5.56 m. long tube section in inches of water. For flow regime definitions please refer to Table 4.2.

for flow regimes with unwaxed surface, as expected, for the two waterflow rates of 0.02074 and 0.1244 m/s. In conclusion, the wetting property of water with respect to the tube surface has a major impact upon the flow patterns. The waxing of tube surface (causing a lower water wettability) has resulted in generating flow regimes which are closer to real vapor-liquid flow regimes that are observed under micro-g conditions. Therefore, for an accurate simulation, the wettability of the simulating "vapor" relative to the wettability of the simulating "liquid" (more viscous liquid) plays a critical part. Since the liquid is more wettable than vapor in real vapor-liquid systems, it is concluded that in our simulated system, the simulating "vapor" should have as little wettability as possible relative to that of the simulating "liquid".

In short, the liquid-liquid system not only should possess equal density, but also should have appropriate **viscosity ratio, interfacial tension, and wettability** characteristics of liquids with respect to tube surface in simulating micro-g vapor-liquid flow behavior.

X. RESULTS AND DISCUSSION

The results of this study are presented in two sections. In Section A, results and discussion of the simulated micro-g vapor-liquid flow regime maps for different equi-density fluid systems are presented and these results are compared with the predictions of Taitel-Dukler and Weisman et al. models. In Section B, the simulated experimental results are compared with the actual micro-g vapor-liquid flow regime data taken in either a drop tower test or an airplane trajectory.

Section A. Simulated Micro-g Flow Regime Maps

In simulating micro-g vapor-liquid flow, the viscosity ratio and relative wettability of the two fluids comprising the system and their interfacial tension are to be comparable to that of typical vapor-liquid systems, e.g. viscosity ratio of water-air system, $\mu_l/\mu_G = 45$ and that of freon-11, $\mu_l/\mu_G = 41$ at 25°C. The search for suitable fluids resulted in using a number of mixtures as discussed in the previous section. These fluids are immiscible and possess essentially equal densities. The surface property of the pyrex glass tube is altered by coating the surface with carnauba wax. This reduced the wettability of water with the glass surface, leaving the wettability of oil with the surface unaltered. In simulating micro-g vapor-liquid flow, the oil which is more viscous and more wettable liquid represents the "liquid" phase and water (less viscous and less wettable with respect to waxed tube surface) although a liquid as well

at test conditions, corresponds to the "vapor" phase. These fluids are introduced into the tube through an annular-type nozzle configuration. The high viscous oil is introduced first through the annular space followed by water through the inner tube.

Flow Regime Map - Fluid System #2

In fluid system #2, water and a mixture of heavy mineral oil and carbon tetrachloride (fluid #2) are used, which are immiscible and possess essentially equal density. A series of flow patterns are observed for an increase in the "liquid" flow rate at a constant "vapor" flow rate. The observed flow patterns are classified into corresponding regimes based on the definitions presented in Table 4.2. The bubble flow is designated when the "liquid" phase is continuous and fills the flow tube while the "vapor" is in the form of bubbles of size less than or equal to the tube diameter. The slug flow is characterized by alternating "bullet" shaped slugs (greater in length than the tube diameter) of "vapor" followed by "liquid" phase flow that completely fills the tube cross-section. In the annular-drop flow, the "liquid" phase completely wets the circumference of the tube and the "vapor" flow containing "liquid" drops, is confined to central core of the tube area. Experimentally observed vapor-liquid flow pattern maps for horizontal flow are shown in Figures 10.1 through 10.3. Data are presented on log-log plots with the following coordinate systems: Figure 10.1 - superficial "vapor" velocity, U_{Gs} versus superficial "liquid" velocity, U_{ls}; Figure 10.2 - superficial momentum flux of "vapor", $\rho_G U_{Gs}^2$ versus superficial momentum flux of "liquid", $\rho_l U_{ls}^2$; and Figure 10.3 - Reynolds number of "vapor", Re_G

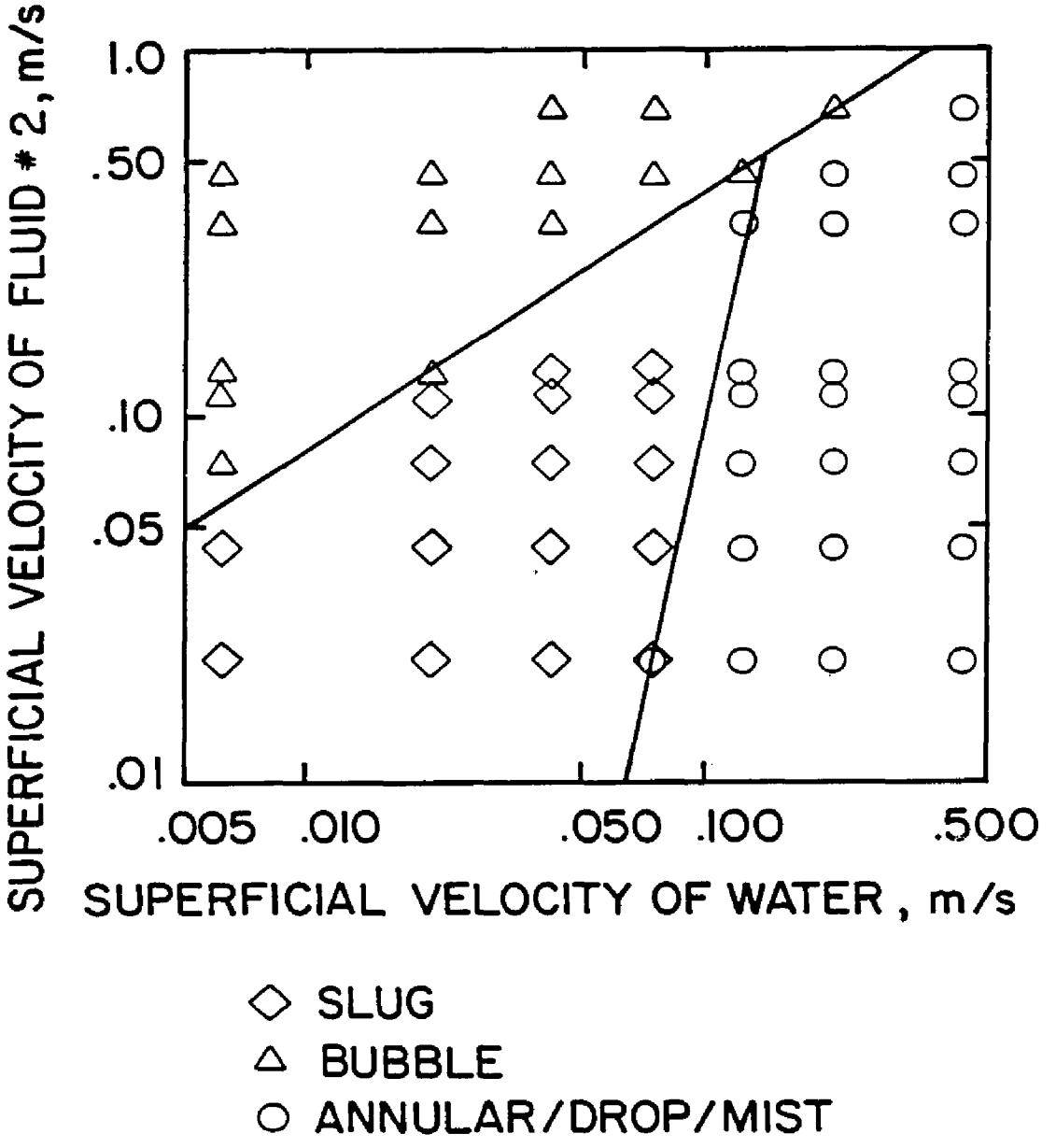

Figure 10.1: Simulated Micro-g Vapor-Liquid Flow Regime Map - Fluid System #2 (Equi-Density Heavy Mineral Oil + CCl_4 and Water).

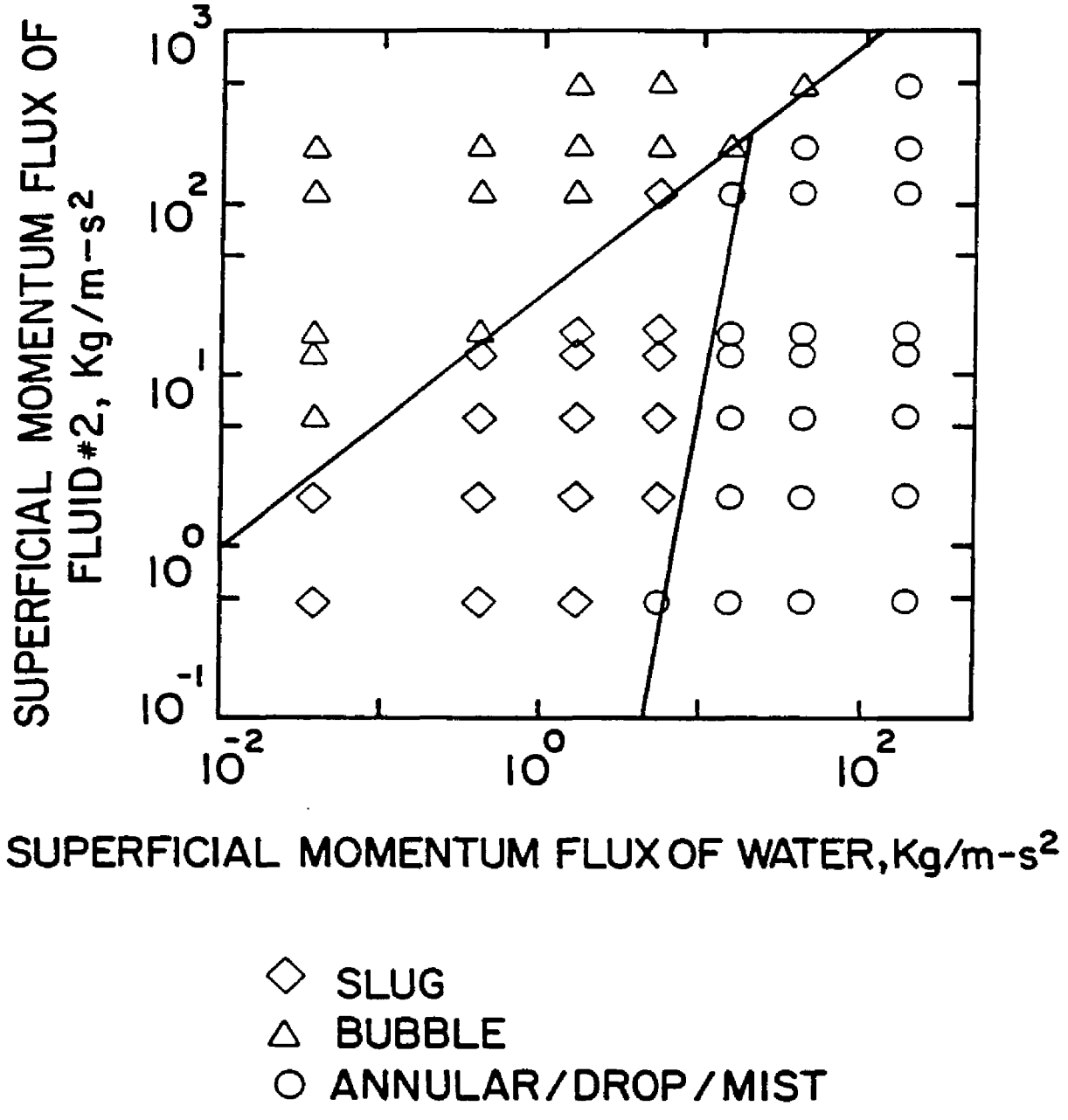

Figure 10.2: Simulated Micro-g Vapor-Liquid Flow Regime Map - Fluid System #2 (Equi-Density Heavy Mineral Oil + CCl_4 and Water).

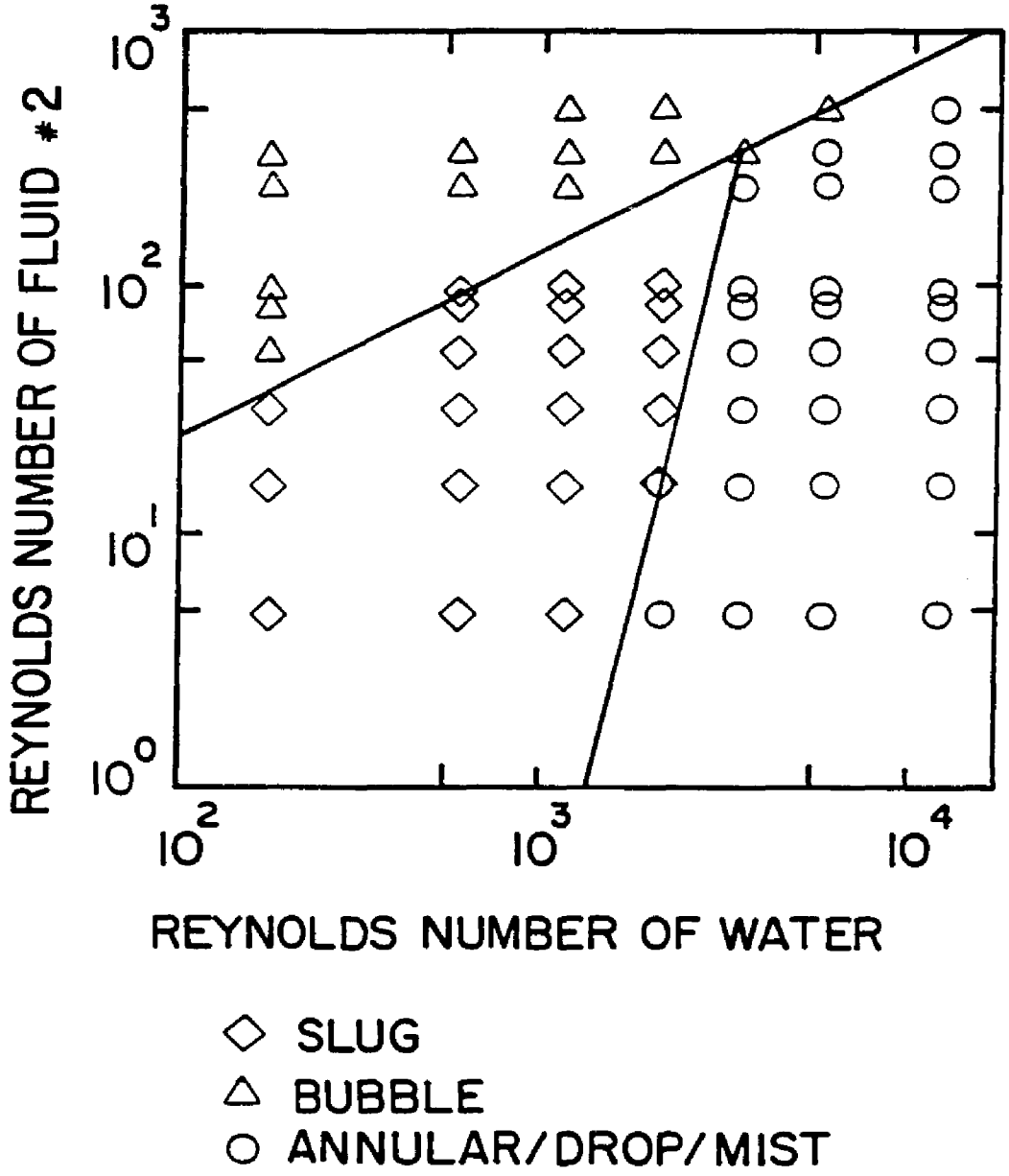

Figure 10.3: Simulated Micro-g Vapor-Liquid Flow Regime Map - Fluid System #2 (Equi-Density Heavy Mineral Oil + CCl_4 and Water).

versus Reynolds number of "liquid", Re_l. The reason for plotting the data on three coordinate systems is discussed in the Chapter IV. A key shows the flow regimes indicated by the various symbols, and lines are drawn between the various flow regimes. The change from one regime to another is not always well defined; however, the lines represent the gradual transitions.

The effect of increasing the "liquid" velocity at the relatively low "vapor" velocity of 0.021 m/s on the flow pattern can be seen in Figure 10.1. At low "liquid" velocities, the bullet shaped slugs (like a classical Taylor bubbles) of "vapor" flow in the continuous phase of "liquid". An increase in "liquid" velocity to about 0.132 m/s causes the "vapor" slugs to disperse as bubbles. This is a typical bubble or dispersed bubble flow.

The effect of increasing "liquid" velocity at the relatively moderate "vapor" velocity of 0.124 m/s on the flow pattern shows that at low to moderate "liquid" velocities the "liquid" phase completely wets the circumference of the pipe and the "vapor" flow is confined to the central core. There are also considerable "liquid" drops flowing in the continuous central core of "vapor" phase. This flow regime is classified as a annular-drop flow. Sometimes the thin film of "liquid" along the wall appears to be washed off into the drop flow in the central core. The "liquid" surface of annular film appears to be rough and occasionally takes the form of roll waves. As the "liquid" velocity increases from 0.02 to 0.46 m/s, the flow pattern changes from annular-drop to bubble flow.

In general, as the "vapor" flow rate is increased for a definite low "liquid" velocity, the flow pattern goes through slug to a

annular-drop flow. At high "vapor" velocities, the "liquid" is thrown out along the circumference of the tube and the "vapor" flows in the central core. Some "liquid" droplets are detached from the fluid interface giving annular-drop flow. At high "liquid" flow rates, the flow is observed to be a bubble flow.

Figures 10.2 and 10.3 show the flow regime maps using superficial momentum fluxes and Reynolds numbers as coordinate systems, respectively. These figures show the same trend in discretizing the flow regimes as discussed for flow regimes in Figure 10.1.

Comparison of Model Predictions with Experimentally Simulated Micro-g Vapor-Liquid Flow Regime Data: For horizontal flow, Taitel and Dukler (1976), and Weisman et al. (1979) have proposed models to predict the various transition lines. The flow regime transition equations as discussed earlier have been used to generate flow pattern boundaries at micro-g levels and are presented in Figures 10.4 through 10.9.

These figures show typical flow regimes for freon-11 vapor-liquid system (25^{o}C, saturation pressure of 1 atm, 2.54 cm ID horizontal tube, and for various values of g/g_n, namely, 10^{-2} and 10^{-3}. The freon-11 was chosen as a reference system because of its potential to be used as a coolant in a two-phase loop for space applications. As a matter of fact, NASA has been seriously considering the use of freon fluids as coolants. The predicted transition lines for the freon-11 system by both models are presented on log-log plots with the following coordinate systems:- Figures 10.4 and 10.5 - Reynolds number of "vapor", Re_G versus Reynolds number of "liquid", Re_l for g/g_n = 10^{-2} and 10^{-3}; Figures 10.6 and 10.7 - superficial "vapor" velocity,

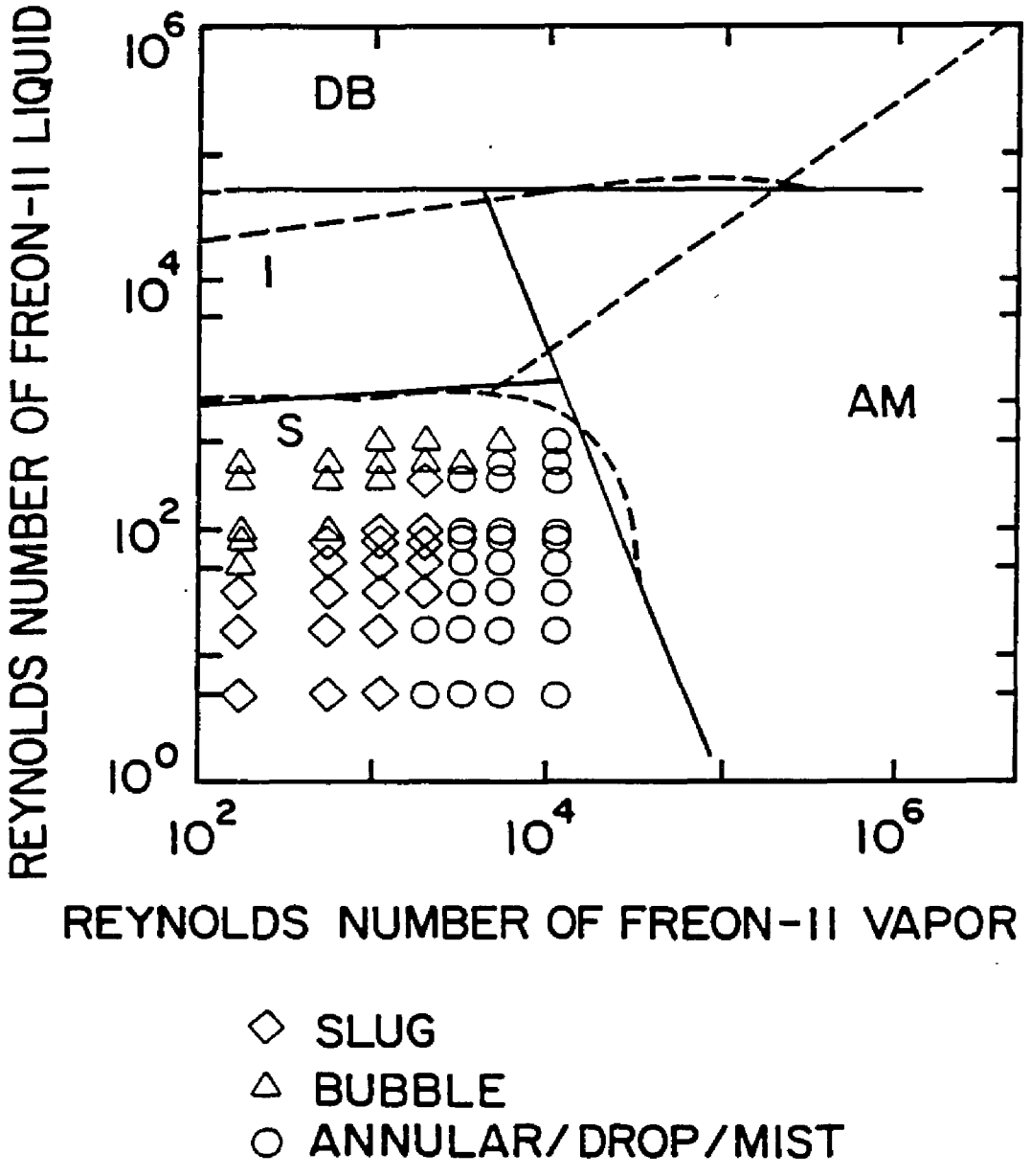

Figure 10.4: Comparison of Simulated vs. Model Predictions; Simulated Micro-g Flow Regime Data - Fluid System #2; Flow Regime Maps: Freon-11, 2.54 cm ID Horizontal, 25°C, Sat. Press., $g/g_n = 10^{-2}$, - - -Taitel-Dukler Model, ———Weisman et al. Model.

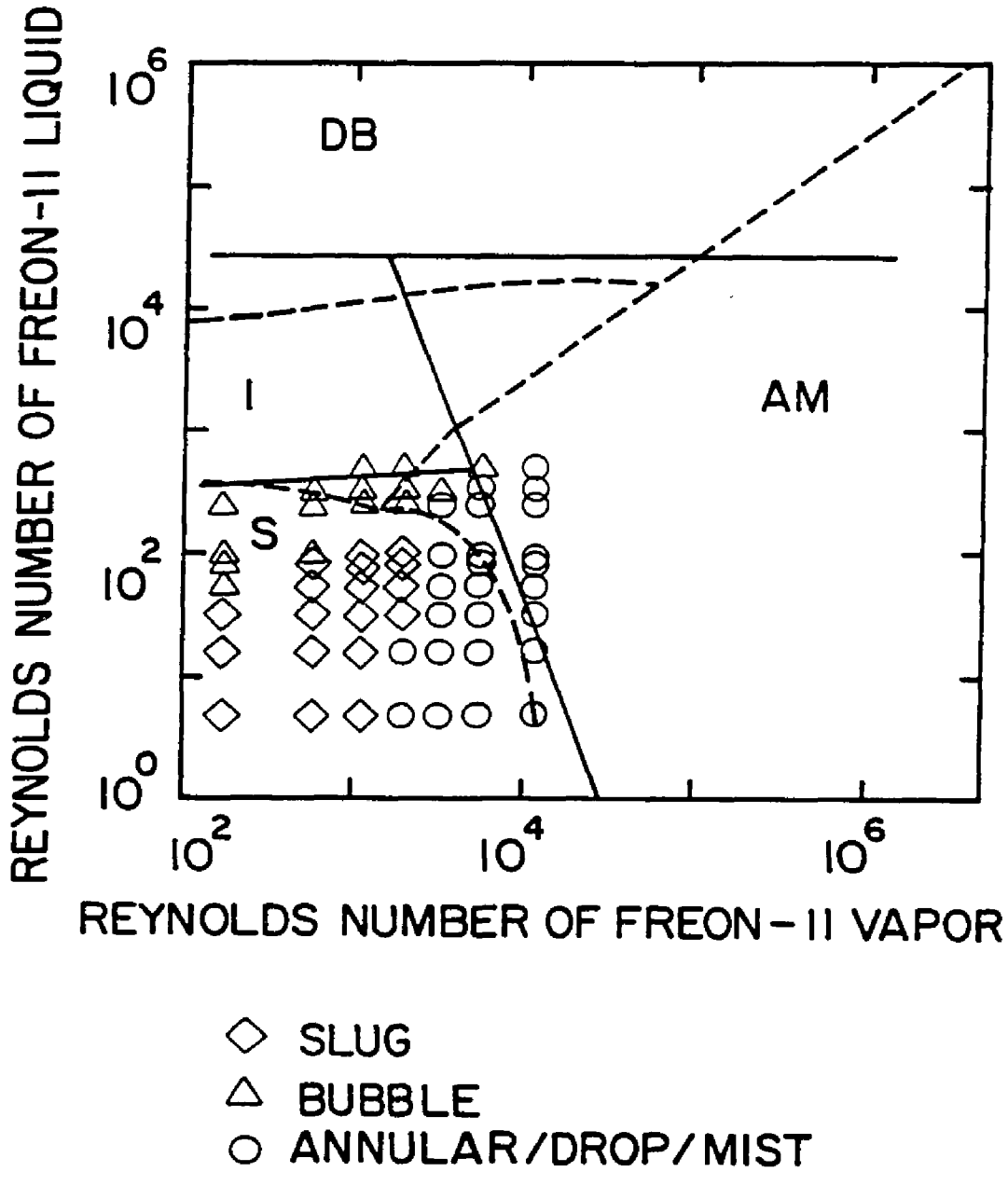

Figure 10.5: Comparison of Simulated vs. Model Predictions; Simulated Micro-g Flow Regime Data - Fluid System #2; Flow Regime Maps: Freon-11, 2.54 cm ID Horizontal, 25°C, Sat. Press., $g/g_n = 10^{-3}$, - - -Taitel-Dukler Model, ———Weisman et al. Model.

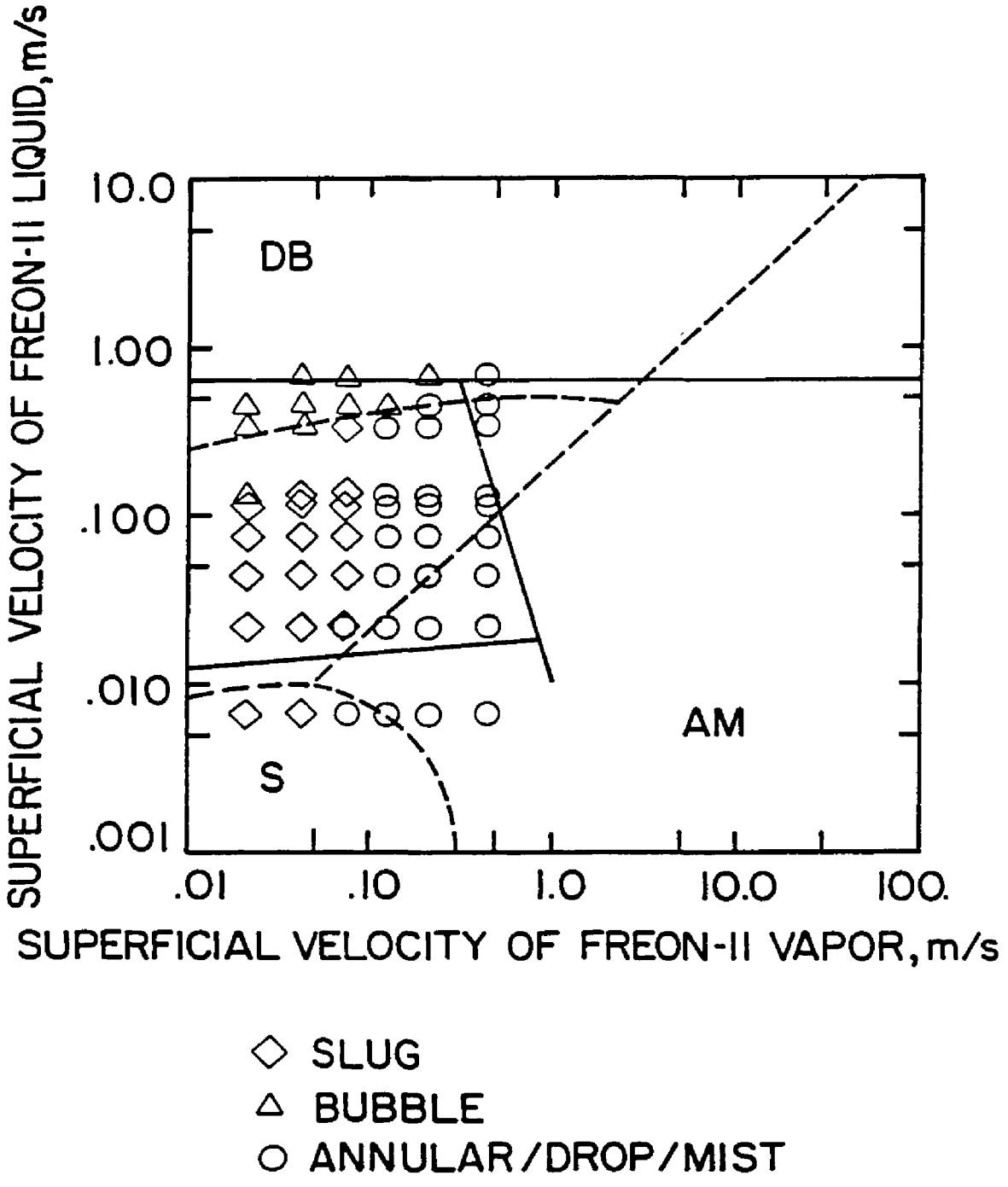

Figure 10.6: Comparison of Simulated vs. Model Predictions; Simulated Micro-g Flow Regime Data - Fluid System #2; Flow Regime Maps: Freon-11, 2.54 cm ID Horizontal, 25°C, Sat. Press., $g/g_n = 10^{-2}$, - - -Taitel-Dukler Model, ———Weisman et al. Model.

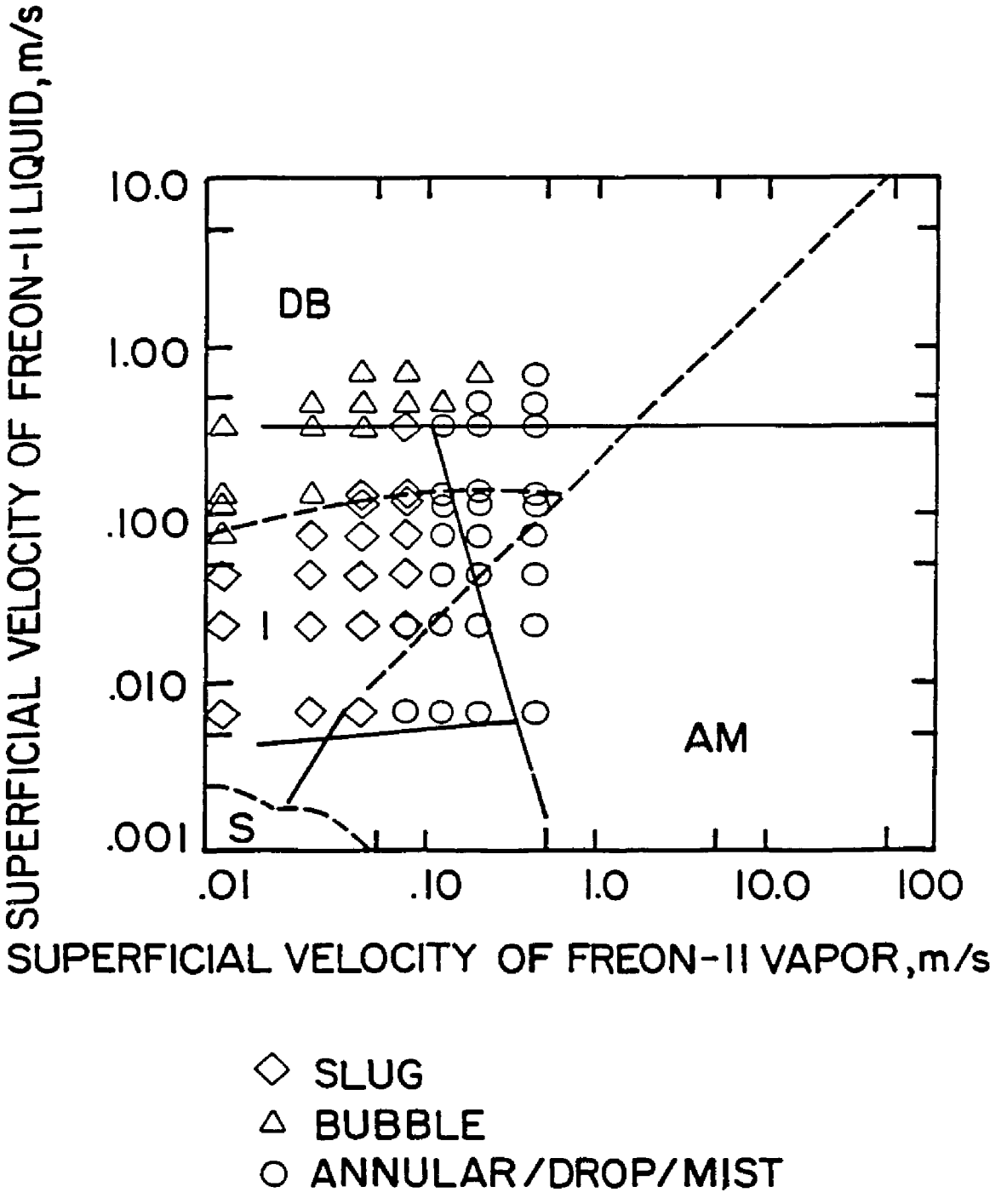

Figure 10.7: Comparison of Simulated vs. Model Predictions; Simulated Micro-g Flow Regime Data - Fluid System #2; Flow Regime Maps: Freon-11, 2.54 cm ID Horizontal, 25°C, Sat. Press., $g/g_n = 10^{-3}$, - - -Taitel-Dukler Model, ———Weisman et al. Model.

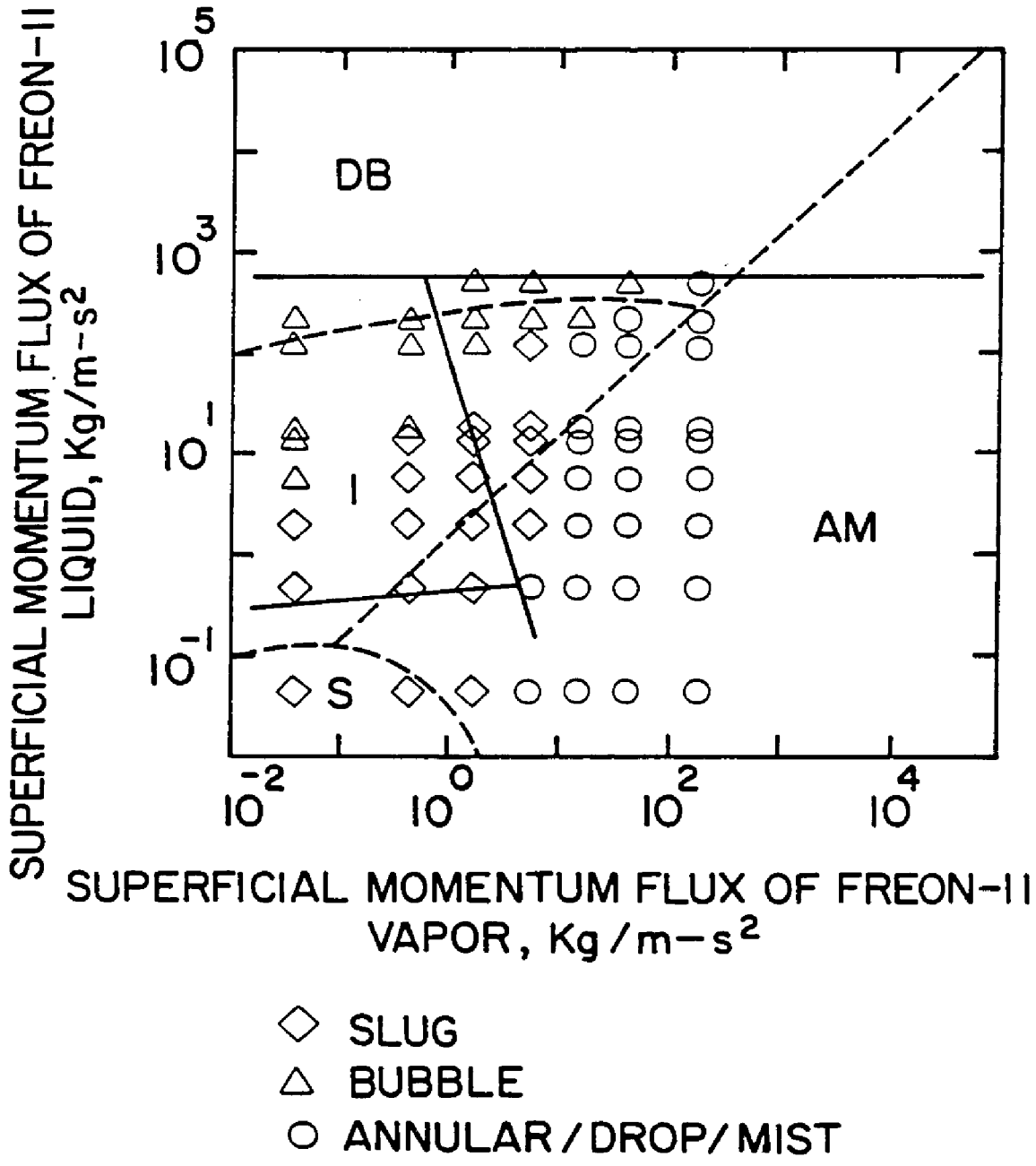

Figure 10.8: Comparison of Simulated vs. Model Predictions; Simulated Micro-g Flow Regime Data - Fluid System #2; Flow Regime Maps: Freon-11, 2.54 cm ID Horizontal, 25°C, Sat. Press., $g/g_n = 10^{-2}$, - - -Taitel-Dukler Model, ———Weisman et al. Model.

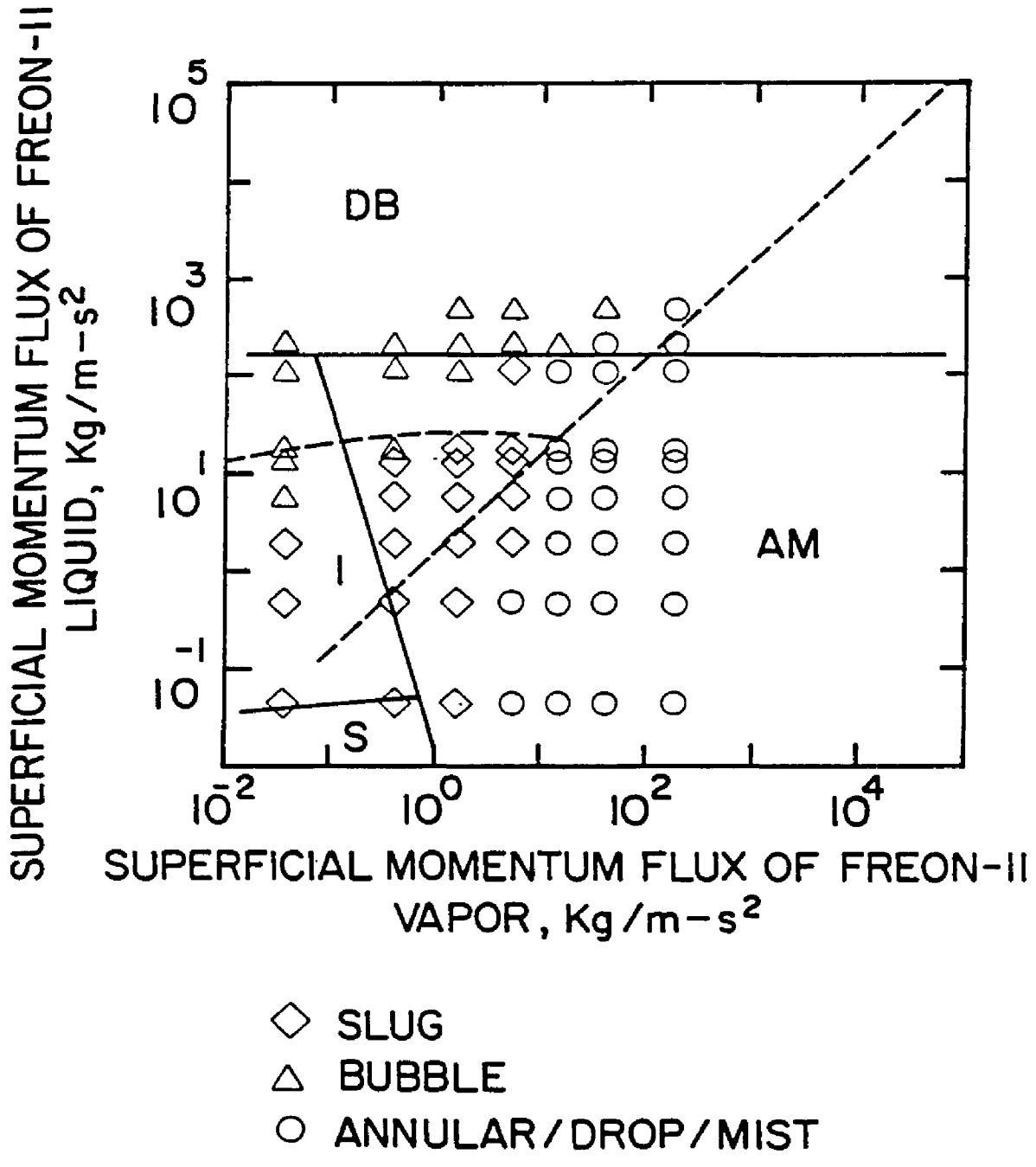

Figure 10.9: Comparison of Simulated vs. Model Predictions; Simulated Micro-g Flow Regime Data - Fluid System #2; Flow Regime Maps: Freon-11, 2.54 cm ID Horizontal, 25°C, Sat. Press., $g/g_n = 10^{-3}$, - - -Taitel-Dukler Model, ———Weisman et al. Model.

U_{Gs} versus superficial "liquid" velocity, U_{ls} for $g/g_n = 10^{-2}$ and 10^{-3}; and Figures 10.8 and 10.9 - momentum flux of "vapor", $\rho_G U_{Gs}^2$ versus momentum flux of "liquid", $\rho_l U_{ls}^2$ for $g/g_n = 10^{-2}$ and 10^{-3}, respectively. In all these flow regime maps, model transition predictions by the Weisman et al. are represented by solid lines, and those of the Taitel-Dukler by broken lines.

The flow regime experimental data of fluid system #2 are superimposed on Figures 10.4 through 10.9 and are identified by legends. The three different coordinate systems have been studied to determine which system best fits the simulated experimental data with model predictions. A comparison of the experimental data with the model predictions in Figures 10.4 and 10.5 for $g/g_n = 10^{-2}$ and 10^{-3}, respectively, reveals that the Reynolds number coordinate system does not provide a good fit for the simulated micro-g experimental data against model predictions. Under the superficial velocity coordinate system (Figures 10.6 and 10.7), the transition lines slug-annular and slug-bubble as predicted by both models are not in good agreement with equi-density fluid experimental data. Under the superficial momentum flux coordinate system (Figures 10.8 and 10.9), the experimental data and model predictions can be compared better at $g/g_n = 10^{-3}$. Basically both the models predict the same type of flow regimes, namely, slug, bubble, and annular-mist. However, the size, shape, and location of the flow regime regions differ considerably from one another. In Figure 10.9, the transition to bubble flow as predicted by both the models, appear to be in reasonable agreement with the experimental data. In addition, the transition lines slug-annular and bubble-annular as predicted by the Taitel-Dukler

model are in better agreement with the experimental data than by the Weisman et al. model. In general, the superficial momentum flux coordinate system shows a better fit between the simulated experimental data and model predictions for micro-g vapor-liquid flow regimes. A detailed analysis for the justification of the use of superficial momentum flux coodinates is provided in Appendix B. Subsequently, the comparison of flow regime data of equi-density fluid systems with actual micro-g vapor-liquid flow will be made on a flow regime map with superficial momentum fluxes as a coordinate system.

The fluid system #2 experimental results are also compared against model prediction for **vertical** flow. Figure 10.10 shows typical flow regimes predicted by both the Taitel et al. and Weisman-Kang models for freon-11 vapor-liquid system (25°C, saturation pressure of 1 atm, 2.54 cm ID vertical tube) at $g/g_n = 10^{-3}$. The experimental data for fluid system #2 are superimposed on Figure 10.10 and the comparison clearly show that the transition lines predicted by both the models deviate considerably with those of simulated experimental data.

Flow Regime Map - Fluid System #3

In fluid system #3, water and a mixture of Dow Corning 200 Fluid (50 cSt) and carbon tetrachloride (fluid #3) are used, which are immiscible and possess essentially equal density. The physical properties of this fluid system at 25°C are: viscosity ratio = 35, density ratio = 1, and interfacial tension = 0.047 N/m between fluid #3 and water. Using the nomenclature of Table 4.2, three flow regimes are observed, namely, bubble, slug, and annular-drop. Figure

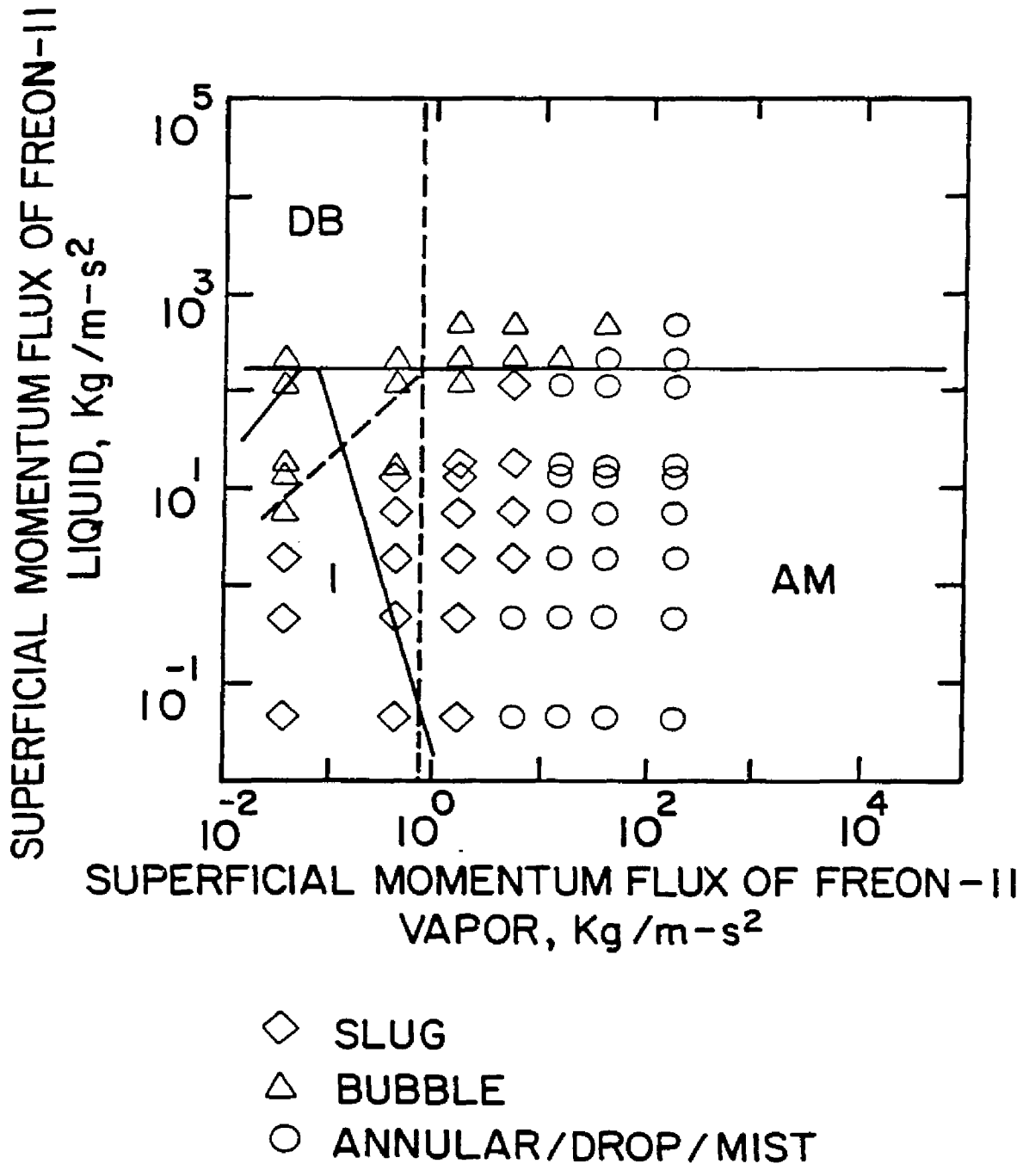

Figure 10.10: Comparison of Simulated vs. Model Predictions; Simulated Micro-g Flow Regime Data - Fluid System #2; Flow Regime Maps: Freon-11, 2.54 cm ID Vertical, 25°C, Sat. Press., $g/g_n = 10^{-3}$, - - -Taitel-Dukler Model, ———Weisman et al. Model.

10.11 with superficial velocities as a coordinate system, shows the observed flow regimes during the experiments at different flow rates. A key shows the flow regimes indicated by the various symbols, and lines are drawn between the various flow regimes. Figure 10.12 utilizing superficial momentum fluxes as a coordinate system, shows the transition lines predicted by the models of Taitel-Dukler and the Weisman et al. for freon-11 system in a horizontal flow at $g/g_n = 10^{-3}$. The flow regime experimental data for fluid system #3 are superimposed on Figure 10.12 and are identified by legends. A comparison reveals that the transition to bubble flow as predicted by both the models, appear to be in reasonable agreement with the simulated experimental data. In addition, the transition lines slug-annular and bubble-annular as predicted by the Taitel-Dukler model are also in better agreement with experimental data than by the Weisman et al. model.

Flow Regime Maps - Fluid Systems #4 and #5

The fluid system #4 is the same as that of fluid system #3 except the interfacial tension between fluid #3 and water is altered by adding small amount of Triton x-100 surfactant to water. The addition of surfactant reduces the interfacial tension from 0.047 to 0.005 N/m. This system is selected to study the effect of interfacial tension keeping the viscous forces the same. The observed flow regimes are shown in Figure 10.13.

The fluid system #5 is chosen to study the effect of viscosity ratio between equi-density fluids on flow regime transitions. In fluid system #5, water and a mixture of kerosene and carbon

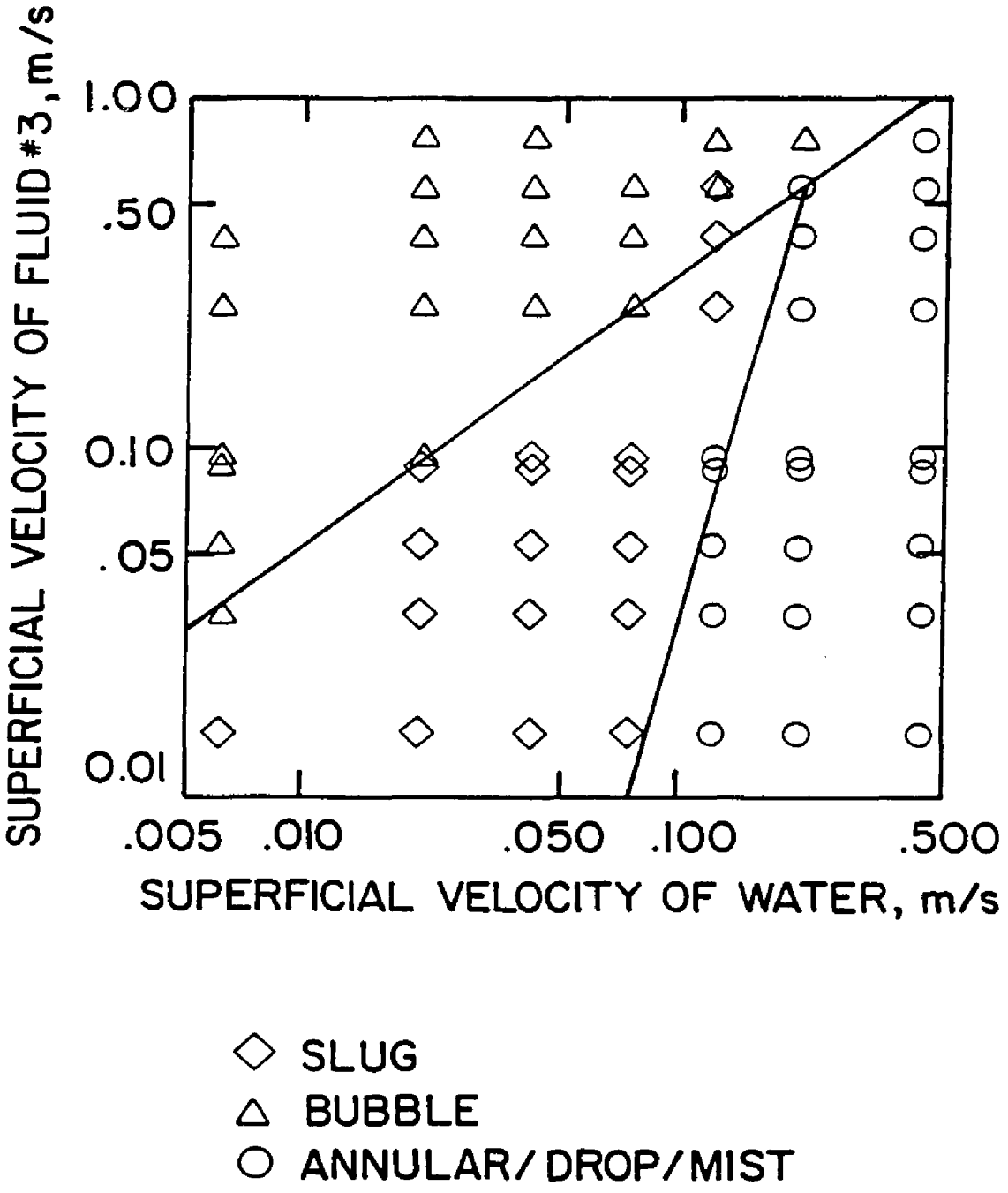

Figure 10.11: Simulated Micro-g Vapor-Liquid Flow Regime Map - Fluid System #3 (Equi-Density Dow Corning 200 Silicone Oil + CCl_4 and Water).

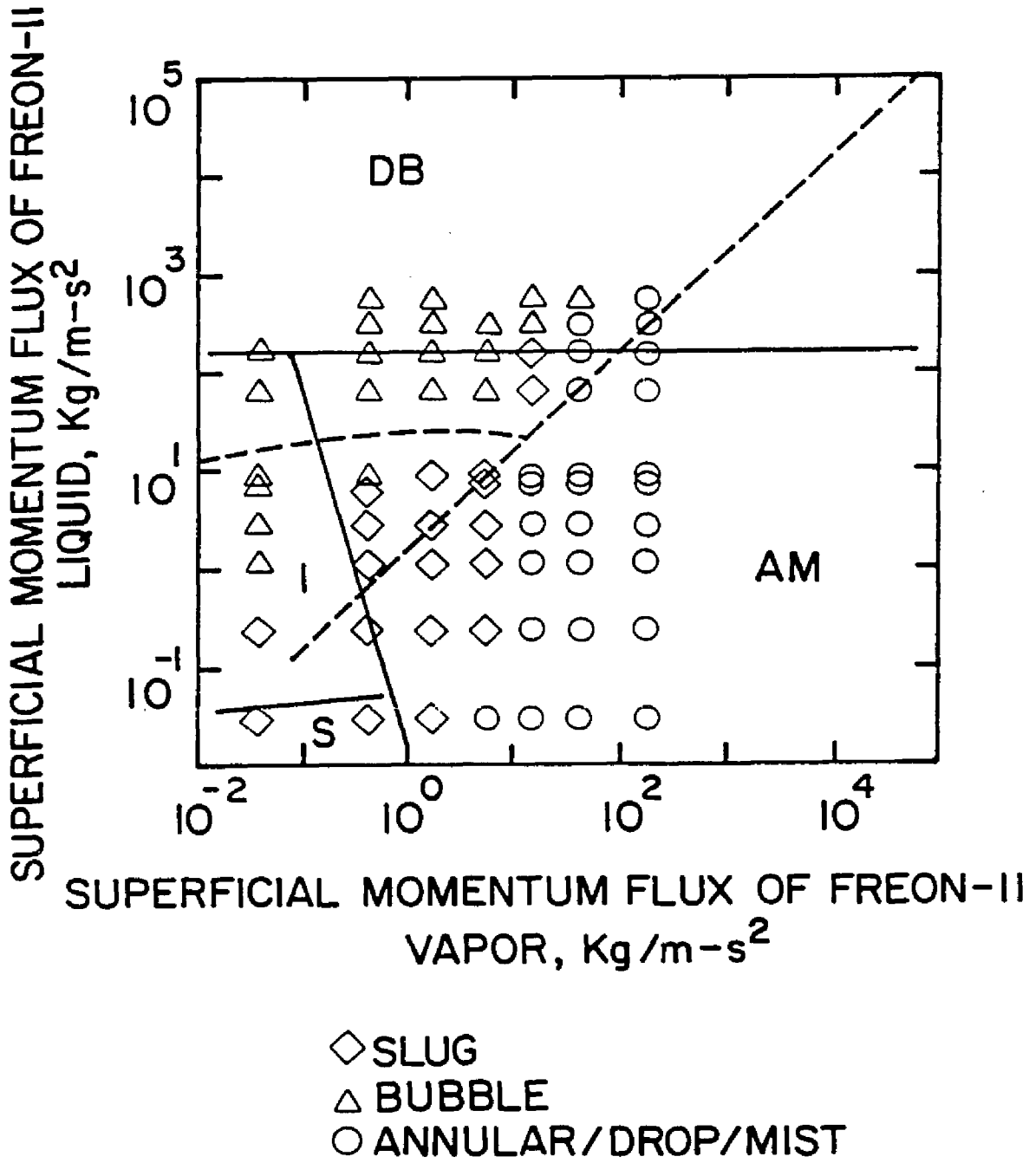

Figure 10.12: Comparison of Simulated vs. Model Predictions; Simulated Micro-g Flow Regime Data - Fluid System #3; Flow Regime Maps: Freon-11, 2.54 cm ID Horizontal, 25°C, Sat. Press., $g/g_n = 10^{-3}$, - - -Taitel-Dukler Model, ———Weisman et al. Model.

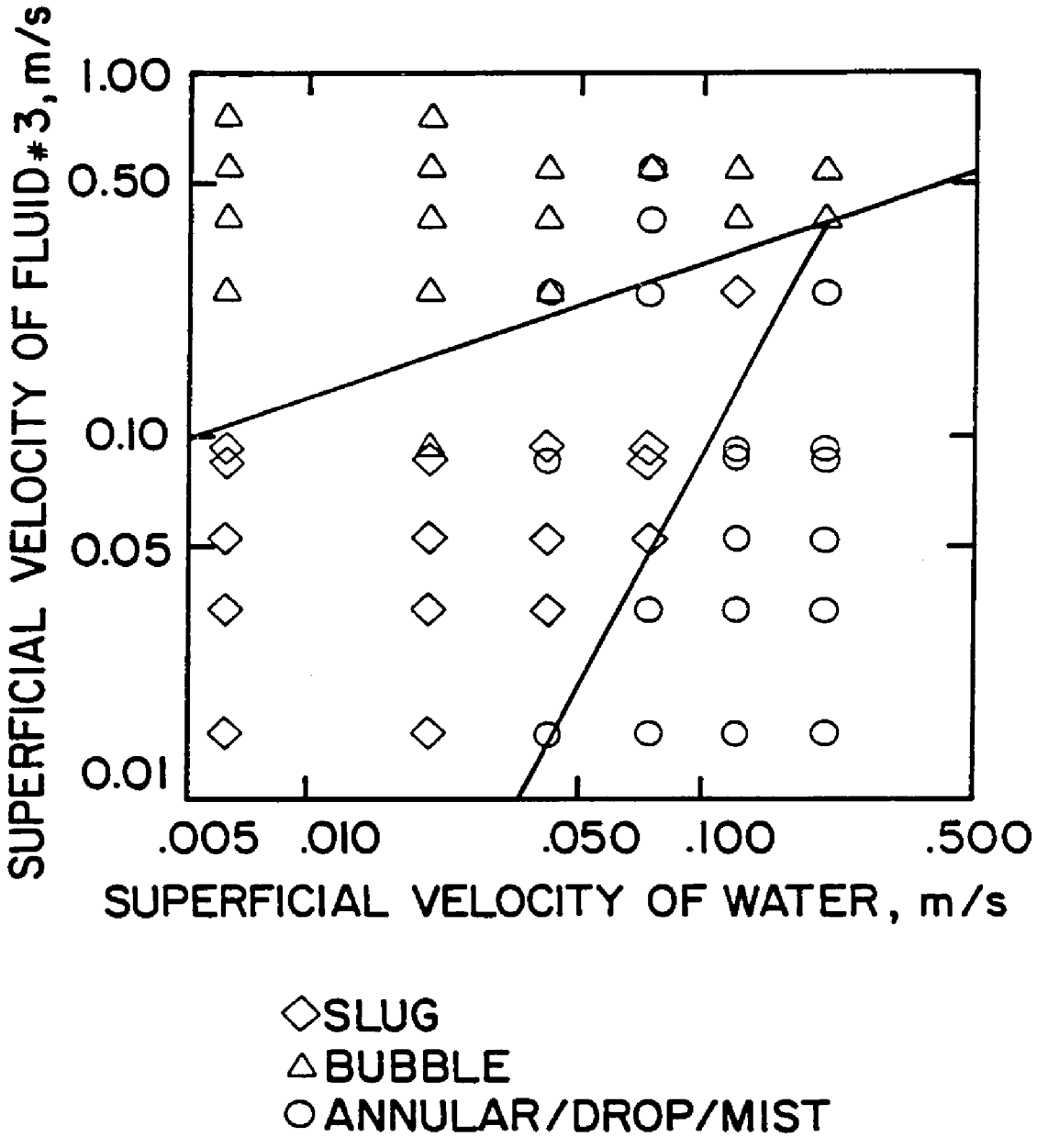

Figure 10.13: Simulated Micro-g Vapor-Liquid Flow Regime Map - Fluid System #4 (Equi-Density Dow Corning 200 Silicone Oil + CCl_4 and Water + Triton x-100).

tetrachloride (fluid #5) are used, whose viscosity ratio = 1.3, density ratio = 1, and an interfacial tension = 0.038 N/m. The observed flow regimes are plotted in Figure 10.14. In both systems #4 and #5, the type of observed flow regimes are bubble, slug, and annular-drop.

Effect of Interfacial Tension on Flow Pattern Transitions

A comparison of fluid systems #2 and #3 shows that the viscosity ratio is about the same order of magnitude (31 and 35, respectively) for both; however, the interfacial tension differs considerably (0.032 and 0.047 N/m, respectively). Therefore the shift of transition lines from one flow regime to another in these two systems as seen in Figures 10.1 and 10.11, could be attributed to the change of interfacial tension. This comparison shows that the transition line to bubble flow for the fluid system #3 is at a somewhat lower "liquid" velocity than for the fluid system #2. On the other hand, the transition line to annular-drop flow for the fluid system #3 is at a somewhat higher "vapor" velocity than for the fluid system #2.

To study the effect of interfacial tension alone on transition lines, experiments are conducted for fluid system #4 which is same as that of fluid system #3 except the interfacial tension between fluid #3 and water is altered (from 0.047 to 0.005 N/m) by adding small amount of Triton x-100 surfactant to water. The qualitative observations of fluid system #4 show that the "vapor" slugs are kind of unstable in the sense they start of as a perfect "Taylor" bubble and could not sustain its shape because of low interfacial tension and tend to become a stratified type flow. This is noticed in most of

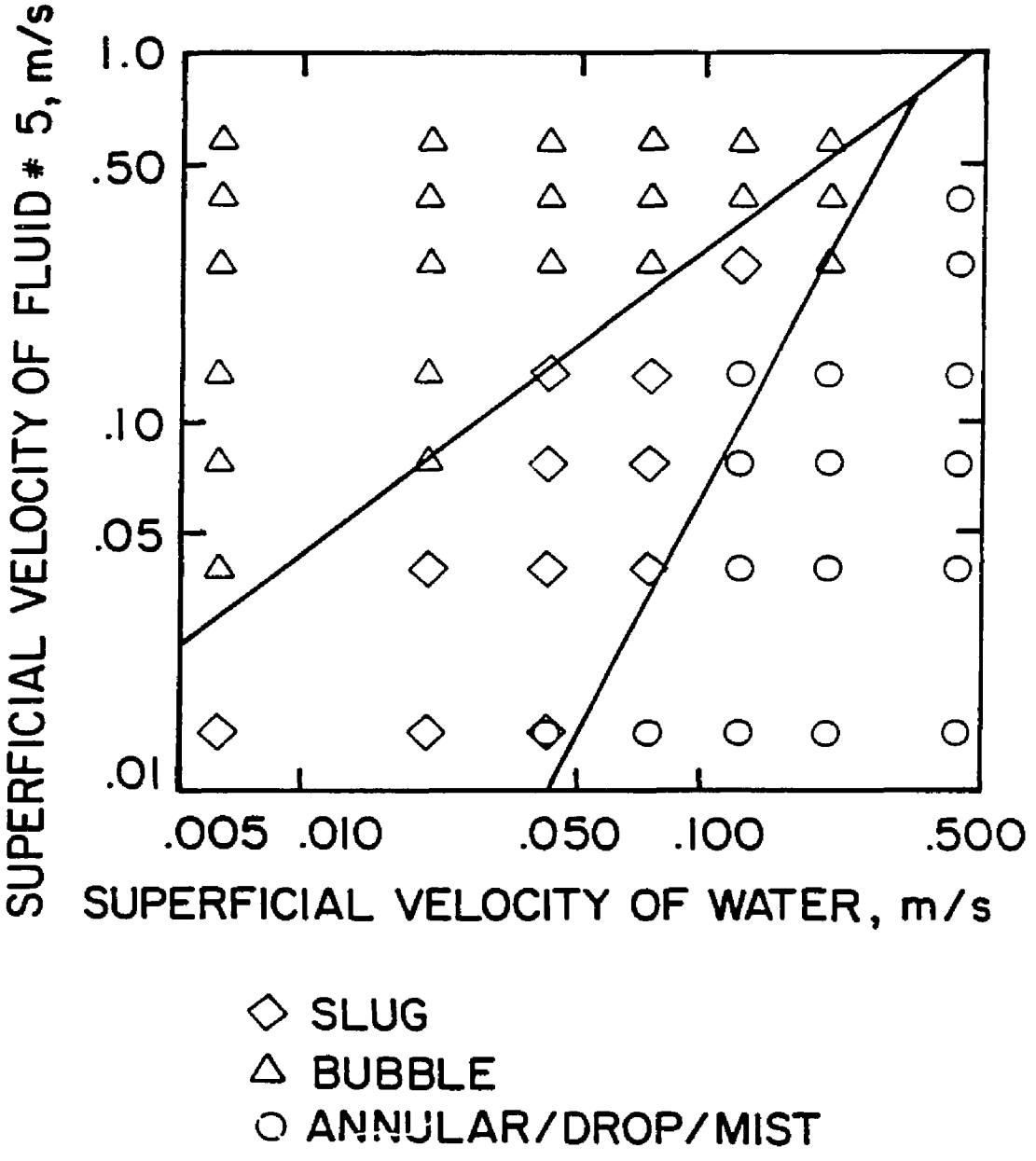

Figure 10.14: Simulated Micro-g Vapor-Liquid Flow Regime Map - Fluid System #5 (Equi-Density Kerosene + CCl_4 and Water).

slug region indicated in Figure 10.13. A comparison of Figures 10.11 and 10.13 show that the transition from slug to bubble flow occurs at somewhat higher "liquid" flow rates and also the transition from slug to annular-drop occurs at relatively lower "vapor" velocities for fluid system #4.

In short, higher the interfacial tension, sooner the flow pattern changes to bubble flow. This is in agreement with the fact that the higher interfacial tension should assist bubble formation. On the other hand, higher interfacial tension delays the transition to annular-drop flow.

Effect of Viscosity ratio on Flow Pattern Transitions

A comparison of fluid systems #2 and #5 shows that the interfacial tension is about the same order of magnitude (0.032 and 0.033 N/m, respectively) for both; however, the viscosity ratio differs considerably (31 and 1.3, respectively). Therefore, the shift of transition lines from one flow regime to another in these two systems as seen from Figures 10.1 and 10.14, could be attributed to the effect of viscosity ratio. This comparison shows that the transition line to bubble flow for the fluid system #2 is at a somewhat higher "liquid" velocity than for the fluid system #5. It is also interesting to note that a comparison of Figures 10.11 and 10.14 (fluid systems #3 and #5, respectively) shows the transition line to bubble flow is at approximately the same position. This may be due to a difference in interfacial tension (0.047 to 0.038 N/m, respectively). A comparison of Figures 10.1, 10.11, and 10.14 shows that the boundary line to annular flow for the fluid system #5 is at

about the same location, but with a small slope when compared to fluid systems #2 and #3.

Effect of Tube Diameter on Flow Pattern Transitions

To study this effect, O'Hearn (1988) has conducted equi-density fluid experiments in 12.7 mm ID tube for fluid system #3. The flow regimes observed are presented in Figure 10.15. A comparison of Figures 10.11 and 10.15 (25.4 and 12.7 mm ID, respectively) shows that tube diameter has a strong effect on the transition line to annular flow. However, the effect of diameter on the transition line to bubble flow doesn't seem very conclusive. The transition to annular flow occurs relatively at lower "vapor" velocities for 12.7 than 25.4 mm ID tube. Further work needs to be done in order to reach definite conclusions for this effect.

These experiments show that flow regimes can be generated by the use of two immiscible liquids of equal density, by controlling viscosity ratio, interfacial tension, and wettability characteristics, which would match with reasonable accuracy the flow regimes as predicted by the Taitel-Dukler and Weisman et al. models when extrapolated to micro-g levels. However, the validity of this technique can only be fully tested by comparing the simulated equi-density flow regimes against the actual micro-g vapor-liquid flow regime data. This aspect of the project will be discussed in Section B of this chapter.

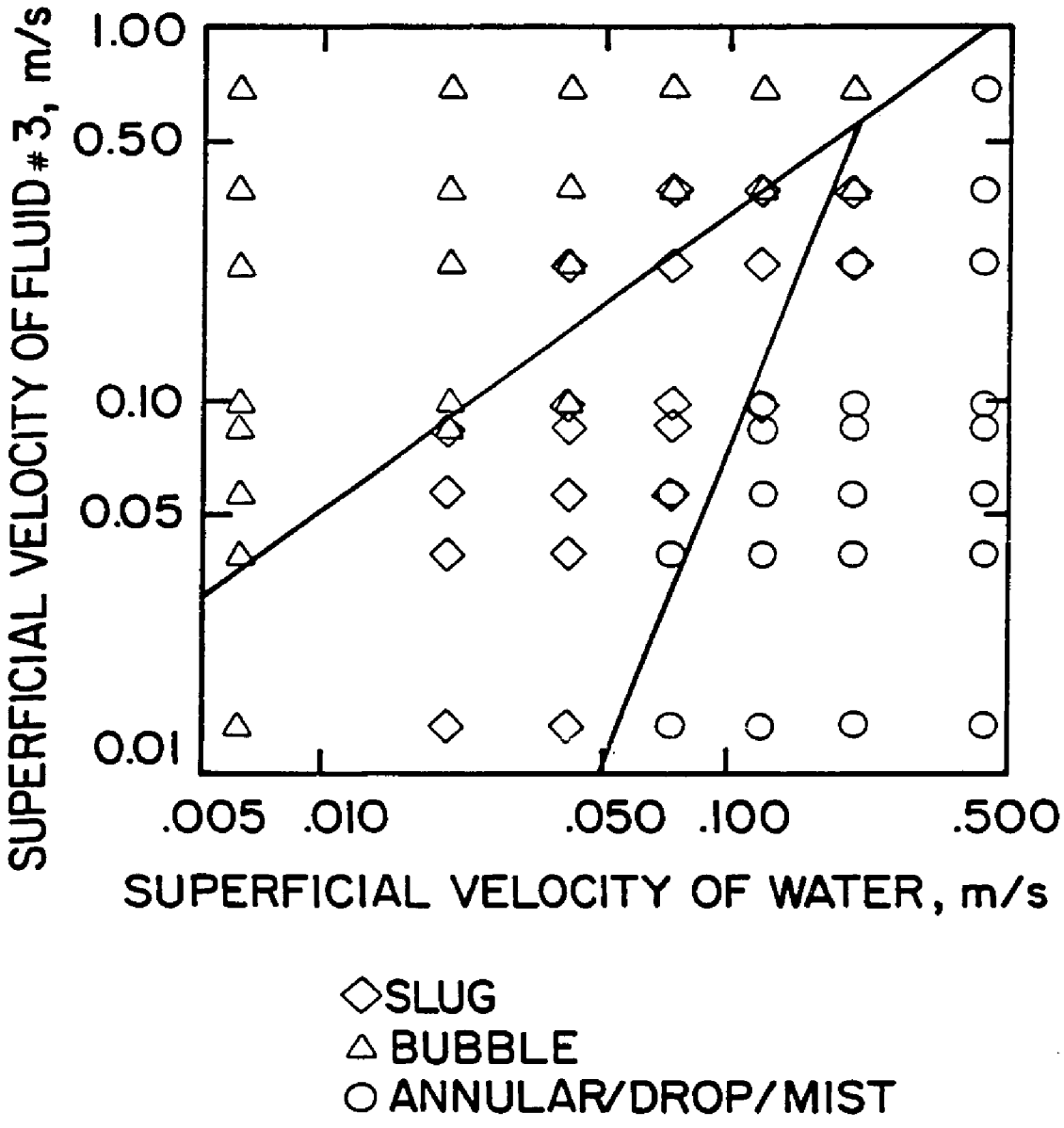

Figure 10.15: Simulated Micro-g Vapor-Liquid Flow Regime Map - Fluid System #3 (Equi-Density Dow Corning 200 Silicone Oil + CCl_4 and Water) on 12.7 mm ID tube.

Section B. Comparison of Simulated vs. Actual Micro-g Vapor-Liquid Flow Regime Data

Heppner et al. (1975) are the first research workers to perform the most extensive work on micro-gravity gas-liquid flow. They have conducted experiments to study the effect of gravity on flow regime transition boundaries and pressure drop. Two-phase flow of air and water in a tube of 2.54 cm ID and 25.4 cm long was examined first on earth, then in a KC-135 aircraft simulating micro-g for about 20 sec. per trajectory. The flow regimes observed are annular, slug, plug (elongated bubble), and bubble flow. Although the test section length was short and duplicate tests gave significantly different results, the work is a landmark study. Unfortunately, the original films apparently are no longer available. The only comparison that can be made is that our simulated experiments predicts the same type of flow patterns, namely, slug, bubble, and annular, as seen by Heppner et al.

In April, 1987, Hill et al. (1987) have conducted experiments in a NASA-JSC KC-135 using a very controlled instrumentation to study the effect of gravity on flow regime boundaries and pressure drop. Observations are made of an adiabatic two-phase flow of freon-114 in a tube of 1.58 cm ID and 1.83 m long (L/D = 116). The aircraft flies a series of parabolas to obtain the reduced gravity for about 25 sec. per parabola. Due to the short duration of each reduced gravity period, the experiments are conducted for three consecutive parabolas for the same operating conditions. The observation of flow regimes are made for different freon-114 qualities (5 to 80 % range). The flow regimes observed are typically classified into slug and annular

flows as shown in Figure 10.16. The flow regime data are presented on log-log plot with superficial momentum flux of both phases as coordinates. The bubble flow is not observed for the qualities they have studied. For freon-114 qualities below 10 percent, continuous liquid slug has been found to be interspersed with bubbles of high vapor void fraction. These bubbles take the form of classical Taylor bubbles which are bullet nosed and boat-tailed. Above about 15 percent, an annular flow has been observed. At the highest qualities, frothy annular-mist flow has been observed. Small dispersed bubbles in annular film are observed most of the time. They have also concluded that the boundary between slug and annular flow was best predicted by Taitel-Dukler (1976) model.

The transition lines for equi-density fluid system #3 are superimposed on Figure 10.16. An important transition on this flow regime map is the transition between annular type flow and slug flow. This transition line compares well with the Hill et al. data. The two data points indicating the slug flow lie within the simulated slug region.

The Dukler et al. (1987) have recently carried out air-water flow experiments both on the Lewis 30.5 m drop tower (9.5 mm ID and 0.457 m long test section and 2.2 seconds long micro-g period) and on the Lewis Learjet (12.7 mm ID and 1.06 m long test section and 12 - 22 seconds long micro-g period). The flow patterns as reported by studying the movie films obtained from both experimental setups, are: annular, slug, and bubble flows as shown in Figure 10.17. Data are presented on log-log plot with superficial momentum flux of both phases as coordinates. Solid (closed) triangles and diamonds show

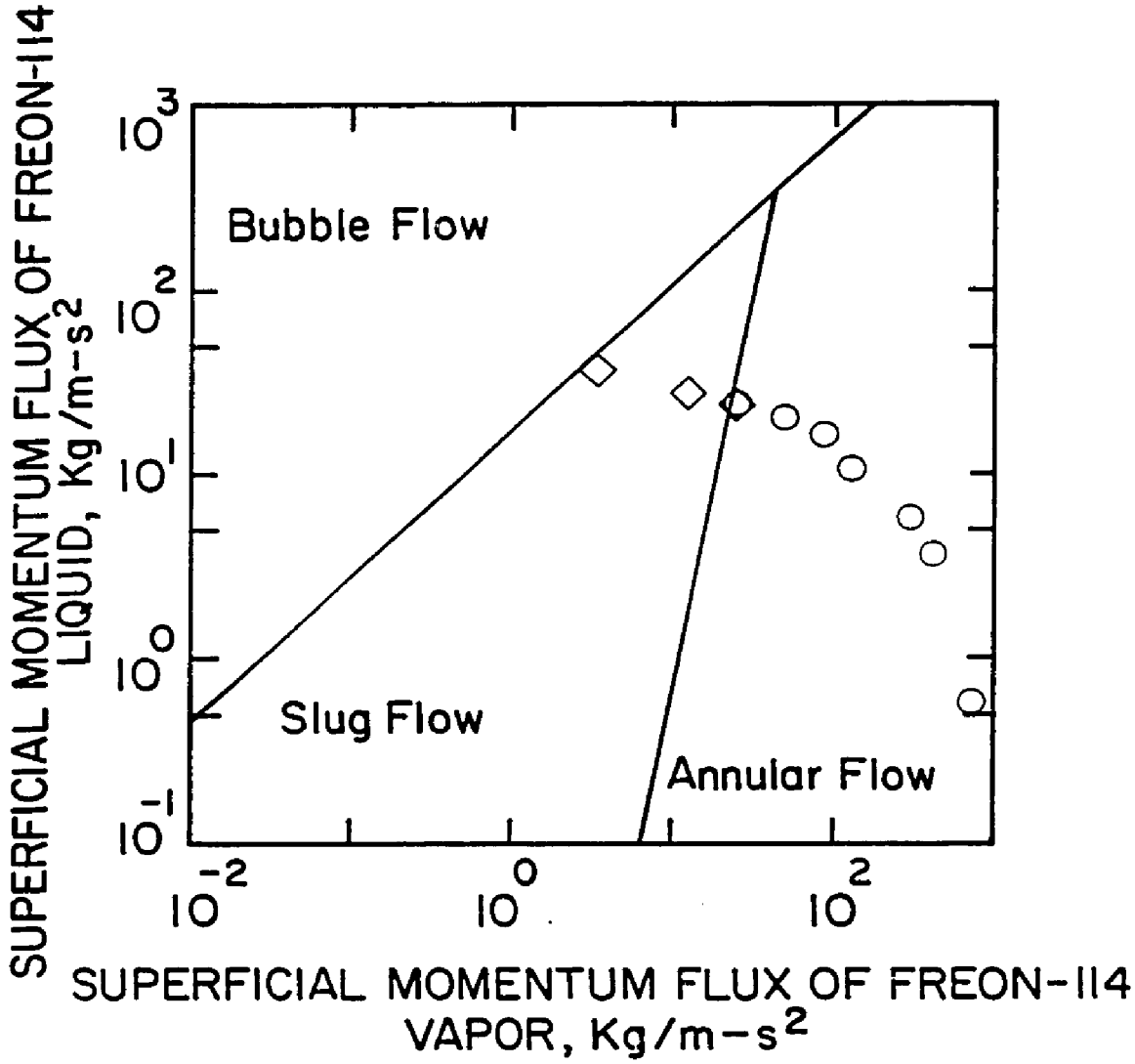

MICRO-g FREON-114 VAPOR-LIQUID FLOW REGIME DATA. HILL et al. (1987)

○ ANNULAR/DROP
△ BUBBLE
◇ SLUG
15.8 mm ID TUBE

TRANSITION LINES FROM SIMULATED EXPERIMENTAL DATA OF FLUID SYSTEM # 3 (25.4 mm ID TUBE)

Figure 10.16: Comparison of Simulated vs. Actual Micro-g Vapor-Liquid Flow Regime Data.

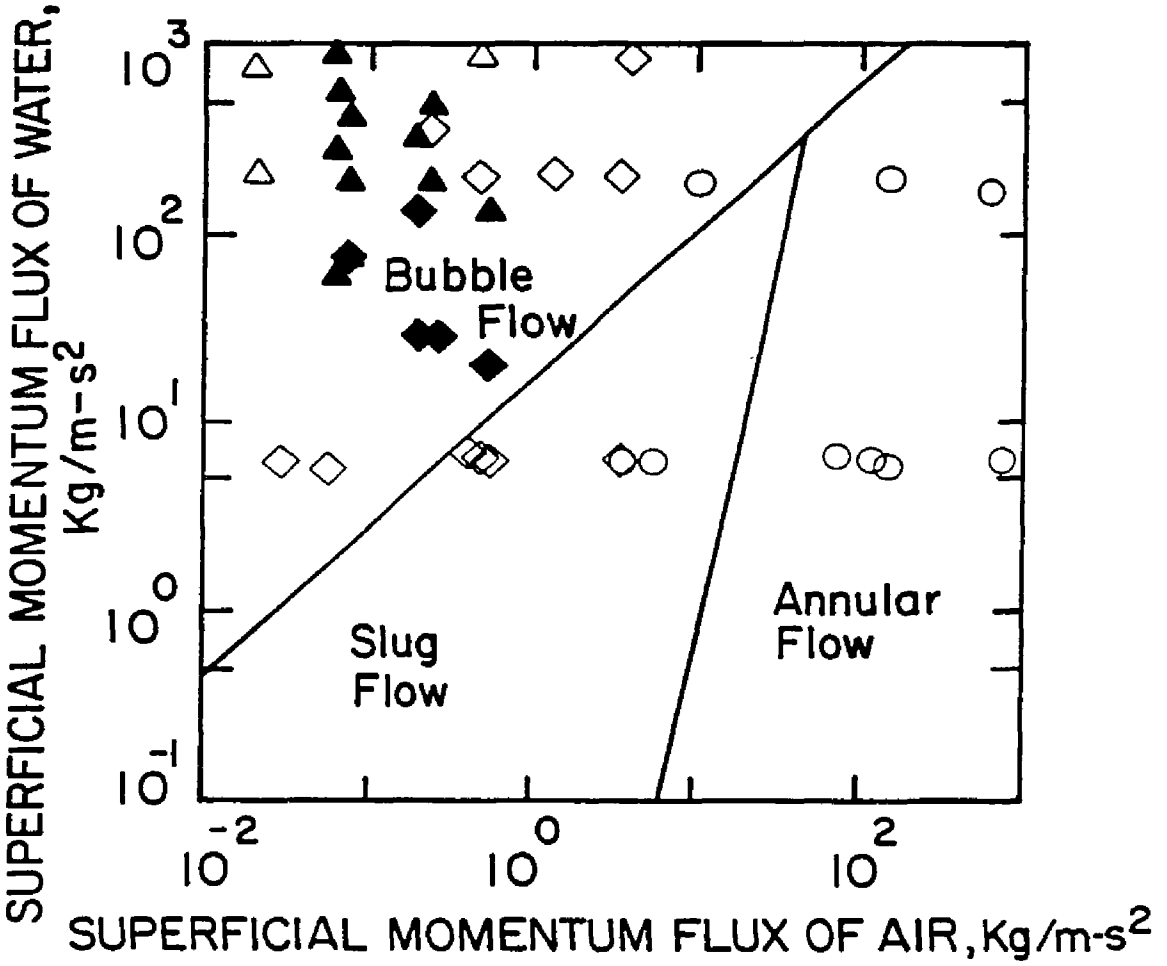

MICRO-g AIR-WATER FLOW REGIME DATA
DUKLER et al (1987)

ANNULAR/DROP
BUBBLE
SLUG
9.5-12.7 mm ID TUBE

TRANSITION LINES FROM SIMULATED EXPERIMENTAL DATA OF FLUID SYSTEM #3 (25.4 mm ID TUBE)

Figure 10.17: Comparison of Simulated vs. Actual Micro-g Vapor-Liquid Flow Regime Data.

the flow regimes obtained from drop tower tests, and the open symbols are data obtained from Learjet experiments.

The gradual transition lines from the flow regime map (Figure 10.11) for equi-density fluid system #3 are superimposed on Figure 10.17. A comparison of flow regime data between the actual micro-g air-water flow and simulated equi-density fluid system shows that the transition to annular flow is in reasonably good agreement; however, the slug-bubble transition for our simulation experiments appears to be occurring at lower liquid flow rates.

In April, 1987, Lovell et al. (1987) have conducted experiments in a NASA-JSC KC-135 to study the effect of gravity on flow regimes and pressure drop. Observations are made of boiling and condensation of water-steam system in a tube of 8 mm ID. The data are still being analyzed. The flow regimes are classified from a study of a high-speed imager videos. Figure 10.18 shows the hand tracings of different micro-g flow regimes from videos. The characteristics of these flow regimes are: bubble flow - well dispersed steam bubbles of varying size, slug flow - stable "Taylor" steam bubbles which are axisymmetric, bullet nosed, flat tailed and separated by clear liquid slugs, annular flow - the annular water film is very wavy with occassional large roll waves sweeping by at velocities approaching the steam velocity and importantly the film is considerably thicker and carries significant number of steam bubbles than for the typical one-g annular flows. To compare qualitatively the flow regimes in our simulation studies against those of actual micro-g flow regimes, the hand traces of different flow regimes of fluid system #3 from videos are presented in Figure 10.19. The comparison of Figures 10.18 and

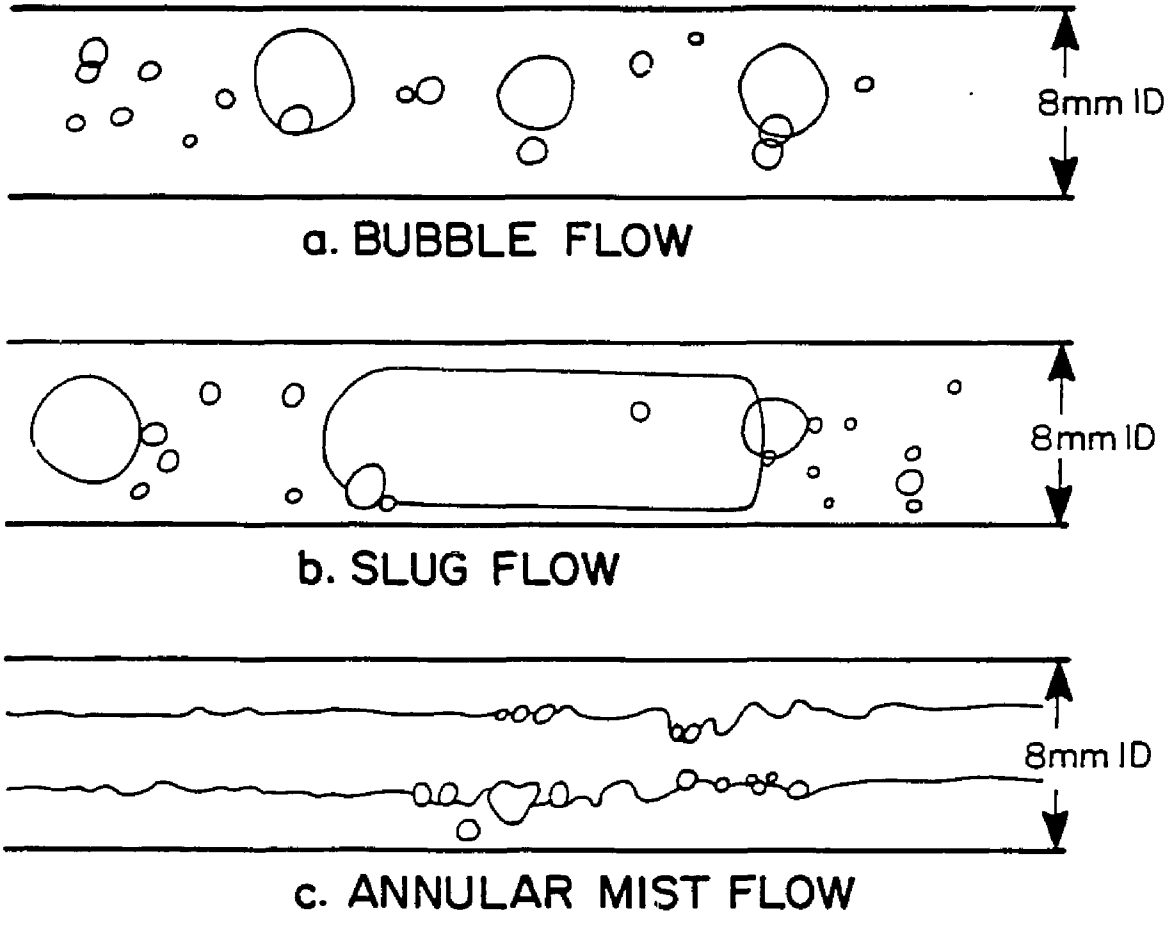

Figure 10.18: Flow Regimes of Water-Steam System in Actual Micro-g Environment.

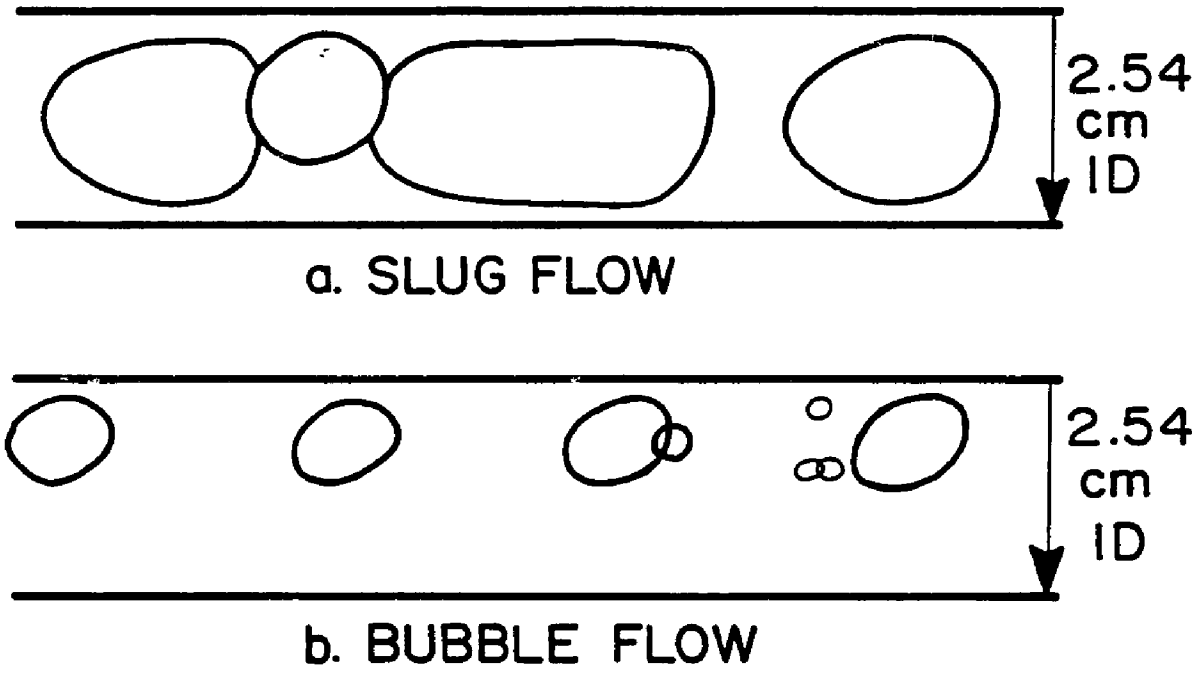

Figure 10.19: Flow Regimes of Fluid System #3 in Simulated Micro-g Environment.

10.19 show that the shape of simulated bubbles in slug flow are in good agreement. The size of bubbles in bubble flow appears to be uniform in our simulation experiments compared to wide distribution of sizes in actual micro-g experiments.

In conclusion, three flow regimes as predicted by our simulated experiments are the same as observed in the micro-g environment, namely, slug, bubble, and annular flows. The transition boundaries among these flow patterns, found in our simulated equi-density fluid systems, are in good agreement with those of actual micro-g vapor-liquid flow regime data. The actual vapor-liquid flow regime data taken under micro-g environment by two independent investigators for two different fluid systems are in good agreement with our simulated equi-density flow regime data.

A technique or method of simulating micro-g vapor-liquid flow has been proposed, discussed, and verified which permits the investigation of two-phase phenomena in a steady-state dynamic flow in a terrestrial laboratory for unlimited periods of time. Preliminary experimental results also show that this technique can be applied for predicting spacial distribution of vapor-liquid phases in a stationary system (please refer to Appendix C). The technique utilizes two immiscible liquids of equal density which in turn offers the possibility of eliminating the buoyancy forces and thus simulating micro-g vapor-liquid flow on earth. The validity of this technique has been confirmed in an experimental program by verifying the simulated data against actual micro-g vapor-liquid flow regime data taken either in a drop tower tests or an airplane trajectory. Finally, flow regime maps for vapor-liquid flow in a micro-g

environment have been developed for usage in designing two-phase systems for space applications.

XI. CONCLUSIONS AND SIGNIFICANCE

A technique or method of simulating micro-g vapor-liquid flow has been proposed, discussed, and verified which permits the investigation of two-phase phenomena in a steady-state dynamic flow in a terrestrial laboratory for a significant period of time. The simulated data obtained by using this technique are in good agreement with the actual vapor-liquid flow regime data taken under micro-g environment by two independent investigators for two different fluid systems.

The following conclusions can be drawn from this study: 1. Micro-gravity vapor-liquid flow can be simulated on earth by the use of two immiscible liquids of equal density, 2. The observed micro-g vapor-liquid flow regimes are: slug, bubble, and annular-mist, 3. Important controlling parameters in the equi-density fluid system are interfacial tension, relative wettability, and viscosity ratio between two fluids, 4. The predicted flow regime transition lines under micro-g conditions by the models of Taitel-Dukler and Weisman et al. differ considerably in type, size, and shape, 5. These model predictions show considerable deviation in flow regimes when compared against experimentally simulated micro-g vapor-liquid flow data, 6. These models need to be refined for micro-g applications, and 7. A comparison of simulated experimental data using equal density fluids against actual micro-g vapor-liquid flow regime data reveals that: a) there is an agreement on type of flow regimes, i.e., slug, bubble, and annular-mist, b) a flow regime map based on superficial momentum flux

coordinates shows better comparison, c) transition to annular flow regime is found to be in better agreement. Finally, the flow regime map for vapor-liquid flow in a micro-g environment has been developed for usage in designing two-phase systems in space applications.

In nucleate pool boiling, bubble departure radii from micro-g data of Siegel and Keshock (1964) are compared against predictions from the proposed static and dynamic force balance approach and five well known correlations. The static and dynamic force balance approach predictions are in good agreement with the experimental data. In particular, the overall effect of surface tension is to delay, not to assist, the bubble departure. The only data needed for predicting the departure radius are the wall superheat, contact angle, and the physical properties of the fluid system. In micro-gravity, the bubbles become quite large and the growth times are longer compared with those in earth gravity.

The side benefit of this study has been the development of a tensiometer to measure interfacial tension between two immiscible liquids of equal/unequal densities. This has been one of the major contributions to the overall project.

XII. RECOMMENDATIONS

The following recommendations are made:

1. For any improvement in this simulation technique, the wettability of liquids with respect to solid surfaces (adhesion tension) should be quantified. In simulating micro-g vapor-liquid flow, the relative wettability properties of equi-density liquids with respect to tube surface need to be matched in the order of magnitude to that of typical vapor-liquid systems. To achieve this, one would require to measure adhesion tension of fluids with respect to tube surface. A literature survey has revealed that there is no reliable instrument which could measure the wettability properties of fluids except measuring the contact angle. The contact angle only refects a qualitative measure, but not the quantitative measure of wettability of fluids. There is a great need to develop an instrument which can measure the adhesion tension of fluids with respect to solids. The applications of such an instrument would be many, such as in electronic material processing, material processing in space, and in the microscopic studies of different processes.

2. The region of interest of flow regime map in which gravity is the dominant force has been defined in this study based on a qualitative reasoning. It is recommended that further work be conducted to well define this gravity dominated region by considering all the forces acting on the two-phase system and comparing their relative orders of magnitude at different phase velocities. This may be accomplished by comparing the following dimensionless groups:

$$\text{Froude number, } Fr = \frac{\text{inertial}}{\text{gravitational}}$$

$$\text{Weber number, } We = \frac{\text{surface tension}}{\text{inertial}}$$

$$\text{Bond number, } Bo = \frac{\text{gravitational}}{\text{surface tension}}$$

$$\text{Grashof number, } Gr = \frac{\text{viscous}}{\text{gravitational}}$$

$$\text{Reynolds number, } Re = \frac{\text{inertial}}{\text{viscous}}$$

3. For a detailed verification of this simulation technique, there is a need for reliable vapor-liquid flow regime data taken in actual micro-g environemnt than available at present. Some studies have been conducted either in drop towers or in aircraft trajectories as discussed earlier in this thesis. Perhaps, the most reliable data could be obtained in either a space shuttle or space station. The advent of a space shuttle presents new opportunities for conducting reduced-gravity experiments for a longer duration of time under fully controlled conditions. Therefore, boiling and/or condensation, and adiabatic two-phase experiments with sensitive, accurate, and reliable intrumentation should be conducted in a space shuttle to augment the database for micro-g two-phase flow.

4. This simulation technique has potentialities to study the dynamic and/or static aspects of micro-g vapor-liquid flow by conducting earth based experiments. Preliminary studies on static vapor-liquid systems are presented in Appendix C. This technique can also be used to study the surface tension driven flow (Marangoni effect) which is significantly important in material processing in space (e.g., crystallization, electronic material processing, etc.). Marangoni effect causes a bubble/drop to move from a higher to lower interfacial

tension region. Interfacial tension decreases with an increase in temperature. This efect can be studied by taking two immiscible liquids 'A' and 'B' of equal density. Take a pool of liquid 'A' in a container and subject it to a series of hot and cold spots. This will establish steady state temperature contours in liquid 'A'. Inject a droplet of known size of liquid 'B' in the pool of liquid 'A'. The only forces acting on the system are surface forces. Temperature contours establish a gradient in interfacial tension. Therefore, the droplet will migrate from low to high temperature contours. Marangoni effect can be studied by monitoring the migration of such droplets. The parameters that may be studied are: droplet size, location of injection, container geometry, location of hot and cold spots, and different fluid systems.

LIST OF REFERENCES

Abou-Sabe, A.H., and H.A. Johnson, "Heat Transfer and Pressure Drop for Turbulent Flow of Air-Water Mixtures in Horizontal Pipe," *Trans. ASME*, **74**, 977 (1952).

Albers, J.A., and R.P. Macosko, "Experimental Pressure-Drop Investigation of Nonwetting, Condensing Flow of Mercury Vapor in a Constant-Diameter Tube in 1-G and Zero-Gravity Environments," *NASA TN D-2838* (1965).

Baker, O., "Simultaneous Flow of Oil and Gas," *Oil and Gas J.* **53**, 185 -195 (1954).

Bartell, F.E., and F.L. Miller,"A Method for the Measurement of Interfacial Tension of Liquid-Liquid Systems," *J. Amer. Chem. Soc.*, **58**, 1961 (1928).

Beer, H., P. Borrow, and R. Best, "Nucleate Boiling; Bubble Growth and Dynamics. *Heat Transfer in Boiling*," H.Hahne, and V. Grigull, Eds. New York: Academic Press, pp.21-52 (1977).

Bell, K.J., J. Taborek, and F. Fenoglio, "Interpretation of Horizontal In-Tube Condensation Heat Transfer Correlations witha Two-Phase Flow Regime Map," *Chem. Engng. Prog. Symp. Ser.*, **66** (102), 150-163 (1970).

Charles, M.E., G.W. Govier, and G.W. Hodgson, "The Horizontal Pipeline Flow of Equal Density Oil-Water Mixtures," *The Can. J. Chem. Engng.*, **39**, 27-36 (1961).

Choe, W.G., and J. Weisman, "Flow Patterns and Pressure Drop in Cocurrent, Vapor/Liquid flow," University of Cincinnati, Ohio, *NTIS No. PB-237261l AS* (1974).

Cochran, T.H., "Forced-Convection Boiling Near Inception in Zero Gravity," *NASA TN D-5612* (1970).

Cole, R., and H.L. Shulman, "Bubble Growth Rates at High Jakob Numbers," *Int. J. Heat Mass Transfer*, **2**, 1377-1390 (1966).

Cole, R., "Bubble Frequencies and Departure Volumes at Subatmospheric Pressures," *AIChE J.*, **13**, 779-783 (1967).

Collier, J.G., "*Convective Boiling and Condensation*," New York: McGraw-Hill (1972).

Congelliere, J.T., W. Unterberg, and E.B. Zwick, "The Zero-G Flow Loop: Steady Flow, Zero-Gravity Simulation for Investigation of Two-Phase Phenomena," *Advances in Astronautical Sciences*, **14**, 223-263 (1963).

Cooper, M.G., A.M. Judd, and R.A. Pike, "Shape and Departure of Single Bubbles Growing at a Wall," Paper presented at the *Sixth International Heat Transfer Conference*, August 7-11, Toronto, Canada (1978).

Dukler, A.E., J.A. Fabre, J.B. Quillen, and R. Vernon, "Gas-Liquid Flow at Microgravity Conditions and their Transitions," Paper presented at *ASME Annual Meeting*, December 12-17, Boston, Massachussetts (1987).

Eastman, R.E., C.J. Feldmanis, W.L. Haskin, and K.L. Weaver, "Two-Phase Fluid Thermal Transport for Spacecraft," *AFWAL-TR-84-3028* (1984).

Feldmanis, J.C., "Pressure and Temperature Changes in Closed Loop Forced Convection Boiling and Condensing Processes Under Zero-Gravity Conditions," *Proc. Inst. Environ. Sci.*, April (1966).

Goldmann, K., H. Firstenberg, and C. Lombardi, "Burnout in Turbulent Flow - A Droplet Diffusion Model," *Trans. ASME J. Heat Transfer*, **83C**, 158 (1961).

Govier, G.W., and W.L. Short, "The Upward Vertical Flow of Air-Water Mixtures," *Can. J. Chem. Engng.*, **36**, 195 (1958).

Griffith, P., and G.B. Wallis, "Two-Phase Slug Flow," *Trans. ASME, J. Heat Transfer*, **83C**, 307 (1961).

Harkins, W.D., and E.C. Humphrey,"Surface Tension at Interface between 2 Liquids," *J. Amer. Chem. Soc.*, **38**, 228 (1916).

Hatton, A.P., and I.S. Hall, "Photographic Study of Boiling on Prepared Surfaces," *Proc. 3rd Int. Heat Trans. Conf., Chicago,* **IV**, 24-37 (1966).

Heppner, D.B., C.D. King, and J.W. Littles, "Zero-G Experiments in Two-Phase Fluid Flow Regimes," *ASME paper 75-ENAs-24* (1975).

Hewitt, G.F., "Liquid-Gas Systems," in *Handbook of Multiphase Flow* (Editor G. Hetsroni), Chapter 2, Washington, D.C.: Hemisphere (1981).

Hewitt, G.F., and D.N. Roberts, "Studies of Two-Phase Flow Patterns by Simultaneous X-Ray and Flash Photography," Report *AERE-M2159* (1969).

Hill, D., R.S. Downing, D. Rogers, D. Teske, and R. Niggeman, "A Study of Two-Phase Flow in a Reduced Gravity Environment," Final Report Under Contrac No. *NAS9-17195* (1987).

Hoogendoorn, C.J., "Gas-Liquid Flow in Horizontal Pipes," *Chem. Engng. Sci.*, **2**, 205 (1959).

Hsu, Y.Y., and R.W. Graham, "Transport Processes in Boiling and Two -Phase Systems," *Hemisphere Publishing*, Washington, D.C. (1976).

Jeffreys, H., "On the Formation of Water Waves by Wind," *Proc. Royal Soc.*, **A 107**, 189 (1925).

Jeffreys, H., "On the Formation of Water Waves by Wind (second paper)," *ibid., Proc. Royal Soc.*, **A110**, 241 (1926).

Jensen, M.K., and G.J. Memmel, "Evaluation of Bubble Departure Diameter Correlations," *Proc. 8th Int. Heat Trans. Conf.*, San Francisco, **4**, 1907-1912 (1986).

Karri, S.B.R., and V.K. Mathur, "Two-Phase Flow Regime Map Predictions Under Microgravity," *AIChE J.*, **34**, 137-139 (1988).

Karri, S.B.R., and V.K. Mathur, "Measurement of Interfacial Tension of Immiscible Liquids of Equal Density," *AIChE J.*, **34**, 155-157 (1988).

Karri, S.B.R., and V.K. Mathur,"Study of Simulated Micro-Gravity Vapor-Liquid Flow Regimes," *Annual AIChE Meeting*, New York, November 15-20, (1987).

Keshock, E.G., G. Spencer, and B.L. French, "A Photographic Study of Flow Condensation in 1-G and Zero-Gravity Environments," Paper presented at the *Fifth International Heat Transfer Conference*, September 3-7, Tokyo, Japan (1974).

Krotiuk, W.J., and Z.I. Antoniak, "Thermal Hydraulic Assessment Report for the Multimegawatt Space Nuclear Power Program," Vol. 1 and 2, *PNL-6061 UC-80* (1986).

Kubie, J., "The Presence of Slug Flow in Horizontal Two-Phase Flow," *Int. J. Multiphase Flow*, **5**, 327-339 (1979).

Kutateladze, S.S., and I.I. Gogonin, "Growth Rate and Detachment Diameter of a Vapor Bubble in Free Convection Boiling of a Saturated Liquid," *High Temperature*, **17**, 667-671 (1979).

Labus, T.L., J,C, Aydelott, and R.F. Lacovic, "Low-Gravity Venting of Refrigerant-11," *NASA TM X-2479* (1972).

Lovell, T., W.J. Krotiuk, and F. Best, Personal Communication (1987).

Mahefkey, T., "Military Spacecraft Thermal Management; The Evolving Requirements and Challenges," *AIAA-82-0827* (1982).

Mandhane, J.M., G.A. Gregory, and K. Aziz, "A Flow Pattern Map for Gas-Liquid Flow in Horizontal Pipes," *Int. J. Multiphase Flow*, **1**, 537-553 (1974).

Namkoong, D., H.B. Block, and R.P. Macosko, "Photographic Study of Condensing Mercury in 0 and 1 g environments," *NASA TN D-4023* (1967).

NASA, "Spacelab 3," *EP203* (1984).

O'Hearn, J., "Effect of Tube Diameter on Flow Regime Transitions at

Micro-Gravity," M.S. Thesis to be submitted to *The University of New Hampshire*, Durham, NH (1988).

Oker, E., and H. Merte, Jr., "Transient Boiling Heat Transfer in Saturated Liquid Nitrogen and F-113 at Standard and Zero Gravity," *NASA CR-120202* (1973).

Petukhov, B.S., and V.G. Zhilin, "Heat Transfer in Turbulent Flow of Liquid Metals in a Magnetic Field," In Heat Transfer in Liquid Metals, ed. O.E. Dwyer, pp.553-568, *Progress in Heat and Mass Transfer*, Vol. **7**, Pergamon Press, New York (1973).

Pike, R.A., *Ph.D. Thesis*, Cambridge University (1977).

Reynolds, W.C.,"Interfacial Tension: Statical Measurement of Interfacial Tension in Absolute Units," *Trans. Chem. Soc.*, **119**, 460 (1921).

Rouhani, S.Z., and M.S. Sohal, "Two-Phase Flow Patterns: A Review of Research Results," *Progress in Nuclear Energy*, **11**, No. 3, 219-259 (1983).

Ruckenstein, E., "A Physical Model for Nucleate Boiling Heat Transfer from a Horizontal Surface," *Bul. Institutului Politech. Bucaresti*, **33**, No. 3, pp.79 (1961); AMR, 16, Rev. 6055 (1963).

Salzman, J.A., "Two-Phase Fluid Management Technology Base," Paper presented at the *NASA In-Space Research, Technology, and Engineering Workshop*, October 8-10, Williamsburg, Virginia (1985).

Schroter, J., Dipl. Arbeit, *Hochschule Dortmund* (1962).

Siegel, R., "Effects of Reduced Gravity on Heat Transfer," In *Advances in Heat Transfer*, Vol. **4**, 143-228, Academic Press, New York (1967).

Siegel, R., and E.G. Keshock, "Effects of Reduced Gravity on Nucleate Boiling Bubble Dynamics in Saturated Water," *AIChE J.*, **10**, 509-517 (1964).

Taitel, Y., D. Barnea, and A.E. Dukler, "Modeling Flow Pattern Transitions for Steady Upward Gas-Liquid Flow in Vertical Tubes," *AIChE J.*, **26**, 345-354 (1980).

Taitel, Y, and A.E. Dukler, "A Model for Predicting Flow Regime Transitions for Steady Upward Gas-Liquid Flow in Vertical Tubes," *AIChE J.*, **22**, 47-55 (1976).

Weisman, J., and S.Y. Kang, "Flow Pattern Transitions in Vertical and Upwardly Inclined Tubes," *Int. J. Multiphase Flow*, **7**, 271-291 (1981).

Weisman, J., D. Duncan, J. Gibson, and T. Crawford, "Effects of Fluid Properties and Pipe Diameter on Two-Phase Flow Patterns in Horizontal Lines," *Int. J. Multiphase Flow*, **5**, 437-462 (1979).

White, P.D., and R.L. Huntington, "Horizontal Co-Current Two-Phase Flow of Fluids in Pipe Lines," *Pet. Engr.*, D-40 (1955).

Wilcox, W.R., et al., "A Preliminary Analysis of the Data from Experiment 77-13 and Final Report on Glass Fining Experiments in Zero Gravity," *NASA CR-161884* (1981).

Williams, J.L, "Space Shuttle Orbiter Mechanical Refrigeration System," *NASA CR-144395* (1974).

Williams, J.L., E.G. Keshock, and C.L. Wiggins, "Development of a Direct Condensing Radiator for Use in a Spacecraft Vapor Compression Refrigeration System," *Trans. ASME J. Eng. for Ind.*, p. 1053 (1973).

Zuidema, H.H., and G.W. Waters,"Determination of Interfacial Tension," *Ind. & Eng. Chem.*, **13**, 312 (1941).

APPENDIX A.

APPENDIX A

EXPERIMENTAL VAPOR-LIQUID FLOW REGIME DATA

Table A.1: Fluid System #1 Runs

U_{Gs} (m/s)	U_{ls} (m/s)	FLOW PATTERNS	$\Delta P/\Delta L$, $x10^3$ ft. water/foot
	0.010	INVERSE ANNULAR	2.64
	0.039	INVERSE ANNULAR	6.59
	0.082	INVERSE ANNULAR	3.28
	0.134	INVERSE ANNULAR	5.27
0.025	0.168	INVERSE ANNULAR	7.46
	0.209	INVERSE ANNULAR	9.65
	0.283	INVERSE ANNULAR	14.3
	0.358	INVERSE ANNULAR	20.9
	0.462	BUBBLE	---
	0.010	INVERSE ANNULAR	2.19
	0.039	INVERSE ANNULAR	5.14
	0.082	INVERSE ANNULAR	4.37
	0.134	INVERSE ANNULAR	3.51
0.042	0.168	INVERSE ANNULAR	--
	0.209	INVERSE ANNULAR	10.97
	0.283	INVERSE ANNULAR	18.8
	0.358	BUBBLE	19.6
	0.462	BUBBLE	20.2
	0.010	DROP	1.11
	0.039	INVERSE SLUG/ANNULAR	2.00
	0.082	INVERSE SLUG/ANNULAR	2.67
	0.134	INVERSE ANNULAR	3.56
0.075	0.209	INVERSE ANNULAR	4.23
	0.283	INVERSE ANNULAR	7.34
	0.358	INVERSE ANNULAR	10.9
	0.462	BUBBLE	14.2
	0.522	BUBBLE	19.1
	0.010	DROP	1.36
	0.039	DROP	2.04
	0.082	INVERSE SLUG	2.45
0.12	0.134	INVERSE ANNULAR	3.40
	0.209	INVERSE ANNULAR	4.62
	0.283	INVERSE ANNULAR	5.71
	0.358	INVERSE ANNULAR	7.88
	0.010	DROP	3.02
	0.039	DROP	3.75
	0.082	DROP	4.89
	0.134	DROP	5.81
0.208	0.209	DROP/INVERSE ANNULAR	6.77
	0.283	DROP/INVERSE ANNULAR	8.45
	0.358	INVERSE ANNULAR	10.9
	0.462	INVERSE ANNULAR	13.0

	0.522	INVERSE ANNULAR	16.0
	0.010	DROP/MIST	10.9
	0.039	DROP/MIST	12.8
	0.082	DROP/MIST	14.5
	0.134	DROP/MIST	15.8
0.436	0.209	DROP/MIST	16.9
	0.283	DROP/MIST	18.8
	0.358	DROP/MIST	21.0
	0.462	DROP/MIST	23.3
	0.522	DROP/MIST	26.7

Table A.2: Fluid System #2 Runs

U_{Gs} (m/s)	U_{ls} (m/s)	FLOW PATTERNS	$\Delta P/\Delta L$, x10^3 ft. water/foot
	0.007	SLUG	2.17
	0.022	SLUG	4.35
	0.044	SLUG	7.88
	0.075	BUBBLE	11.7
0.006	0.114	BUBBLE	17.4
	0.132	BUBBLE	18.2
	0.338	BUBBLE	46.2
	0.461	BUBBLE	75.0
	0.007	SLUG	2.72
	0.022	SLUG	6.52
	0.044	SLUG	11.1
	0.075	SLUG	15.5
0.021	0.114	SLUG	21.5
	0.132	BUBBLE	21.7
	0.338	BUBBLE	47.5
	0.461	BUBBLE	81.0
	0.007	SLUG	2.72
	0.022	SLUG	5.98
	0.044	SLUG	10.3
	0.075	SLUG	13.9
0.042	0.114	SLUG	19.8
	0.132	SLUG	24.5
	0.338	BUBBLE	54.3
	0.461	BUBBLE	86.3
	0.693	BUBBLE	121.0
	0.007	ANNULAR-DROP	--
	0.022	SLUG/ANNULAR-DROP	5.71
	0.044	SLUG	9.24
	0.075	SLUG	14.9
0.075	0.114	SLUG	19.0
	0.132	SLUG	34.5
	0.338	SLUG	63.0
	0.461	BUBBLE	92.1
	0.693	BUBBLE	127.0
	0.007	ANNULAR-DROP	2.72
	0.022	ANNULAR-DROP	7.88
	0.044	ANNULAR-DROP	6.52
	0.075	ANNULAR-DROP	13.3
0.124	0.114	ANNULAR-DROP	--
	0.132	ANNULAR-DROP	30.4
	0.338	ANNULAR-DROP	69.0
	0.461	BUBBLE	86.0
	0.007	ANNULAR-DROP	5.43
	0.022	ANNULAR-DROP	5.98
	0.044	ANNULAR-DROP	7.06
	0.075	ANNULAR-DROP	7.34
0.207	0.114	ANNULAR-DROP	8.15

	0.132	ANNULAR-DROP	10.1
	0.338	ANNULAR-DROP	23.0
	0.461	ANNULAR-DROP	63.0
	0.693	BUBBLE	207.0
	0.007	ANNULAR-MIST	16.6
	0.022	ANNULAR-MIST	18.2
	0.044	ANNULAR-MIST	19.8
	0.075	ANNULAR-MIST	19.8
0.436	0.114	ANNULAR-MIST	20.9
	0.132	ANNULAR-MIST	26.0
	0.338	ANNULAR-MIST	34.5
	0.461	ANNULAR-MIST	49.0
	0.693	ANNULAR-MIST	58.0

Table A.3: Fluid System #3 Runs

U_{Gs} (m/s)	U_{ls} (m/s)	FLOW PATTERNS	$\Delta P/\Delta L$, $x10^3$ ft. water/foot
	0.006	SLUG	2.56
	0.015	SLUG	3.52
	0.034	SLUG/BUBBLE	7.36
	0.053	BUBBLE	11.2
0.006	0.087	BUBBLE	15.7
	0.094	BUBBLE	17.9
	0.253	BUBBLE	45.1
	0.403	BUBBLE	74.5
	0.006	SLUG	3.20
	0.015	SLUG	8.14
	0.034	SLUG	11.8
	0.053	SLUG	14.4
	0.087	SLUG	20.8
0.021	0.094	BUBBLE	22.7
	0.253	BUBBLE	50.0
	0.403	BUBBLE	75.0
	0.557	BUBBLE	108.0
	0.762	BUBBLE	150.0
	0.006	SLUG	3.52
	0.015	SLUG	8.0
	0.034	SLUG	11.0
	0.053	SLUG	12.0
	0.087	SLUG	14.0
0.042	0.094	SLUG	26.0
	0.253	BUBBLE	55.0
	0.403	BUBBLE	88.1
	0.557	BUBBLE	122.0
	0.762	BUBBLE	156.0
	0.006	ANNULAR-DROP	3.0
	0.015	SLUG	10.0
	0.034	SLUG	13.0
	0.053	SLUG	20.0
	0.087	SLUG	26.0
0.075	0.094	SLUG	28.0
	0.253	BUBBLE	61.0
	0.403	BUBBLE	95.0
	0.557	BUBBLE	122.0
	0.006	ANNULAR-DROP	6.4
	0.015	ANNULAR-DROP	6.4
	0.034	ANNULAR-DROP	6.4
	0.053	ANNULAR-DROP	12.0
	0.087	SLUG/ANNULAR-DROP	45.0
0.125	0.094	SLUG/ANNULAR-DROP	37.0
	0.253	SLUG	74.5
	0.403	SLUG	102.0
	0.557	SLUG/BUBBLE	135.0
	0.762	BUBBLE	170.0

	0.006	ANNULAR-DROP	6.4
	0.015	ANNULAR-DROP	7.0
	0.034	ANNULAR-DROP	8.0
	0.053	ANNULAR-DROP	9.0
	0.087	ANNULAR-DROP	11.0
0.208	0.094	ANNULAR-DROP	12.0
	0.253	ANNULAR-DROP	45.0
	0.403	ANNULAR-DROP	108.0
	0.557	ANNULAR-DROP/BUBBLE	156.0
	0.762	BUBBLE	183.0
	0.006	ANNULAR-MIST	16.0
	0.015	ANNULAR-MIST	20.0
	0.034	ANNULAR-MIST	20.0
	0.053	ANNULAR-MIST	21.0
	0.087	ANNULAR-MIST	22.7
0.436	0.094	ANNULAR-MIST	23.0
	0.253	ANNULAR-MIST	37.0
	0.403	ANNULAR-MIST	54.0
	0.557	ANNULAR-MIST	88.1
	0.762	ANNULAR-DROP	142.3

Table A.4: Fluid System #4 Runs

U_{Gs} (m/s)	U_{ls} (m/s)	FLOW PATTERNS	$\Delta P/\Delta L$, $x10^3$ ft. water/foot
	0.006	SLUG (UNSTABLE)	0.32
	0.015	SLUG (")	0.96
	0.034	SLUG (")	1.6
	0.053	SLUG (")	4.2
0.006	0.087	SLUG (")	7.4
	0.094	SLUG (")	9.9
	0.253	BUBBLE	47.0
	0.403	BUBBLE	74.5
	0.557	BUBBLE	95.0
	0.762	BUBBLE	142.0
	0.006	SLUG (UNSTABLE)	0.64
	0.015	SLUG (")	0.96
	0.034	SLUG (")	0.96
	0.053	SLUG (")	1.92
	0.087	SLUG (")	2.88
0.021	0.094	BUBBLE	11.2
	0.253	BUBBLE	42.0
	0.403	BUBBLE	61.0
	0.557	BUBBLE	88.0
	0.762	BUBBLE	115.0
	0.006	ANNULAR-DROP	0.64
	0.015	ANNULAR-DROP	0.64
	0.034	SLUG	1.3
	0.053	SLUG	3.52
	0.087	SLUG/ANNULAR-DROP	9.6
0.042	0.094	SLUG	9.0
	0.253	ANNULAR-DROP/BUBBLE	47.3
	0.403	BUBBLE	67.7
	0.557	BUBBLE	88.1
	0.006	ANNULAR-DROP	0.96
	0.015	ANNULAR-DROP	1.6
	0.034	ANNULAR-DROP	1.6
	0.053	SLUG	2.2
	0.087	SLUG	2.9
0.075	0.094	SLUG	4.2
	0.253	ANNULAR-DROP	61.0
	0.403	ANNULAR-DROP	81.3
	0.557	ANNULAR-DROP/BUBBLE	129.0
	0.006	ANNULAR-DROP	4.5
	0.015	ANNULAR-DROP	1.9
	0.034	ANNULAR-DROP	1.9
	0.053	ANNULAR-DROP	2.2
	0.087	ANNULAR-DROP	4.5
0.125	0.094	ANNULAR-DROP	5.4
	0.253	SLUG	17.0
	0.403	BUBBLE	47.4
	0.557	BUBBLE	129.0

	0.006	ANNULAR-MIST	2.9
	0.015	ANNULAR-MIST	2.9
	0.034	ANNULAR-MIST	3.2
	0.053	ANNULAR-MIST	3.5
	0.087	ANNULAR-MIST	5.1
0.208	0.094	ANNULAR-MIST	5.8
	0.253	ANNULAR-MIST	13.8
	0.403	ANNULAR-DROP	33.9
	0.557	BUBBLE	47.4

Table A.5: Fluid System #5 Runs

U_{Gs} (m/s)	U_{ls} (m/s)	FLOW PATTERNS	$\Delta P/\Delta L$, $x10^3$ ft. water/foot
	0.014	SLUG	0.96
	0.040	BUBBLE	1.28
	0.078	BUBBLE	1.28
0.006	0.135	BUBBLE	1.9
	0.272	BUBBLE	8.0
	0.409	BUBBLE	11.8
	0.579	BUBBLE	20.2
	0.014	SLUG	0.91
	0.040	SLUG	1.28
	0.078	SLUG/BUBBLE	1.60
0.021	0.135	BUBBLE	2.2
	0.272	BUBBLE	8.6
	0.409	BUBBLE	12.5
	0.579	BUBBLE	22.7
	0.014	ANNULAR-DROP/SLUG	0.96
	0.040	SLUG	1.28
	0.078	SLUG	1.92
0.042	0.135	SLUG	2.2
	0.272	BUBBLE	8.96
	0.409	BUBBLE	14.4
	0.579	BUBBLE	24.6
	0.014	ANNULAR-DROP	0.96
	0.040	SLUG	1.92
	0.078	SLUG	2.56
0.042	0.135	SLUG	3.84
	0.272	SLUG/BUBBLE	8.96
	0.409	BUBBLE	13.8
	0.579	BUBBLE	27.2
	0.014	ANNULAR-DROP	2.6
	0.040	ANNULAR-DROP	2.9
	0.078	ANNULAR-DROP	3.5
0.125	0.135	ANNULAR-DROP/SLUG	8.6
	0.272	SLUG	11.8
	0.409	BUBBLE	19.5
	0.579	BUBBLE	31.3
	0.014	ANNULAR-DROP	3.2
	0.040	ANNULAR-DROP	3.8
	0.078	ANNULAR-DROP	5.1
0.210	0.135	ANNULAR-DROP	8.0
	0.272	BUBBLE	16.3
	0.409	BUBBLE	24.0
	0.579	BUBBLE	34.2
	0.014	ANNULAR-MIST	13.1
	0.040	ANNULAR-MIST	13.4
	0.078	ANNULAR-MIST	17.6
0.436	0.135	ANNULAR-MIST	21.8
	0.272	ANNULAR-MIST	29.4
	0.409	ANNULAR-MIST	33.9

The flow rates in Table A.6 to Table A.9 are based on tube diameter of 1 inch.

Table A.6: Calibration of Flow Meter for Fluid #1
Brooks Flow Meter : Sl. No. 7305-49938

Scale Reading	Flow Rate, m/s
10	0.0096
20	0.0396
30	0.0821
40	0.1342
45	0.1680
50	0.2087
60	0.2834
70	0.3579
80	0.4624
90	0.5220

Table A.7: Calibration of Flow Meters for Fluid #2

a. Brooks Flow Meter : Sl. No. 7305-49938

Scale Reading	Flow Rate, m/s
10	0.1316
20	0.3382
30	0.4605
40	0.6930
50	0.8857

b. Fisher&Porter Flow Meter : Sl. No. A-4578

Scale Reading	Flow Rate, m/s
5	0.0067
10	0.0218
15	0.0439
20	0.0748
25	0.1144

Table A.8: Calibration of Flow Meters for Fluid #3

a. Brooks Flow Meter : Sl. No. 7305-49938

Scale Reading	Flow Rate, m/s
10	0.0939
20	0.2528
30	0.4034
40	0.5572
50	0.7615

b. Fisher&Porter Flow Meter : Sl. No. A-4578

Scale Reading	Flow Rate, m/s
5	0.0055
10	0.0154
15	0.0336
20	0.0525
25	0.0868

Table A.9: Calibration of Flow Meters for Fluid #5

a. Brooks Flow Meter : Sl. No. 7305-49938

Scale Reading	Flow Rate, m/s
10	0.272
14	0.409
20	0.579
30	0.866

b. Fisher&Porter Flow Meter : Sl. No. A-4578

Scale Reading	Flow Rate, m/s
15	0.1157
17	0.1354

c. Fisher&Porter Small Flow Meter : No Identification

Scale Reading	Flow Rate, m/s
20	0.014
50	0.040
80	0.061
100	0.078

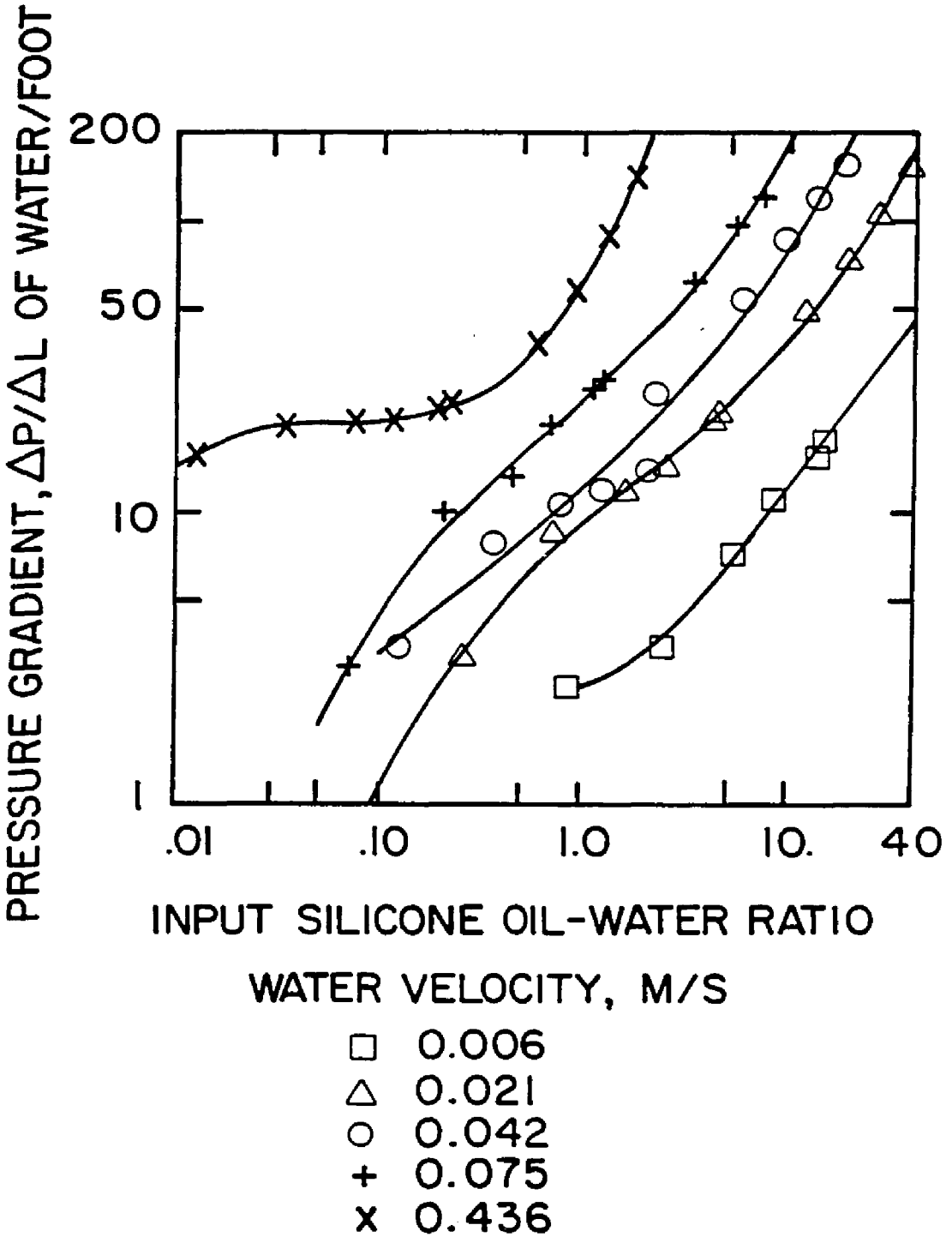

Figure A.1 : Pressure Gradients for Fluid System #3 as a Function of the Input Water-Oil Ratio and Waer Velocity.

APPENDIX B.

APPENDIX B.

Equilibrium Annular Flow in Micro-Gravity

In the literature review (Chapter II), it is reported that the annular flow is a common flow regime under micro-g conditions. The process of analyzing the transitions between flow regimes can be viewed to start from the condition of annular flow, and then to determine the mechanism by which a transition from annular flow to either a slug or bubble flow would take place. The development of mathematical equations to describe these transition lines is beyond the scope of this thesis. However, this analysis would not only help in drawing similitude between simulated and actual micro-g vapor-liquid flow but could also become the starting point for deriving equations to describe the transitions lines.

Consider an equilibrium annular flow as shown in Figure B.1. The orientation of the pipe is unimportant due to the absence of gravity component. A momentum balance on each phase yields:

$$\text{Liquid:} \quad -A_l\left[\frac{dP}{dx}\right] - \tau_l S_l + \tau_i S_i = 0 \tag{B.1}$$

$$\text{Vapor:} \quad -A_G\left[\frac{dP}{dx}\right] - \tau_i S_i = 0 \tag{B.2}$$

Equating the pressure drop in the two phases gives the following results

$$\tau_l \frac{S_l}{A_l} - \tau_i S_i \left[\frac{A_l A_G}{A_l + A_G}\right] = 0 \tag{B.3}$$

where geometrical parameters are given by

$$A_l = \frac{\pi}{4}(D^2 - d^2) \quad \text{and} \quad A_G = \frac{\pi}{4} d^2 \tag{B.4}$$

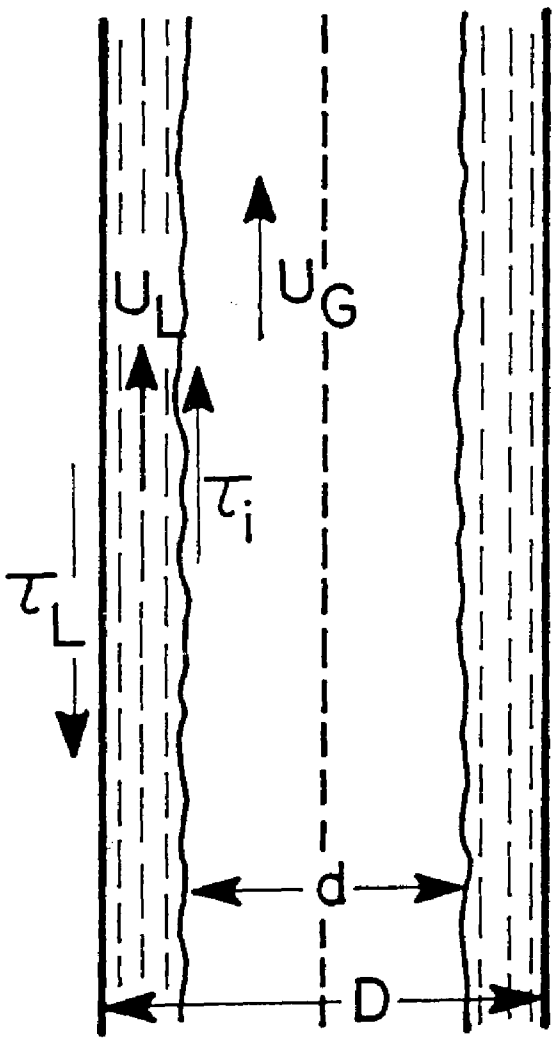

Figure B.1 : Annular Vapor-Liquid Flow in a Micro-g Environment

$$S_l = \pi D \qquad \text{and} \qquad S_i = \pi d \tag{B.5}$$

Substituting these in equation B.3 and upon simplifying gives

$$\tau_l = \tau_i \, D/d \tag{B.6}$$

The shear stresses are evaluated in a conventional manner with U being the average phase velocity

$$\tau_l = f_l \frac{\rho_l U_l^2}{2} \quad \text{and} \quad \tau_i = f_i \frac{\rho_G (U_G - U_i)^2}{2} \approx f_G \frac{\rho_G U_G^2}{2} \tag{B.7}$$

with the liquid and vapor friction factors evaluated from

$$f_l = C_l \left[\frac{D_l U_l}{\nu_l}\right]^{-n} \quad \text{and} \quad f_G = C_G \left[\frac{D_G U_G}{\nu_G}\right]^{-m} \tag{B.8}$$

where D_l and D_G are the hydraulic diameter evaluated from

$$D_l = \frac{4A_l}{S_l} = D - d \quad \text{and} \quad D_G = \frac{4A_G}{S_G + S_i} = d \tag{B.9}$$

In this work, the following coefficients were utilized: $C_G = C_l = 0.046$, $n = m = 0.2$ for the turbulent flow, and $C_G = C_l = 16$, $n = m = 1.0$ for laminar flow. It is useful to transform equation B.6 for different flow conditions such as laminar liquid - laminar vapor, turbulent liquid - turbulent vapor, etc.

Laminar Liquid - Laminar Vapor

Substituting equations B.7 through B.9 in B.6 for laminar flow conditions gives:

$$\frac{U_G}{U_l} = \frac{\mu_l}{\mu_G} \left[\frac{d^2}{D(D-d)}\right] \tag{B.10}$$

However, in terms of superficial velocities, by substituting $U_G = U_{Gs}/\epsilon$, $U_l = U_{ls}/(1-\epsilon)$ in equation B.10 results in

$$\frac{U_{Gs}}{U_{ls}} = \frac{\mu_l}{\mu_G} \left[\frac{\epsilon^2}{(1-\epsilon)(1-\sqrt{\epsilon})}\right] \tag{B.11}$$

where $\epsilon = (d/D)^2$ = void fraction.

It is interesting to note that U_{Gs} and U_{ls} are linearly related for a given void fraction if both vapor and liquid are flowing in a laminar flow, i.e., the interaction of these two phases may be represented on a flow regime map with superficial velocities as a coordinate system

Turbulent Liquid - Turbulent Vapor

Substituting equations B.7 through B.9 in B.6 for turbulent flow conditions gives

$$\left[\frac{U_G}{U_l}\right]^{1.8} \left[\frac{\rho_G}{\rho_l}\right]^{0.8} = \left[\frac{\mu_l}{\mu_G}\right]^{0.2} \left[\frac{d}{D-d}\right]^{0.2} \frac{d}{D} \qquad \text{(B.12)}$$

However, in terms of superficial velocities, by substituting $U_G = U_{Gs}/\epsilon$, $U_l = U_{ls}/(1-\epsilon)$ in equation B.12 results in

$$\left[\frac{U_{Gs}}{U_{ls}}\right]^{1.8} \left[\frac{\rho_G}{\rho_l}\right]^{0.8} = \left[\frac{\mu_l}{\mu_G}\right]^{0.2} \left[\frac{\epsilon^{2.4}}{(1-\epsilon)^{1.8}(1-\sqrt{\epsilon})^{0.2}}\right] \qquad \text{(B.13)}$$

This equation shows that the relationship between the two phases for a given void fraction and viscosity ratio can be approximated in terms of $\rho_G U_{Gs}^2$ for vapor phase and $\rho_l U_{ls}^2$ for liquid phase, i.e., the interaction of these two phases can be represented on a flow regime map with superficial momentum fluxes as a coordinate system.

Laminar Liquid - Turbulent Vapor

Substituting equations B.7 through B.9 in B.6 for laminar liquid and turbulent vapor flow conditions gives

$$\left[\frac{U_{Gs}}{U_{ls}}\right]^{1.8} \rho_G^{0.8} = \left[\frac{\mu_l}{\mu_G^{0.2}}\right] \left[\frac{348\,\epsilon^{2.4}}{D^{0.8}(1-\epsilon)(1-\sqrt{\epsilon})}\right] \qquad \text{(B.14)}$$

This equation shows that the relationship between the two phases

for a given void fraction and viscosity ratio can be approximated in terms of $\rho_G U_{Gs}^2$ for turbulent vapor phase and U_{ls} for laminar liquid phase.

Similitude Analysis

Simulation of micro-g vapor-liquid flow is accomplished by the selection and use of two immiscible liquids of equal density. It is important to have a flow regime map with coordinates on which one could compare flow regime data of simulated equi-density liquid system and actual micro-g vapor-liquid system. It is critical to know which combination of coordinates (U_{Gs}, $\rho_G U_{Gs}^2$, Re_G, etc.) to use for comparison.

In simulating micro-g vapor-liquid flow, comparable viscosity ratio and interfacial tension between equi-density fluids as that of typical vapor-liquid systems are used. For a given viscosity ratio, equations B.11, B.13, and B.14 show the relationships between the two phases (liquid-liquid or vapor-liquid) for various flow conditions. That is, the interaction of two phases can be graphically represented with the following coordinate systems for various flow conditions:

laminar vapor - laminar liquid : U_{Gs} vs. U_{ls}

turbulent vapor - turbulent liquid : $\rho_G U_{Gs}^2$ vs. $\rho_l U_{ls}^2$

turbulent vapor - laminar liquid : $\rho_G U_{Gs}^2$ vs. U_{ls}

As discussed in Chapter IV, region of interest (Figure 4.2) in which gravity force is dominant, consists of turbulent vapor - laminar liquid. Laminar vapor - laminar liquid region is of no practical importance because of very low flow rates. In the simulation experiments, water which is simulating the real "vapor" goes from

laminar to turbulent and fluid #2 which is simulating the "liquid" does remain in laminar in the range of flow rates studied as shown in Figure 10.3. Therefore these equi-density liqud systems do simulate the region of interest quite well. Since the region of interest basically consists of turbulent vapor - laminar liquid, the comparison between simulated vs. actual micro-g data can be made on a flow regime map with a coordinate system : superficial momentum flux of vapor, $\rho_G U_{Gs}^2$ vs. superficial velocity of liquid, U_{ls}. Since the density of our simulating "liquid" (oils) is of the same order of magnitude as that of typical liquids, the y-coordinate can be changed from U_{ls} to $\rho_l U_{ls}^2$ without introducing any significant error. Therefore, the comparison between simulated vs. actual is made on a flow regime map with a coordinate system : superficial momentum flux of vapor, $\rho_G U_{Gs}^2$ vs. superficial momentum flux of liquid, $\rho_l U_{ls}^2$ throughout this study.

It is interesting to compare modified coordinates (as discussed in Chapter V.) of Baker's flow regime map (Bell et al., 1970) with the superficial momentum fluxes from this analysis. Baker uses G_G/λ and $G_l\psi$ which are essentially square root of corresponding superficial momentum fluxes as coordinates. The similarities are:

$$\text{(i)} \quad r_l U_{ls}^2 = G_l^2 (1 - x)^2 / \rho_l \simeq (G_l \psi)^2$$

$$\text{(ii)} \quad r_G U_{Gs}^2 = G_G^2 x^2 / \rho_G \simeq (G_G/\lambda)^2$$

This comparison shows that these coordinates are similar in nature. Hewitt and Roberts (1969) are the first ones to use superficial momentum flux as coordinates to represent a flow regime map.

APPENDIX C.

APPENDIX C.

SIMULATION OF VAPOR-LIQUID STATIC SYSTEMS IN MICRO-GRAVITY

Consider a stationary container filled with any vapor and liquid under normal earth gravity conditions. It would be quite easy to figure out the spatial distribution of the vapor and liquid. It will be essentially a stratified configuration in which the liquid occupies the bottom and the vapor the top part of the container. This is because the difference in the buoyancy forces of these two phases (liquid is heavier than vapor). The question is what would be the spatial distribution of these two phases if the container is placed in a micro-g environment (i.e., absence of buoyancy forces). This is an important problem in a number of space applications, e.g., vapor-liquid configuration in a solar thermal energy storage system in which heat transfer rate is dependent, to a large extent, on the position, shape, and location of the vapor.

In the absence of gravity and other body forces as in the case for a vapor-liquid static system in micro-g, the surface forces determine the shape and location of the void(s). The use of two immiscible liquids of equal density offers the possibility to eliminate the buoyancy forces and thus simulate a micro-g vapor-liquid static system on earth. In simulating micro-g vapor-liquid static system, the fluid which is more wettable with the container surface simulates the "liquid" phase and the fluid which is less wettable would simulate the "vapor" phase. By matching the surface forces of equal density liquid-liquid system to that of a real vapor-liquid

system, it is possible to simulate micro-g vapor-liquid static system on earth.

Proof of Concept: This technique is used to simulate an air-water (surface tension is 0.072 N/m) static system in micro-g environment. The simulating fluid system consists of the mixture of silicone oil + CCl_4 and water of equal density (interfacial tension between these two liquids is about 0.047 N/m). Figure C.1 shows the result of our simulation technique. Stationary spherical droplet (less wettable and low viscous water) simulates micro-g "air" surrounded by more wettable and high viscous liquid (silicone oil + CCl_4) simulates micro-g "water". An air-water experiment in a stationary system has been conducted during parabolic trajectories in a KC-135 aircraft. The spatial configuration of air and water in this experiment is shown in Figure C.2. It can be seen that the air formed a single spherical bubble surrounded by water. When the static system is disturbed by shaking the container, it is observed that the dispersed air bubbles quickly coalesce back and form a single spherical bubble. It can be concluded that our technique has been successful in simulating air-water system in micro-g.

Mathematical Analysis - Thermodynamic Considerations

A thermodynamic analysis of the morphological nature of the possible spatial distribution of vapor in the vapor-liquid static system may be obtained by considering the free energy changes taking place for a hypothetical case. The spatial distribution of vapor could be of any shape all the way from stratified to perfect spherical vapor bubble(s). Since no mixing or demixing is involved, the only

Figure C.1 : Schemiatic of Simulated Micro-g Vapor-Liquid in a Stationary System.

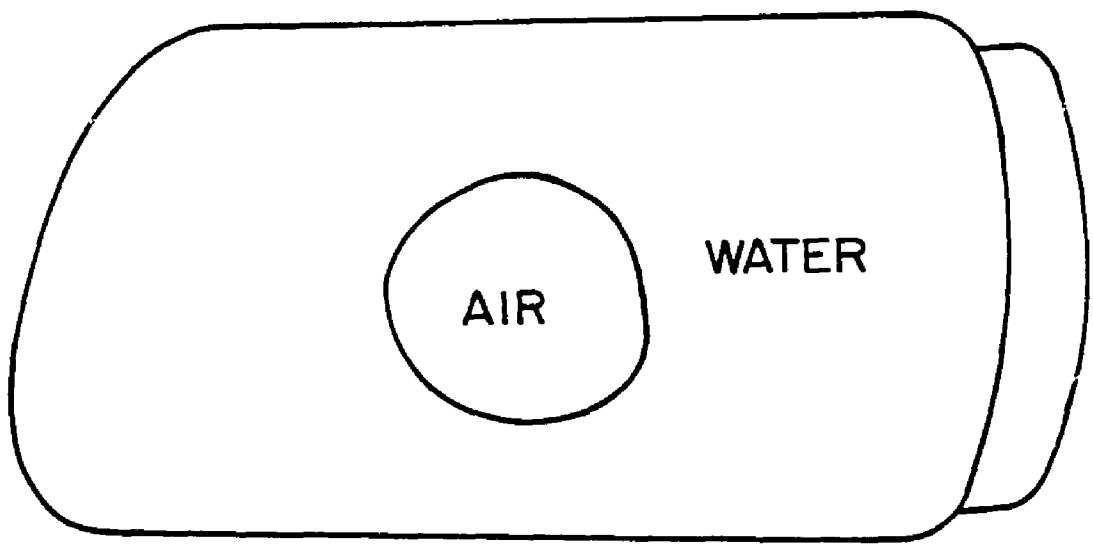

Figure C.2 : Schematic of Air-Water Experiment in a Stationary System Under Micro-g Environment (KC-135 Aircraft).

contribution to the free energy change is due to the creation of a new interface. This free energy change, ΔG can be expressed as

$$\Delta G = \Sigma \gamma_i A_i \qquad C.1$$

where, γ_i is the interfacial tension of the i-th interface and A_i is the corresponding interfacial area. Each of the different morphologies will have different combinations of $\gamma_i A_i$ due to their respective geometric shapes. This makes the analysis straight forward as long as the interfacial forces are constant and can be measured. The thermodynamics dictates that the system will reach static equilibrium when ΔG is minimum for a particular configuration of the vapor in the system. In other words the spatial distribution of vapor in vapor-liquid static system will take a form for which ΔG predicted by equation C.1 is minimum. To verify this model, it is necessary to measure all the interfacial forces including interfacial tension and adhesion tension and adhesion wetting of liquid and vapors with respect to container surfaces.

APPENDIX D.

APPENDIX D.

Sources of Chemicals and Equipment

1. Polypropylene Glycol-2000	John R. Hess and Sons, Inc. P.O. Box 2096 Providence, R.I. 02905 (401) 785-9300
2. Heavy Mineral Oil (340-360 USP @ 100°F)	General Chemical 133 - Leland Street Framingham, MA 01701 (617) 872-500
3. Carbon Tetrachloride	Bulk Sales Department Aldrich Chemicals 940 West Saint Paul Avenue Milwaukee, WI 53233 (800) 556-2426
4. Dow Corning 200 Fluid (50 cSt)	George Mann & Co., Inc. P.O. Box 9066 Providence, R.I. 02940 (800) 556-2426
5. Kerosene	H & H Oil Co., Inc. Portsmouth Avenue Greenland, NH 03840 (800) 322-0313
6. Amyl Benzoate, Anisole, Benzonitrile, Butyl Benzoate, Diethyl Adipate, Diethyl Dimethylmalonate, Diethyl-1-Naphthylamine, 1-Phenyl-1-Propanol, and 3-Phenyl-1-propanol	Pfaltz & Bauer, Inc. 172 E. Aurora St. Waterbury, CT 06708 (203) 574-0075
7. All Glass Ware and Accessories	Ace Glass, Inc. P.O. Box 688 1430 Northwest Boulevard Vineland, New Jersey 08360 (609) 692-3333